SYNTHESIS AND CHARACTERIZATION OF GRAPHENE ON COPPER SUBSTRATE: EFFECTS OF HYDROGEN AND COPPER SURFACE MORPHOLOGY ON GRAPHENE CHARACTERISTICS

BY

AHMED IBRAHIM ALI IBRAHIM

A Dissertation Presented to the

DEANSHIP OF GRADUATE STUDIES

KING FAHD UNIVERSITY OF PETROLEUM & MINERALS

DHAHRAN, SAUDI ARABIA

In Partial Fulfillment of the

Requirements for the Degree of

DOCTOR OF PHILOSOPHY

In

MECHANICAL ENGINEERING

May, 2015

KING FAHD UNIVERSITY OF PETROLEUM & MINERALS

DHAHRAN-31261, SAUDI ARABIA

DEANSHIP OF GRADUATE STUDIES

This thesis, written by **Ahmed Ibrahim Ali Ibrahim** under the direction of his thesis advisor and approved by his thesis committee, has been presented and accepted by the Dean of Graduate Studies, in partial fulfillment of the requirements for the degree of **DOCTOR OF PHILOSOPHY IN MECHANICAL ENGINEERING.**

Dr. Tahar Laoui
(Advisor)

Dr. Muataz Atieh
(Member)

Dr. Zafarullah Khan
(Member)

Dr. Saheb Nouari
(Member)

Dr. Muhammad M. Hussain
(Member)

Dr. Zuhair Gasem
Department Chairman

Dr. Salam A. Zummo
Dean of Graduate Studies

30/ 7/ 2015

Date

عمادة الدراسات العليا
DEANSHIP OF GRADUATE STUDIES

To my loving family

ACKNOWLEDGMENTS

I would like to thank Professor Tahar Laoui and Professor Muataz A. Atieh for providing me the opportunity to conduct research in their groups, a special thanks for Professor Tahar Laoui for his continuous supervision and guidance during the experimental work and thesis writing. I wish to thank Mr. Jerwin for training me on field emission scanning electron microscopy apparatus (FE-SEM) and Mr. Saheed for training me on Horiba Raman spectroscopy apparatus. I want also to give great thanks for Mr. Lateef and Mr. Sadaqah for their assistance during the lab work.

Moreover, I would like to thank Dr. Sultan Akhtar for useful discussions and suggestions about some results reported in my thesis. Lastly, I would like to thank my parents, wife and children for their unconditional love, support and patience during my four years PhD program.

TABLE OF CONTENTS

ACKNOWLEDGMENTS ..... **V**

TABLE OF CONTENTS ..... **VI**

LIST OF TABLES ..... **IX**

LIST OF FIGURES ..... **X**

LIST OF ABBREVIATIONS ..... **XVI**

ABSTRACT ..... **XVII**

ARABIC ABSTRACT ..... **XIX**

CHAPTER 1 INTRODUCTION **1**

CHAPTER 2 LITERATURE REVIEW **4**

2.1 CVD technique **4**

2.2 Graphene growth mechanism **5**

2.3 APCVD versus LPCVD synthesized graphene **8**

2.4 Factors affecting CVD synthesis of graphene on copper **9**

2.4.1 Methane flow rate 9

2.4.2 Hydrogen flow rate 12

2.4.3 Growth temperature and time....14
2.4.4 CVD chamber geometry....16
2.4.5 Cu substrate....18
2.5 Raman spectroscopy of CVD-graphene....24
CHAPTER 3 EXPERIMENTAL WORK....32
3.1 Pre-cleaning of Cu substrate....32
3.2 CVD process....32
3.3 Graphene transfer....35
3.4 Graphene Characterization....36
3.4.1 Scanning Electron Microscopy (SEM)....37
3.4.2 X-Ray Diffraction (XRD)....37
3.4.3 Optical Microscopy (OM)....38
3.4.4 Raman Spectroscopy....38
3.4.5 Atomic Force Microscopy (AFM)....39
3.4.6 Transmission Electron Microscopy (TEM)....40
CHAPTER 4 RESULTS AND DISCUSSION....41
4.1 Effect of hydrogen on Cu surface during annealing stage....41
4.2 Effect of hydrogen during Cu annealing on nucleation and growth of graphene....49
4.3 Effect of hydrogen during graphene growth step....64

4.4 Effect of Cu substrate on growth and transfer of graphene 68

4.5 Effect of growth temperature on the quality and thickness uniformity of graphene film 84

CHAPTER 5 CONCLUSIONS 92

REFERENCES 94

CURRICULUM VITAE 107

LIST OF TABLES

Table 1: Graphene growth recipe by APCVD 35

Table 2: CVD parameters to study the effect of H_2 concentration on Cu surface morphology evolution during annealing stage..... 45

Table 3 Crystallite size calculations of annealed Cu samples as a function of H_2 concentrations 48

Table 4: CVD-graphene growth parameters to study the effect of H_2 concentration (during annealing stage) on Cu surface morphology evolution and deposited graphene properties..... 50

Table 5: Calculations of I_D/I_G and I_{2D}/I_G ratios for Raman spectra shown in Figure 43(e) 61

Table 6: CVD-graphene growth parameters to study the effect of H_2 concentration (2.5-20%) on the deposited graphene properties 65

Table 7: CVD-graphene growth parameters to study the effect of Cu substrate on graphene properties..... 68

Table 8: CVD-graphene growth parameters to study the effect of H_2 concentration (during annealing stage) and increased growth temperature (1040^{o}C) on deposited graphene properties on AA and HA-Cu substrates respectively 84

LIST OF FIGURES

Figure 1: Graphical representation of the different mechanisms in which carbon forms graphene layers: (a) surface adsorption process at Cu surface (B) segregation process at Ni surface. [8][9] 6

Figure 2: Schematic representation of graphene growth mechanism. [12] 7

Figure 3: SEM images of grown graphene at different growth conditions (a), (b) by increasing temperature from 985 to 1035 oC, (b), (c) by decreasing methane flow rate from 35 to 7 sccm, (c), (d) by decreasing partial pressure from 460 to 160 mTorr [38] .. 11

Figure 4: SEM images of the CVD graphene domains grown under different hydrogen flow rates: (a) 100 sccm, (b) 200 sccm, (c) 500 sccm, and (d) 1000 sccm. The carrier gas used here was pure hydrogen, the methane flow rate was 5 sccm and the growth time was set to be 10 min.[42] 13

Figure 5: SEM images for synthesized HGFs at different growth temperatures, (a) at 1120^{o}C, (b) 1140^{o}Cand (c) 1160^{o}C. [50] 15

Figure 6: SEM images of the CVD graphene domains grown at different growth times, (a) 10 min, (b) 30 min, (c) 60 min. The carrier gas used here was pure hydrogen at a flow rate of 800 sccm, and the methane flow rate was 5 sccm [42] 16

Figure 7: Structure evolution of the graphene films as a function of growth time. (a) SEM image of the graphene films prepared for 1 min without the use of H2 during the growth. (b),(c), and (d) SEM images of the graphene films prepared with different growth periods, where H2:Ar is 150:150 SCCM [51] 17

Figure 8: Schematic of boundary layer above copper foil. The copper foil substrate surface is parallel (a) and tilted (b) to the bulk gas flow 17

Figure 9: Optical micrographs of graphene flakes grown by (a) polished and (b) unpolished Cu substrate at early growth stage [23] 18

Figure 10: SEM images of graphene grown on NR copper foil type for (a) untreated, (b) HNO3 treated, and (c) electropolished treated substrate [24] 19

Figure 11: SEM images of graphene on Cu foil with different purities [24] 20

Figure 12: Shape and orientation dependence of LPCVD graphene domains on polycrystalline Cu. (a) SEM image LPCVD graphene domain shape and orientation on different Cu grains. (b) EBSD map of the same region of polycrystalline Cu using the standard EBSD color key. (c), (d), (e), (f) SEM images of representative LPCVD graphene domain shapes grown on different Cu grains [55]. 23

Figure 13: Graphene grains grown on Cu substrates. (a) An optical microscopy image (b) SEM image (c) SEM image of as-grown grains (d) SEM image showing graphene grains across Cu grain boundaries [56] 24

Figure 14: Raman spectra of graphene films with different numbers of stacked layers[7] 27

Figure 15: Raman characterizations of HGFs transferred onto 300 nm SiO2/Si substrate [50]……. 28

Figure 16: Raman map of a single layer graphene grown on bulk Cu substrate and transferred onto an insulating substrate [63]..... 29

Figure 17: Raman Spectroscopy maps (90x90μm2). (a)I2D/IG map, (b) 2D peak position map and (c) G peak position map[55]..... 30

Figure 18: Spectroscopic Raman mapping of graphene grains and grain boundaries. (a–c) Intensity maps of the D, G and 2D bands, respectively, for a two coalesced graphene grains with a single grain boundary [56] 31

Figure 19: (a) SEM image of graphene transferred on SiO2/Si (b) Optical microscope image of the same regions as in (a). (c) Raman spectra from the marked spots ,(d to f) Raman maps of the D , G and 2D bands [7] 31

Figure 20: Schematic diagram of the CVD process for growing graphene on Cu substrate…..... 34

Figure 21: CVD-graphene growth cycle..... 34

Figure 22: Graphene transfer process 36

Figure 23: Schematic diagram of AFM instrument [64]. 39

Figure 24: Surface morphology characteristics of as-received AA-Cu foil. (a, b) OM and SEM images of as-received Cu surface morphology, (c, d, e) 2D AFM images of primary

, waviness and roughness surface profiles respectively (f, g, h) corresponding 3D AFM images, (i, j, k) surface height profiles corresponding to the locations indicated by the scan lines shown in (c, d, e), the length of scan line was 5 μm in each case 43

Figure 25: Effect of H2 during annealing stage on evolution of Cu surface morphology.(a-d) SEM micrographs of Cu annealed at different H2 concentration corresponding to 0, 2.5, 20 and 50% respectively, (e-h) high magnification images of Cu foils shown in (a-d), (i) XRD spectra of as-received and annealed Cu foils, (j) zoomed–in plot of Cu(200) reflections shown in (i). Scale bars corresponding to 20 μm for (a-d) and 1 μm for (e-h) 46

Figure 26: Effect of H2 on Cu surface evolution after annealing only. (a-d) SEM micrographs of Ann-Cu samples at different H2 concentrations corresponding to 0, 2.5, 20 and 50% respectively (e-h) 2D AFM images of Cu surfaces shown in (a-d), (i-l) cross-sectional surface profiles at locations indicated by the scan lines 48

Figure 27: (a-d) SEM micrographs of graphene/Cu that pre-annealed at different H_2 concentrations (0 to 50%). Some graphene domains are indicated by white arrows in a, b, and a particle with white arrowhead in (c) 50

Figure 28: OM images and Raman spectra of transferred graphene onto 300 nm SiO_2/Si wafers, (a-d) OM images of transferred graphene grown on Cu-foils that annealed at different H2 concentrations (0-50%), (i) Raman spectra of transferred graphene samples and (j) plot of I_{2D}/I_G and ID/IG ratios measured from Raman spectra shown in panel (i) 52

Figure 29: AFM micrographs of as grown graphene on Cu foils; the foils were annealed at 0% (a), 2.5% (b), 20% (c) and 50% of H_2 (d). The micron-sized particles were emerged on the Cu foils both as individuals (blue arrows) and aggregates (red arrows)… 55

Figure 30: Elemental analysis composition of particles formed on Cu surface after graphene growth (Cu was annealed at 0% H_2), (a-c) SEM images of investigated Cu areas, (d- f) corresponding EDX spectra of areas highlighted by square shapes, as shown in panel (a- c) 55

Figure 31: Schematic illustration of Cu surface morphology evolution of only annealed-Cu and graphene/Cu. (a) surface morphology of as-received Cu, (b, c) after Ar and H_2-annealing respectively, the insets are zoomed-in views of annealed-Cu and (d, e) Cu surface morphologies after graphene growth on Cu shown in the insets of (b, c)..... 57

Figure 32: (a-d) SEM images of G-Cu samples (3 min growth) as a function of different H2 concentrations (0-50%), (e-h) 2D AFM images of corresponding SEM images shown in (a-d), (i-l) surface profiles of 2D AFM images shown in (e-h) corresponding to the cross-sectional lines indicated by white color 59

Figure 33: (a-d) OM images of transferred graphene/SiO2 which grown on Cu substrates, which pre-annealed at different H_2 concentrations (0- 50%) of the total gas mixture consisting of Ar and H_2, (e) Raman spectra of graphene/SiO2 samples shown in (a-d), (f) plot of I_{2D}/I_G and I_D/I_G ratio of corresponding spectra shown in (e) 61

Figure 34: AFM images of transferred graphene onto SiO_2 which were deposited on Cu substrates (pre-annealed at different H_2 concentrations corresponding to (a) 0%, (b) 2.5%, (c) 20% and (d) 50% of the total gas mixture consisting of Ar and H_2 63

Figure 35: Effect of H_2 concentration on morphology evolution of as-graphene films during growth step. (a-c) SEM micrographs of as-grown graphene/Cu substrates under different H2 concentrations corresponding to 2.5, 10 and 20% respectively, (d-f) OM images of graphene/SiO2 wafers, (g-i) Raman spectroscopy analysis of graphene/SiO2 67

Figure 36: SEM micrographs of grown graphene on (a) AA and (b) HA Cu respectively. It is obvious that AA exhibited higher density of multilayer; irregular graphene domains nucleated mostly on Cu step edges, in contrast HA showed less number of nucleation sites with bi and multilayer, hexagonal graphene domains on monolayer graphene with increased number of wrinkles and cracks indicating its one atom thickness..... 69

Figure 37: Surface morphology and roughness of Cu substrate before and after graphene growth. AFM micrographs of (a) bare AA, (b) graphene/HA, (c) bare HA, (d) graphene/HA. (e, f) surface roughness profiles of as-received(blue line) and as-grown graphene(red line) on AA and HA Cu foils respectively, associated with their corresponding RMS roughness values..... 70

Figure 38: High magnification AFM images (shown in Figure 1 (b), (c) respectively) of Cu foils after graphene growth, (a, c) AA-Cu surface morphology, and corresponding height profile of surface nanoparticles, (b, d) HA-Cu surface morphology and its corresponding particles heights analysis. It is observed particles emerged on AA case are larger in size (~ 70 nm) than found on HA Cu whose size (~15 nm)..... 72

Figure 39: Schematic diagram shows the evolution of AA and HA Cu foils after annealing and graphene growth steps 72

Figure 40: XRD patterns of AA and HA C1gu substrates before and after graphene growth (a, b) of AA and (c, d) for HA 75

Figure 41: OM and Raman spectroscopy analysis of grown graphene on AA and HA Cu substrates respectively, (a, b) OM images of graphene/AA and HA respectively after transferred onto SiO2 wafer, (c, d) Raman spectra of graphene/SiO_2 shown in (a), (b) respectively 77

Figure 42: AFM micrographs of graphene transferred onto SiO_2/Si substrate, (a,b) graphene grown on AA and HA respectively, (c, d) height profiles along the rectangles marked in (a), (b) respectively 78

Figure 43: TEM analysis of graphene (a,d) transferred from AA and HA Cu foils respectively, (b,e) EDS spectra of corresponding images (a,d), (c, f) Typical selected area electron diffraction (SAED) patterns of graphene taken from the flat area in each case, (g) High resolution image taken from the folding edge of graphene (as marked with black arrow in (h) where, the inset is the intensity profile taken from the indicated area (white line) show 3-4 layers of graphene 80

Figure 44: Schematic diagram shows the transfer of graphene from Cu substrate to SiO2/Si wafer and generation of graphene nanometer pores as a result of Cu-etching process…… 82

Figure 45: OM and AFM images of etched graphene/ AA and HA Cu foils respectively. (a, b, c) graphene grown by AA, (d, e, f) graphene grown on HA 83

Figure 46: Effect of H2 concentration on graphene grown on AA-Cu at 1040^{o}C for 30 sec growth time. (a- c) SEM micrographs of deposited graphene/AA-Cu foils, which preheated and annealed under different H_2 concentrations corresponding to 0, 2.5 and 20% respectively of the total gas mixture consisting of Ar and H_2 gases, (d-f) OM images of transferred graphene onto SiO_2 wafers shown in panels a-c , (g-i) Raman spectra of graphene/AA-Cu samples shown in panels (d-f). It is clear that as H2 concentration increases, the defects density measured by D-band increases, indicating that high H2 exposure during Cu pre-heating and annealing promotes formation of multilayer, highly defective graphene films 85

Figure 47: Effect of H_2 concentration on graphene grown on HA-Cu at 1040^{o}C for 30 sec growth time. (a- c) SEM micrographs of deposited graphene/HA-Cu foils, which preheated and annealed under different H_2 concentrations corresponding to 0, 2.5 and

20% respectively of the total gas mixture consisting of Ar and H_2 gases, (d-f) OM images of transferred graphene onto SiO_2/Si substrates shown in panels a-c , (g-i) Raman spectra of as-transferred graphene films shown in panels (d-f). It is clear that as H_2 concentration increases, the defects density measured by D-band increases, indicating that high H_2 exposure during Cu pre-heating and annealing promotes formation of multilayer, highly defective graphene films 87

Figure 48: SEM and OM images of growth graphene on AA and HA Cu foils at elevated temperature corresponding to 1040^{o}C. Other growth parameters were set as follows; H_2: Ar = 0 (during annealing step-30 min), 5 sccm CH4, for 5 minutes (a, b) SEM images of graphene/AA and HA respectively, (c,d) OM images of transferred graphene (shown in (a,b)) onto 300 nm SiO_2/Si wafer, (e,f) Raman spectra of transferred graphene samples shown in (c,d). It is clear that AA promoted multilayer, high density, very small, high defective graphene, however, HA exhibited bilayer, low defective graphene with high density of graphene grain boundaries 90

LIST OF ABBREVIATIONS

AA	:	Alfa Asear copper foil
AFM	:	Atomic force microscopy
APCVD	:	Atmospheric pressure chemical vapor deposition
BLG	:	Bilayer graphene
Cu	:	Copper
CVD	:	Chemical vapor deposition
DI	:	De-ionized
HA	:	JX Nippon Mining & Metals HA Foil
LPCVD	:	Low pressure chemical vapor deposition
MLG	:	Multilayer graphene
OM	:	Optical microscopy
SCCM	:	Standard cubic centimeter per minute
SEM	:	Scanning electron microscopy
SLG	:	Single layer graphene
TEM	:	Transmission electron microscopy
XRD	:	X-ray diffraction

ABSTRACT

Full Name : [Ahmed Ibrahim Ali Ibrahim]

Thesis Title : [Synthesis and Characterization of Graphene on Copper Substrate: Effects of Hydrogen and Copper Surface Morphology on Graphene characteristics]

Major Field : [Manufacturing and Materials]

Date of Degree : [May, 2015]

Understanding both graphene growth mechanism on Cu substrate by chemical vapor deposition and the interplay between the Cu surface morphology and the deposited graphene film characteristics is crucial for production of high-quality graphene. In the present work, we investigated the effect of H_2 concentration during annealing on evolution of Cu surface morphology, and on deposited graphene characteristics. In addition, we studied the effect of Cu surface morphology on graphene growth and its subsequent transfer onto SiO_2/Si substrate.

Our results revealed that although H_2 had a smoothening effect on Cu surface as its surface roughness was reduced significantly at high H_2 concentration, it promoted formation of other surface features such as; facets, dents and particles. Furthermore, H_2 content influenced the graphene morphology and its quality. A low H_2 concentration (0 and 2.5%) during annealing promoted uniform and good quality bilayer graphene. In contrast, a high concentration of H_2 (20 and 50%) resulted in multilayer, non-uniform and

defective graphene. Interestingly, it was found that the annealed Cu surface morphology differed considerably from that obtained after deposition of graphene, indicating that graphene deposition has its own impact on Cu surface.

In addition, we found that a smooth Cu surface promoted growth of continuous and uniform monolayer graphene film with fewer structural defects. Whereas, a relatively rougher Cu surface exhibited relatively porous, non-uniform, bilayer graphene film, associated with a higher density of multilayer graphene domains preferentially located along the Cu surface striations. Interestingly, compared with graphene grown on rough Cu foil, graphene grown on smooth Cu yielded better protection for the underlying Cu foil against the attack of Cu-etchant (APS) as evidenced by etching-pit experiments.

This study is believed to bring about more insight on the role of H_2 on Cu surface morphology evolution after being annealed only and after graphene deposition. Furthermore, it emphasizes the importance of Cu morphology in controlling structural defects in graphene, which has implications on synthesis of graphene for applications as a barrier material or as a selective membrane.

ARABIC ABSTRACT

الاسم الكامل: أحمد إبراهيم على إبراهيم

عنوان الرسالة: تحضير وتوصيف الجرافين على ركيزة النحاس: تأثير الهيدروجين وسطح ركيزة النحاس على خصائص الجرافين

التخصص: الهندسة الميكانيكية- المواد والتصنيع

تاريخ الدرجة العلمية: مايو-2015

فهم كل من آلية نمو الجرافين على النحاس بواسطة الترسيب بالتبخير الكيميائى والتأثير المتبادل بين سطح النحاس وخصائص طبقة الجرافين المترسبة أمر بالغ الأهمية لانتاج جرافين عالى الجودة. في هذا العمل تم دراسة تأثير تركيزغازالهيدروجين على تطور مورفولوجيا سطح النحاس خلال مرحلة التليين ، وأيضا تأثيره على خصائص الجرافين المترسب. بالإضافة إلى ذلك، قمنا بدراسة تأثير مورفولوجيا سطح النحاس على نمو الجرافين ونقله لاحقا إلى رقاقة SiO_2/Si.

كشفت النتائج أن الهيدروجين يساعد على تقليل خشونة سطح رقائق النحاس بشكل ملحوظ خاصة في تركيز الهيدروجين العالى، ولكن فى نفس الوقت ساهم فى ظهور بعض السمات السطحية الأخرى مثل؛ الأوجه، الخدوش والجسيمات. وعلاوة على ذلك، تبين أن تركيز الهيدروجين له تأثير واضح على تشكل الجرافين وجودته فعلى سبيل المثال التركيزات المنخفضة للهيدروجين (0 و 2.5٪) خلال مرحلة التليين ساعدت على تكوين طبقة ثنائية من الجرافين ذات نوعية جيدة. في المقابل، أدى تركيزات الهيدروجين المتوسطة والعالية من (20 و 50٪) إلى تكوين جرافين متعدد الطبقات، وذات جودة سيئة. ومن المثير للاهتمام أن مورفولوجيا سطح النحاس اختلفت بشكل كبير عن تلك التي تم الحصول عليها بعد ترسيب الجرافين، مشيرا إلى أن ترسيب الجرافين له تأثيره الخاص على سطح النحاس.

بالإضافة إلى ذلك، وجدنا أن سطح النحاس الناعم يعزز نمو مستمر ومنتظم لطبقة أحادية من الجرافين مع عيوب هيكلية أقل. في المقابل، سطح النحاس الخشن نسبيا ساعد على تكوين طبقة ثنائية من الجرافين الغير منتظم، حيث احتوى على مساحات صغيرة من الجرافين متعدد الطبقات بكثافة عالية. ومن المثير للاهتمام، أن الجرافين المتكون على سطح النحاس الناعم أعطى حماية أكثر للنحاس ضد إختبار تاكل السطح بالمقارنة مع الجرافين الذى تكون على سطح النحاس الخشن، مشيرا إلى ان أسطح النحاس الخشنة تساعد على تكوين عيوب هيكلية بعدد أكثر فى الجرافين المترسب بالمقارنة بالجرافين المتكون على الأسطح الناعمة.

يعتقد أن هذه الدراسة سوف توفر مزيد من الفهم حول دور الهيدروجين فى تطور مورفولوجية سطح النحاس خلال كلا من مرحلة التليين، و أثناء ترسيب الجرافين. علاوة على ذلك، فإنها تؤكد على أهمية تشكل النحاس في السيطرة على وجود العيوب الهيكلية في طبقة الجرافين و التي لها آثار على تطبيقات الجرافين المختلفة كمادة حاجزة أو غشاء انتقائي.

CHAPTER 1

INTRODUCTION

Graphene, a monoatomic layer of carbon atoms in the form of honey-comb lattice has attracted much attention due to its remarkable structure, properties and potential applications in science and technology [1][2][3][4]. Graphene can be synthesized using different techniques such as liquid-phase exfoliation [5], mechanical exfoliation [6] and chemical vapor deposition (CVD). Synthesis of graphene by CVD is one of the most promising routes for producing large-area and good quality graphene films on suitable substrates [7]. Synthesis of graphene using CVD consists of four steps; heating, annealing, graphene deposition, and cooling. Gas flow rates (e.g. H_2, Ar and CH_4) need to be selected carefully during each step to deposit graphene with desired characteristics. Copper (Cu) and nickel (Ni) are the most commonly used substrates/catalysts for graphene fabrication. Cu is extensively used as it promotes more uniform, relatively large-area graphene compared to that obtained on Ni substrate [8],[9].

Extensive work has been reported to control synthesis of graphene on Cu substrate by CVD process. In this regard, some researchers have studied the influence of various CVD parameters (gas flow rates (e.g. Ar, H_2 and CH_4), pressure, growth temperature and time) on the uniformity and quality of graphene [10] [11] [12] [13] [14] [15]. These studies revealed that H_2 plays a crucial role in controlling both of graphene uniformity and quality during CVD process. it was reported that H_2 had a smoothening effect on Cu surface

morphology and thus it promoted growth of uniform, large area and good quality graphene [16][17]. In contrast, it was demonstrated by other researchers that H_2 could have a roughening effect on Cu surface (due to the formation of voids and hillocks), leading to increased nucleation density, and resulting in the formation of multilayer, defective graphene [18][19][20].

Cu surface plays also a crucial role on the thickness uniformity and quality of deposited graphene film. For instance, smooth Cu features favor formation of mono- or bi-layer graphene domains, while rough features (e.g. grain boundaries, impurities and Cu particles) promote multilayer and defective graphene [18]. These features could also trap high amount of decomposed carbon species favoring deposition of amorphous or turbostatic graphene regions [21]. Thus, the quality of graphene film relies strongly on the surface morphology of underlying Cu substrate [22]. Considering the importance of Cu surface morphology on the deposited graphene characteristics, a lot of efforts have been devoted to smoothen the Cu surface either before or during the CVD process [23] [24] [25]. Other researchers replaced commercial Cu foils by sputter-deposited thin Cu film to grow large area, high quality graphene [26][27]. However, growth of graphene on commercially available Cu foils offers more advantages than these thin Cu films as it saves time and efforts, and avoids introducing more complicated steps to graphene growth process.

Although intensive work has been performed to optimize the CVD parameters to achieve certain graphene characteristics, there is still a lack of full understanding concerning the following points; (1) the correlation among the CVD parameters, graphene characteristics and the Cu surface morphology, (2) the actual role of H_2 on Cu surface evolution and

graphene growth during different CVD steps, and (3) the interplay between Cu surface and graphene during growth and transfer onto insulating substrates. In order to contribute towards a better understanding on the above mentioned points, the following objectives were addressed:

1- Investigate the effect of H_2 concentration (0, 2.5, 20 and 50%) on the evolution of Cu surface morphology during the annealing stage (prior to graphene growth)
2- Elucidate the effect of H_2 concentration during annealing on the quality and thickness uniformity of synthesized graphene film
3- Understand the Cu-surface reconstructuring mechanism by comparing as-annealed Cu surface to that obtained after graphene growth
4- Study the effect of Cu substrate morphology and purity on graphene growth and its subsequent transfer onto SiO_2/Si substrate
5- Investigate the effect of growth temperature on graphene characteristics

CHAPTER 2

LITERATURE REVIEW

Graphene has attracted attention in recent years because of its unique structure and special properties, making it attractive for electronics, optoelectronics, nanoelectromechanical systems, chemical and biosensing applications. Besides, it has been reported that graphene can be used in membrane applications due to its size-selective transport properties through nanometer-scale holes in its lattice structure [28] [29] [30]. Graphene can be synthesized by many techniques such as liquid-phase[5], mechanical [6] exfoliation, however, Synthesis of graphene by chemical vapor deposition (CVD) process is one of the most promising ways for producing large area, uniform and low defects graphene film on suitable substrate [31].

2.1 CVD technique

In CVD, carbon source (e.g. methane) is introduced at high temperature (~1000°C) in the presence of thin transition metal, on which it is decomposed into carbon atoms, resulting in nucleation and growth of graphene film. There are many parameters which greatly influence the quality and characteristics of grown graphene. The first category of parameters is related to the CVD system such as; precursor gases (H_2, Ar and CH_4), pressure, growth temperature, growth time and cooling rate. The second group of parameters is related to the substrate/catalyst such as; its carbon solubility degree, surface morphology, crystallographic orientation, purity and cleanness of substrate surface [31]. Understanding the interaction among those synthesis parameters and their influence on

deposited graphene film is crucial in controlling and optimizing the quality and characteristics of fabricated graphene. It is intended in this chapter, to get comprehensive understanding on CVD graphene synthesis process by investigating the effect of various growth parameters on the quality and structure of grown graphene. In addition, we will explore the most common graphene characterization techniques, which are used effectively to investigate the characteristics of fabricated graphene.

2.2 Graphene growth mechanism

Graphene can be synthesized over many types of transition substrates using CVD technique. Among those metal substrates are Ni[32], Pd[33], Ru[34], Ir[35] or Cu[7]. Researchers had investigated extensively synthesis of graphene onto Ni and Cu because they relatively yield large, uniform graphene domains compared to the remaining transition metal types. Graphene can be synthesized according to different growth mechanisms, the first mechanism is surface segregation, and the second one is surface reaction. Each mechanism is correlated strongly to the substrate type, and their carbon solubility degree[31].

The most important factor which controls the graphene growth mechanism is the solubility of carbon species in different substrates types. For instance, solubility of carbon into Ni and Co are relatively high (> 0.1 atomic %), therefore, the growth mechanism depends on surface segregation process as depicted in **Figure 1**, in which the growth is due to a combination of diffusion into the metal thin film at growth temperature, and segregation of carbon at the surface of the metal upon cooling stage [31]. In such cases the cooling rate determines if the graphene is successfully formed or not. Fast cooling

rejects carbon atoms from the substrate. However, very slow cooling rate causes the carbon to be diffused into the metal [12]. Therefore, cooling rate must be carefully controlled in order to achieve equilibrium segregation process and hence ensure formation of graphene. Because graphene growth on Ni is dominated by carbon segregation and precipitation process, medium cooling rates are favorable to yield few layer graphene. Besides the role of cooling rate in controlling the graphene properties, microstructure of Ni film plays also crucial role in the formation of graphene film morphology. Polycrystalline Ni substrate leads to formation of continuous monolayer and multilayers regions mostly located at the grain boundaries of Ni substrate [36].

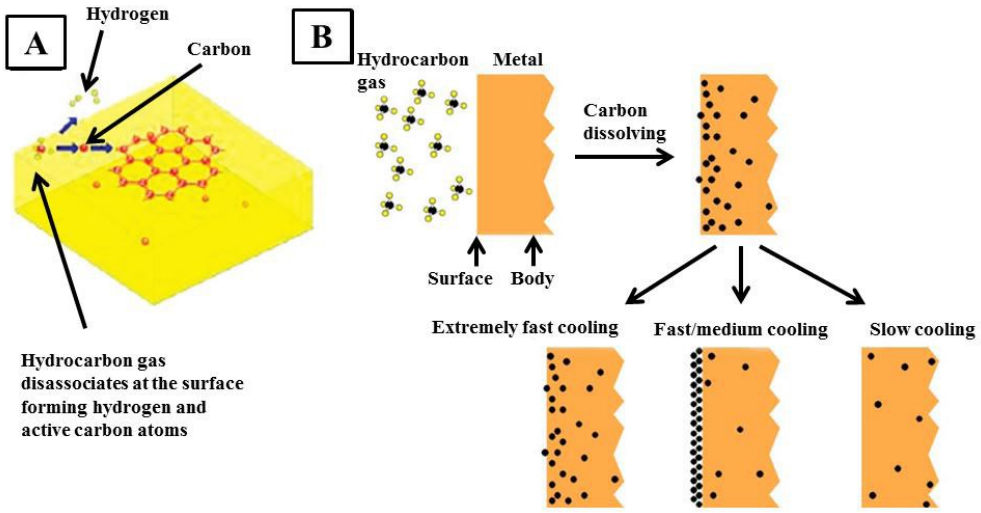

Figure 1: Graphical representation of the different mechanisms in which carbon forms graphene layers: (a) surface adsorption process at Cu surface (B) segregation process at Ni surface [8][9]

However, in case of Cu substrate because of its lower solubility of carbon (<0.001 atomic %) graphene growth mechanism is limited only to the interaction to the catalyst surface. **Figure 2** explains the graphene growth steps on Cu substrates; (1) methane diffuse through the stagnant boundary layer (formed by steady state gases flow close to the catalyst surface), (2) it is then adsorbed on the substrate surface and disassociated into

carbon and hydrogen atoms, the carbon atoms are attached to the Cu surface in order to form graphene nucleation sites. (3) The growth begins by diffusion of other dissociated carbon atoms on copper surface to form graphene lattice planes and hence, forming graphene domains. (4) These domains keep growing till they join together and forming a large graphene sheet. The other inactive hydrogen species will escape and get removed by the bulk gas flow through the boundary layer. This is the reason why this mechanism can provides a uniform mono-layer of graphene on the Cu surface compared to the non-uniform graphene layer obtained by segregation process occurring in Ni substrate.

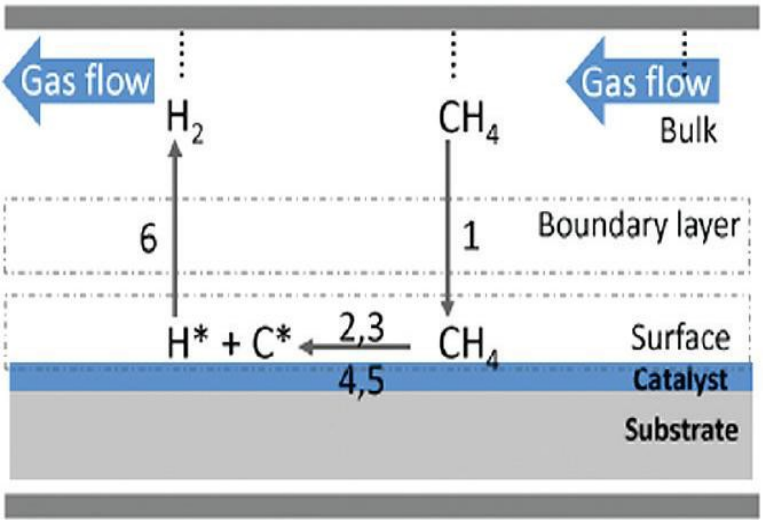

Figure 2: Schematic representation of graphene growth mechanism [12]

Dissociation of CH_4 into C and H species can be expressed by the following equations;

$$CH_4 \rightarrow CH_3 + H \quad \text{.....(1)}$$

$$CH_3 \rightarrow CH_2 + H \quad \text{.....(2)}$$

$$CH_2 \rightarrow CH_1 + H \quad \text{.....(3)}$$

$$CH \rightarrow C + H \quad \text{.....(4)}$$

2.3 APCVD versus LPCVD synthesized graphene

In both of APCVD and LPCVD the thermodynamics of the synthesis system remains the same, however the growth kinetics are different, resulting in a variation in the graphene thickness uniformity over large areas.

In APCVD, graphene quality is controlled by many factors such as; amount of flow gases, surface geometry, position of the substrate and the amount of active species. It was reported in [31] that high flow rate of different precursors gases causes thick, non-uniform boundary layer attached to the catalyst surface, thus this region usually significantly reduces carbon species diffusion rate. Consequently enough amount of precursor gases are needed to efficiently diffuse through that large boundary layer, in order to reach the Cu substrate surface. Adversely, this high gases flow rate may lead to more gaseous reactions, which deposits some particulates on the catalyst surface during graphene synthesis [12]. This can result in higher defect densities, and hence more nucleation sites. After enough synthesis time, multilayer, non-uniform graphene layer can be obtained. Thus, it is believed that, active species (methane and hydrogen) effectively control the quality and thickness of grown graphene in APCVD. Robertson and Warner [37] declared that APCVD yielded few layer hexagonal-shaped single crystal graphene domains. The number of layer was in the range from 5-10 layers in the central region and thinning out toward the domains' edges.

On the other hand, in LPCVD, the diffusion of active species is enhanced through the boundary layer, consequently the growth kinetics is no longer mass transport limiting rate, and hence it becomes dominated by surface reaction rate. As a result this method

promotes formation of more uniform, large area and single layer graphene if compared to that obtained by APCVD [12]. Li, et al. [7] successfully grew continuous, large-area graphene films using LPCVD across copper surface steps and grain boundaries. The as-grown film consisted of monolayer graphene occupying more than 95% of investigated area along with small fraction of bilayer and few-layer (<5%). Li, et al. [38] demonstrated that, at low concentration of methane, graphene growth terminated before achieving full surface coverage, even if the entire copper surface was exposed to methane. As a result, they needed to introduce a second step process to get full graphene surface coverage by increasing the partial pressure for 1min growth time. However, high concentration of carbon species exhibited formation of multilayer graphene domains via an epitaxial growth under the top single layer [39].

2.4 Factors affecting CVD synthesis of graphene on copper

CVD process parameters consist of the precursor gases (CH_4, H_2 and Ar), annealing time, growth temperature and time, heating and cooling rates. These parameters play crucial role in controlling the deposited graphene characteristics. The interaction among these parameters needs to be understood to control the nucleation and growth of graphene on certain substrate. Consequently, a lot of experimental work has been conducted to find the proper balance among these parameters [16].

2.4.1 Methane flow rate

Methane (CH_4) is usually used as the carbon source needed to deposit graphene during CVD process. High CH_4 concentration provides more carbon atoms which leads to more nucleation sites and more growth rate. As a result it promotes formation of multilayer

graphene domains. However, very low concentration of CH_4 gas (~ 0.01 to 0.02% vol) yields monolayer, large area with coverage percentage up to 99% on copper substrate surface.

Li, et al [38] demonstrated that by decreasing the precursor gas flow rate from 35 to 7 sccm, the graphene nuclei density was decreased and as a result, the graphene domain size was increased (**Figure 3)**. Moreover, they mentioned that according to the growth conditions, the Cu surface could be under-saturated, saturated or super-saturated with carbon species; local supersaturation will lead to formation of graphene nuclei, which afterwards will grow to form graphene islands. Consequently by controlling other growth parameters, it was possible to achieve full Cu surface coverage of graphene. They also declared that in order to get full coverage of graphene on Cu surface, it must be supersaturated with CxHy species, so that, the graphene domains will continue growing until they join together and fully cover the Cu surface at the end.

Liang, et al, [40] investigated the effect of methane concentration on the single crystal graphene domains. Results showed that, low concentration methane (mixed gas with 10% methane and 90% Argon) gave better quality and larger graphene domain size than those produced by pure methane, because low methane concentration leaded to less graphene nucleation seeds and hence larger domains by increasing growth time up to ~ 15 min. During their studies, other growth parameters are kept fixed, such as; 1000 sccm argon, 40 sccm hydrogen and 1.5 sccm methane. In addition, they demonstrated that, low methane concentration enhanced hydrogen etching effect, which enabled large area single crystal graphene domain synthesis. According to their study, the best parameters which

yielded approximately continuous graphene film were 1000 ^{o}C, growth temperature, 1.5 sccm low concentration methane, 40 sccm hydrogen and 1000 sccm Argon, the growth time should be between 15 to 18 min.

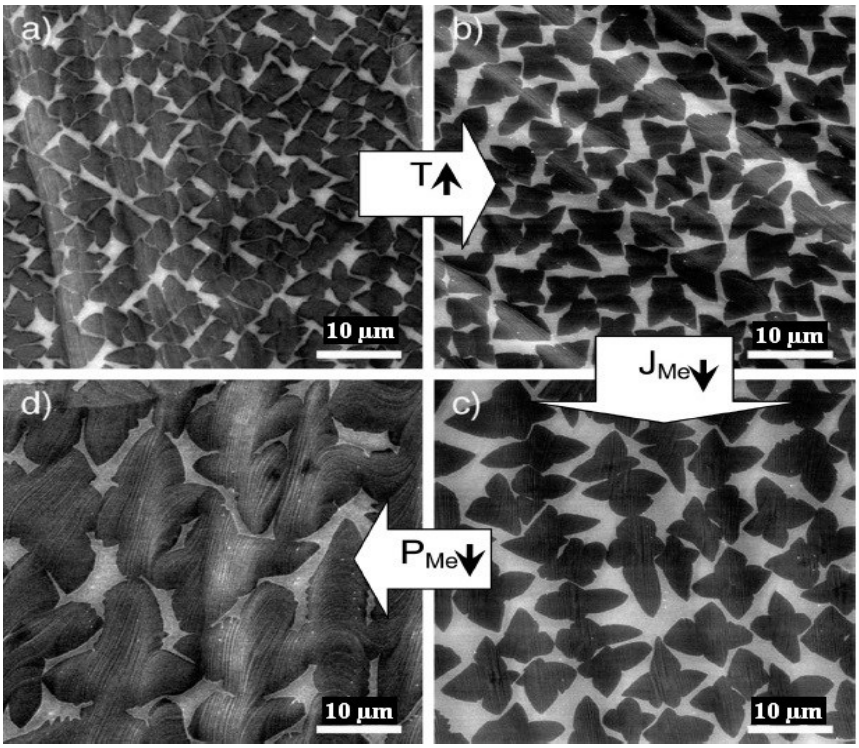

Figure 3: SEM images of grown graphene at different growth conditions (a), (b) by increasing temperature from 985 to 1035 oC, (b), (c) by decreasing methane flow rate from 35 to 7 sccm, (c), (d) by decreasing partial pressure from 460 to 160 mTorr [38]

Rossela et al. [41] had studied the effect of methane flow rate, partial pressure on the grown graphene layer thickness and quality; they demonstrated that, multilayered graphene film was obtained when using high methane concentration of 25 sccm, and high partial pressure of 760 Torr. Therefore, it was reported that graphene growth on Cu was not a self-limiting process. In addition, they stated that when CH_4 flow rate was reduced to 3 sccm, and the partial pressure to 440 Torr, a significant reduction of the film thickness was obtained.

2.4.2 Hydrogen flow rate

Recent studies demonstrated that H_2 flow rate is another crucial factor that can control the graphene properties during growth step. It was reported that presence of H_2 was crucial for growing large area, high quality graphene, as it (1) encourages conversion of adsorbed methane into its hydrocarbon radicals which is essential for formation of graphene [42]. Consequently, activating surface bound carbon which was necessary to grow monolayer [43] and/or bilayer graphene [44]. (2) H_2 could also regulate the diffusion of carbon species on the surface of the copper, thus affording a balanced carbon environment to further ensure the quality of the graphene formed [42]. (3) In addition, H_2 is playing as etching reagent which could control both size, morphology, and the number of layers of grown graphene [42] [43].

Zhang et al. [42] investigated the effect of hydrogen flow rate on the quality and thickness of APCVD synthesized graphene. They conducted some experiments to study the effect of pure hydrogen with different flow rates in the range from 100 sccm to 1000 sccm (**Figure 4**), while the flow rate of methane was fixed at 5 sccm and the growth time set typically for 10 min. they found that hydrogen flow rate of 500 sccm afforded formation of perfect hexagonal single layer graphene domains, and higher hydrogen flow rate of 1000 sccm, leaded to excessive etching of hexagonal graphene domains edges, which suggested the competitive etching effect of hydrogen. In addition, it was observed that, by increasing hydrogen flow rate, the number of graphene layer were reduced and graphene domains became thinner and single-layered graphene structure was obtained at hydrogen flow rate of 500 sccm. Therefore, large area, hexagonal graphene domains

could be synthesized by carefully controlling the competitive etching effect of hydrogen gas during graphene formation.

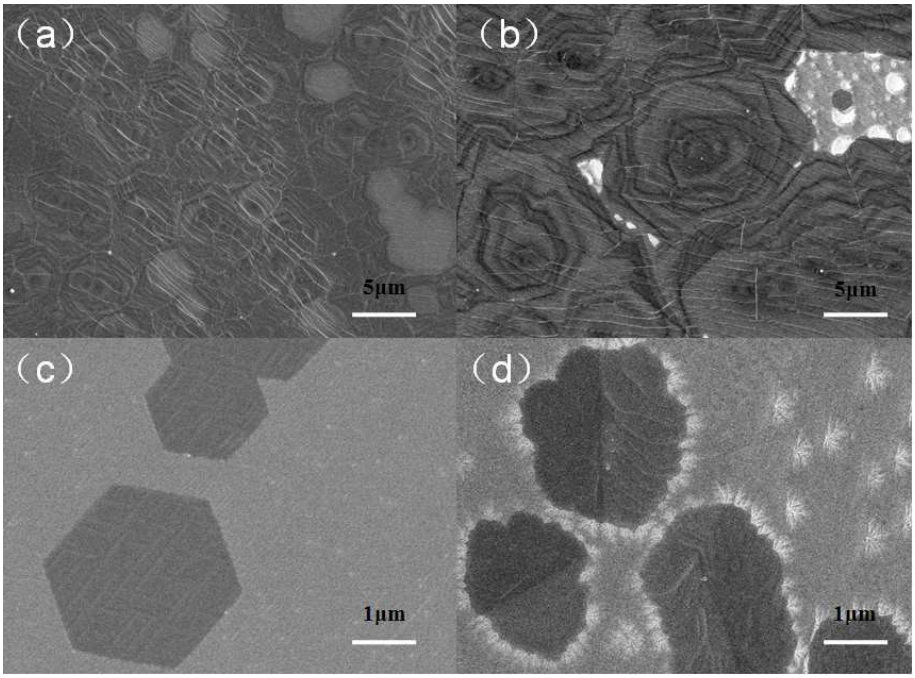

Figure 4: SEM images of the CVD graphene domains grown under different hydrogen flow rates: (a) 100 sccm, (b) 200 sccm, (c) 500 sccm, and (d) 1000 sccm. The carrier gas used here was pure hydrogen, the methane flow rate was 5 sccm and the growth time was set to be 10 min [42]

Therefore, many researchers found that after excluding H_2 from growth step, amorphous carbon batches were grown on Cu surface, as absence of H_2 lead to formation of weak carbon coverage, consisting mostly of oxidized and amorphous carbon obtained on the copper catalyst. The oxidation originates from the inevitable occurrence of residual oxidizing impurities in the reactor's atmosphere, leading to oxygen-related functional groups (H_2 was considered as defect suppressor agent) [15] [42] [45].

On the other hand, many researchers gave completely different explanation concerning H_2 role during growth. H_2 competes with CH_4 dehydrogenation leading to suppression of graphene formation and growth, associated by formation of defective graphene consisting

basically of C-H defects [46], high H_2 supply can cause also SP3-style defects resulting in increased I_D/I_G ratio [44]. Other researchers claimed that H_2 could be the main reason behind growing few-layer graphene, leading to thick and discontinuous multilayer flakes observed mainly at high H_2 concentrations, as it could prevent the transport and adsorption of active carbon species, leading to aggregation of the activated C atoms around the active sites to form stacked graphene flakes, associated by low growth rate [47]. Therefore, by excluding H_2 during growth step, high quality graphene with large area could be synthesized similarly to those obtained by LPCVD confirming that absence of H_2 might convert the growth kinetics from mass-transport to surface-reaction regime [19].

2.4.3 Growth temperature and time

Many researchers asserted that growth temperature effectively influence the quality and characteristics of CVD synthesized graphene. It was reported by many researchers that high growth temperature (~1000-1035^{o}C) is beneficial in decreasing nucleation sites and promoting higher growth rate, resulting in large size graphene domains and low density of defects. In contrast low growth temperature (~750^{o}C) promoted small size graphene domains associated with high density of structural disorder. These results are likely attributed to the increased nucleation density. It is demonstrated that high growth temperature not only does improve hydrocarbon dissociation into carbon species but also it increases diffusion of carbon atoms on the Cu surface. In addition, it helps reduction of volatile impurities, contaminants, and defects on the copper surface and improves surface flatness, and consequently suppressed graphene nucleation on the copper surface [48] [49].

When temperature was further increased in the range from 1120 to 1160^{o}C, large sized hexagonal graphene flakes (HGFs) with average sizes of approximately 50 and 120 μm were obtained as shown in **Figure 5.** By controlling the synthesis time, uniform and continuous single-layered graphene film was eventually obtained. It was explained that at this elevated temperature level Cu was melted, resulting in elimination of grain boundaries which normally found in solid Cu that utilized at lower growth temperatures. Consequently, it led to low nucleation density, better growth rate and larger sized graphene domains uniformly distributed throughout Cu surface [50].

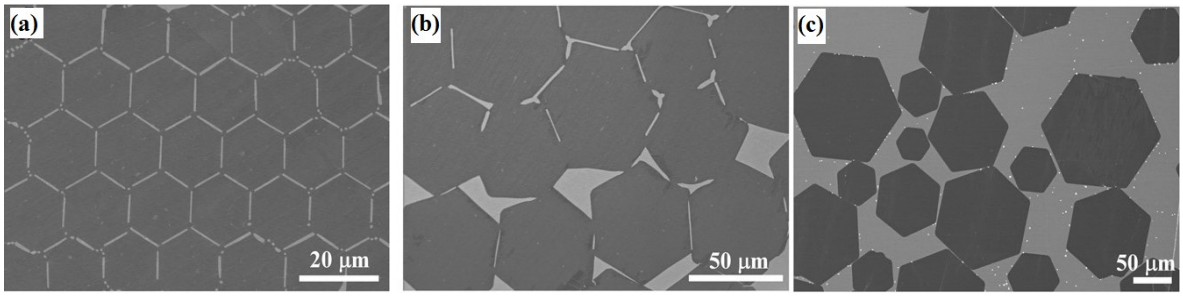

Figure 5: SEM images for synthesized HGFs at different growth temperatures, (a) at 1120^{o}C, (b) 1140^{o}Cand (c) 1160^{o}C [50]

In contrary it was reported elsewhere [39] that high growth temperature (~1035^{o}C) could promote high nucleation density and hence led to small size graphene domains associated with increased defect density.

It was reported that increasing growth time is important for obtaining continuous, full coverage of graphene film [50]. Zhang et al. [39] demonstrated that large area, monolayer graphene with coverage up to 99% could be obtained by increasing the growth time from 2 to 20 min, at 1035^{o}C growth temperature and low CH_4 concentration of 0.02 vol% . Zhang et al. [42] mentioned that prolonged growth time (from 10 to 60 min) was

associated with change of graphene domain edges and increase in domain sizes as depicted in **Figure 6**. Interestingly, Geo, et al. [51] found that by increasing the growth time from 1 to 10 min, graphene film fully covered the Cu foil and there was no distinguishable difference after that period up to 30 minutes as shown in **Figure 7**. Similar results were reported in [7]. These findings reveal that under specific CVD conditions, growth of graphene on Cu is dominated by self-limiting kinetic, in which graphene growth is surface-catalyzed process rather than a precipitation process, resulting in formation of monolayer graphene film on Cu foil. However, it was demonstrated elsewhere [41] that increased growth time was responsible for increasing both graphene film thickness (number of layers) and the amount of structural disorders.

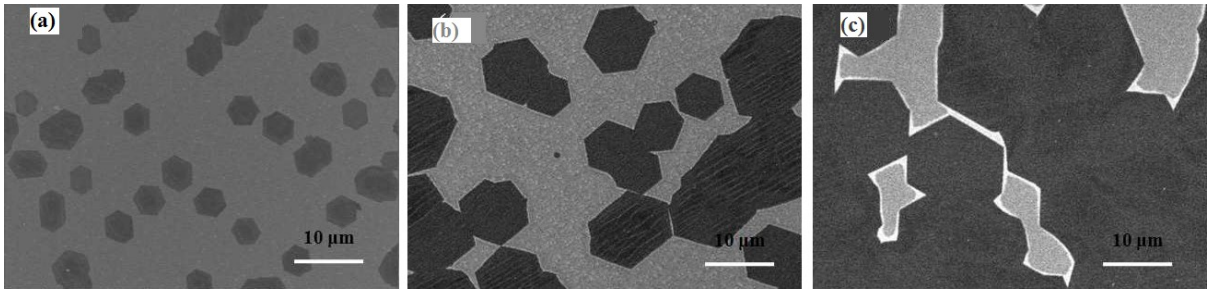

Figure 6: SEM images of the CVD graphene domains grown at different growth times, (a) 10 min, (b) 30 min, (c) 60 min. The carrier gas used here was pure hydrogen at a flow rate of 800 sccm, and the methane flow rate was 5 sccm [42]

2.4.4 CVD chamber geometry

It was reported that, geometry of CVD chamber would have pronounced effect in the deposition rate of carbon species, because it would be a function in generated gas flow patterns (turbulent and laminar types). Zhang et al. [39] demonstrated that, high quality, large area graphene can be obtained using APCVD, by tilting the copper foil during synthesis process. They claimed that when the substrate is tilted against the gaseous flow,

high uniformity of graphene can be obtained due to geometrical fluidic dynamics. Non-uniform boundary layer leads to non-uniform diffusion of carbonaceous species and cannot preclude the reactant depletion effect from one side to the other side in the CVD reactor as can be depicted in **Figure 8**.

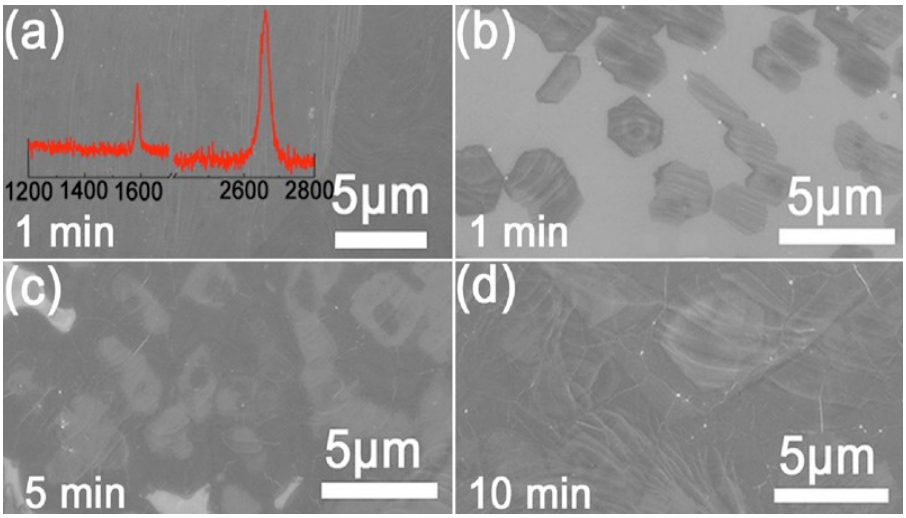

Figure 7: Structure evolution of the graphene films as a function of growth time. (a) SEM image of the graphene films prepared for 1 min without the use of H2 during the growth. (b),(c), and (d) SEM images of the graphene films prepared with different growth periods, where H2:Ar is 150:150 SCCM [51]

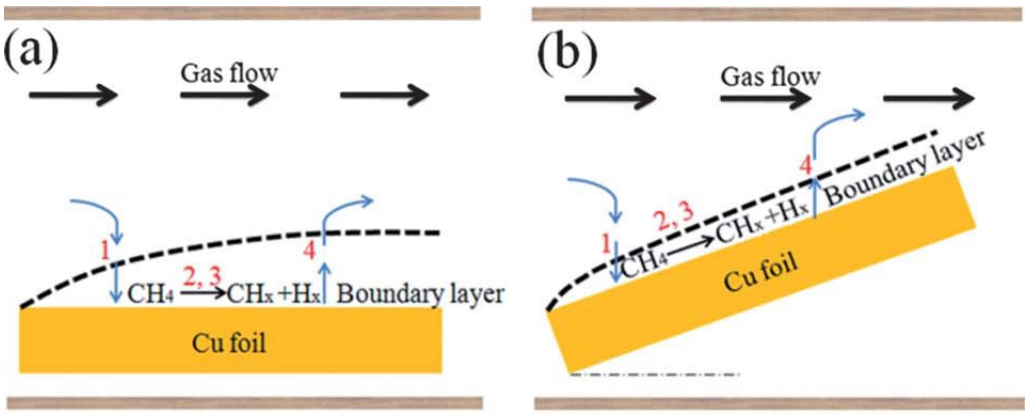

Figure 8: Schematic of boundary layer above copper foil. The copper foil substrate surface is parallel (a) and tilted (b) to the bulk gas flow

2.4.5 Cu substrate

Rasool et al [52] had investigated the continuity of grown graphene on polycrystalline copper substrates. They reported that, irrespective of the amorphous morphology of substrate surface, which exhibits a multitude of surface features, the graphene remain continuous. Han, et al. [23] investigated the influence of copper morphology on the grown graphene quality synthesized by APCVD process. In that work, two copper foils with different surface morphologies were prepared as substrate as shown in **Figure 9**; the first copper sheet was polished using a chemical mechanical method, and the other was used without any surface preparation process. Results showed that, graphene nucleation density was strongly dependent on surface impurities (Cu or alumina particles introduced to the surface during polishing), artificial scratches and grain boundary. Consequently, polished Cu foil exhibited lower density of graphene nucleation seeds, and larger size graphene domains associated with higher growth rate than those grown over unpolished Cu film.

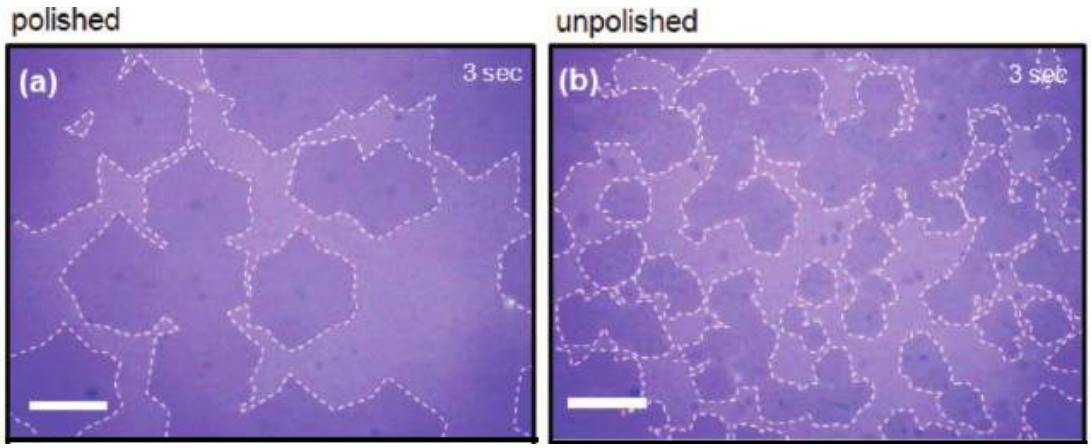

Figure 9: Optical micrographs of graphene flakes grown by (a) polished and (b) unpolished Cu substrate at early growth stage [23]

It was reported also that, impurities and roughness of unpolished Cu foil increased graphene nucleation density, and hence were the main reasons behind formation of multilayered small regions by increasing the growth time. On the other hand, polished Cu surface, exhibited minimum graphene nuclei seeds, and hence facilitated formation of monolayer graphene even at longer growth time. This ensured the self-limiting growth conditions.

Vlassiouk, et al. [24] adopted a study to investigate the effect of Cu substrate surface pretreatment on the quality of APCVD synthesized graphene. They found that, electropolishing pretreatment resulted in superior graphene quality (regular hexagons) in terms of graphene single domain size and nucleation density compared with no treatment or with etching of the foils by nitric or acetic acids as depicted in **Figure 10** That is because it produced lowest contamination and minimal roughness.

Jia, et al. [53] also studied the effect of copper foil pretreatment on the impurities and defects density on investigated Cu films, it was found that, after pretreatment by acetic

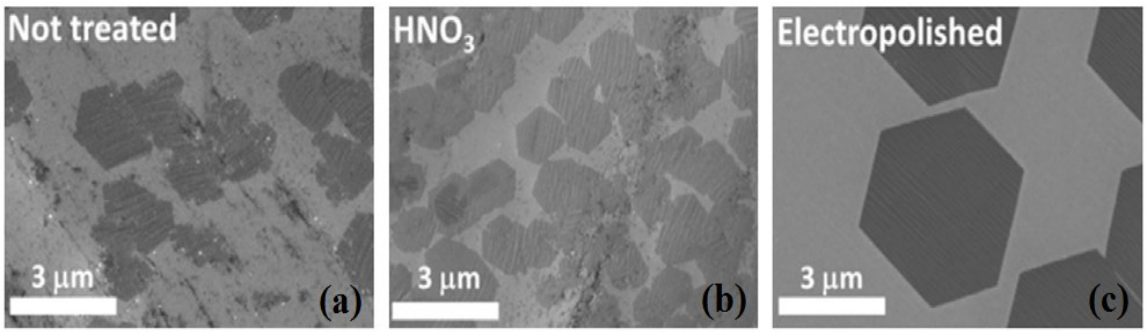

Figure 10: SEM images of graphene grown on NR copper foil type for (a) untreated, (b) HNO3 treated, and (c) electropolished treated substrate [24]

acid for 5 min, and then washed with copious ultrapure water and ethanol, the density of graphene domains on Cu foils was drastically decreased, which was due to the reduction

of nucleation sites, as acetic acid etched the active defect sites and thus decreased the nucleation sites.

Impurities in the copper substrate detract the growth process by encouraging nucleation sites and thus hindering the formation of contiguous carbon domains, therefore, proper chemical cleaning of the copper is essential. Annealing time of the copper also affects the level of impurity for the same reason. Vlassiouk, et al. [24] mentioned that , Cu foil with highest purity (99.999%) promoted single layer graphene synthesis than those produced on copper foils with 99.8% purity which showed some regions with bilayer and multilayer graphene domains (**Figure 11**). Those results might be related to the influence of purity level on solubility, diffusion and adsorption of carbon species with respect to the Cu foil.

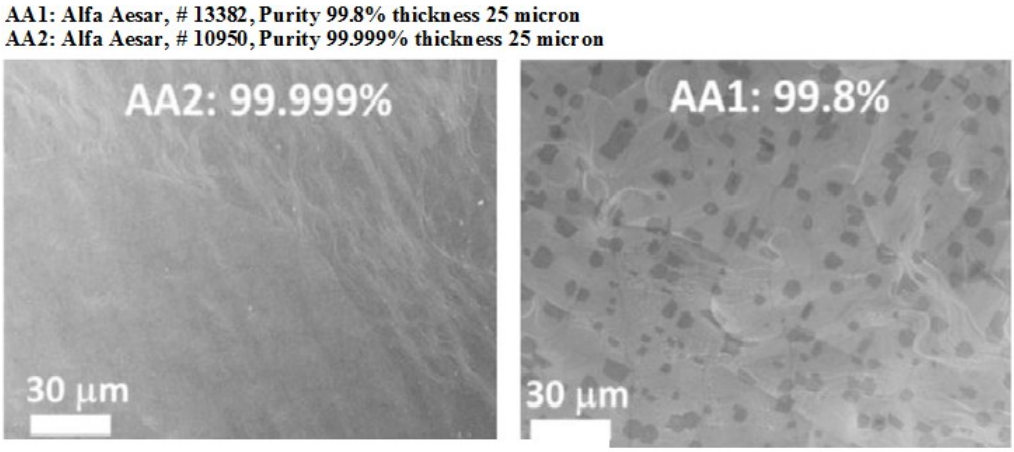

Figure 11: SEM images of graphene on Cu foil with different purities [24]

Many researchers investigated the effect of heat treatment of copper foil on the characteristics of synthesized graphene. Annealing of copper substrate before graphene synthesis is very important step, as it helps reduce the Cu foils, increase grain size and clean the Cu surface. Li, et al. [38] annealed copper substrate at high temperature

(~1035°C) under low hydrogen flow rate (~2 sccm) for 20 min, to minimize graphene nucleation density. Liang, et al, [40] reported also that pre-annealing of copper foil before graphene synthesis for 3 h in the presence of H_2 effectively reduced graphene nucleation density, because hydrogen suppressed the nucleation on copper foil surface at high temperature and hence promoted formation of single-crystal graphene domains larger than 10 μm.

Lu et al. [54] depicted that heat-treated Cu foil promoted a large-area single-crystalline feature Cu(111) orientation of already polycrystalline copper microstructure. Wood et al. [48] mentioned that, longer pre-growth annealing at 900 oC can help promoting formation of predominant Cu (111) facets, while avoiding Cu sublimation and GB migration. Vlassiouk, et al. [24] mentioned that, different copper foil types resulted in different crystallographic surface orientations upon annealing process, as indicated by XRD results. The Alfa Aesar (AA) foil was dominated by (100) facets, however, Nimrod Hall (NH) foils was mixed of (111) and other high index facets.

Many researchers had studied the effect of copper foil microstructure on the quality and number of graphene layer synthesized using CVD technique. One group of researchers reported that crystalline orientations of copper foil have significant effect on the shape, size, and number of layers of individual graphene domains [55].

Wood et al. [48] asserted that the Cu substrate significantly influences graphene nucleation and growth, and showed that a monolayer, high quality graphene with large area coverage grew efficiently on Cu (111), and with faster growth rate, compared to the multilayer graphene grown on Cu(100) facets. They attributed this to high diffusion and

improved carbon adsorption on Cu (111). Murdock et al. [55] had mentioned that there was very strong relationship between the orientation, edge geometry and thickness of grown individual graphene domains and the crystallographic orientations of polycrystalline copper foil.

Figure 12 reveals that the synthesized graphene domains characteristics, depends strongly on the crystallographic planes on which they are synthesized. For example, single layer graphene domains were grown on Cu (111) and Cu (101), while bilayer domains were found on Cu (001). Moreover, they clarified also that, the shape of individual graphene domain changes when it is spanning across two orientations, Cu(001) and Cu(101), as can be indicated by the yellow arrow, while the edge of graphene domain can change across two misoriented grains sharing the same surface normal, Cu(101), as depicted by the red arrow.

In contrary, it was reported by Yu, et al. [56], that grown single-crystal graphene was not restricted by the polycrystallinity of the underlying Cu substrate, as can be depicted in Figure 13 As, the hexagonal shape of APCVD synthesized graphene domains did not change while passing through different Cu facets. In addition, it was demonstrated also in [52] that, pristine graphene was not also restricted to specific copper crystallographic orientation and efficiently can be overgrown on different crystallographic planes Cu(100) and Cu(311), which have different fundamental symmetries than graphene, and hence, the graphene growth was not controlled neither by the morphology nor the atomic arrangement of the underlying substrate. Vlassiouk, et al. [24] found that overall graphene growth on (100) planes of Alfa Aesar (AA) foils was higher than for those

synthesized on (111) planes of Nimrod Hall (NR) foils at ambient pressure, which actually contradicted the other studies results reported elsewhere. [48]

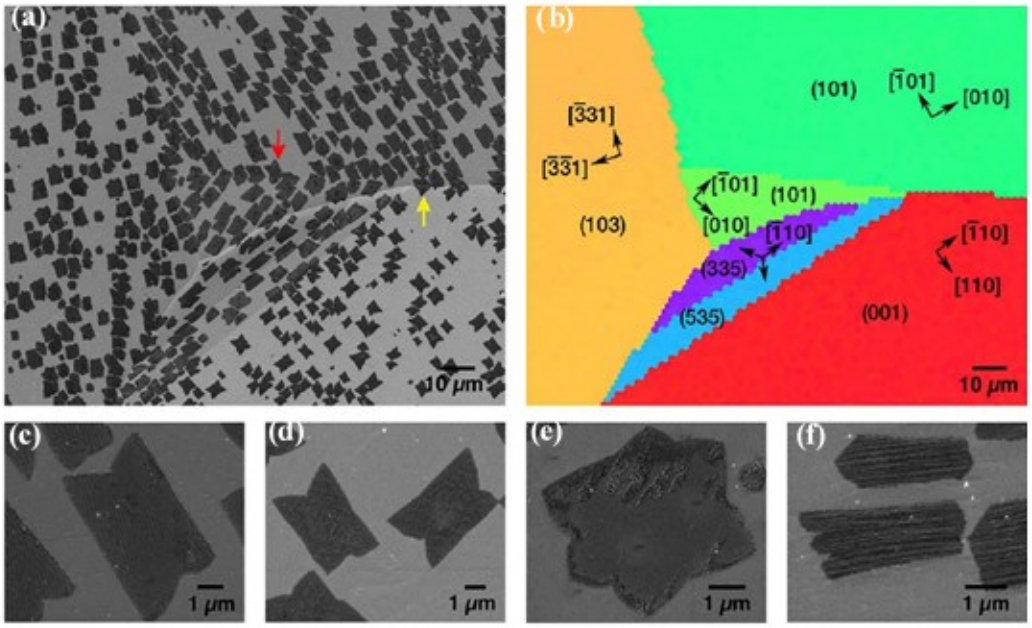

Figure 12: Shape and orientation dependence of LPCVD graphene domains on polycrystalline Cu. (a) SEM image LPCVD graphene domain shape and orientation on different Cu grains. (b) EBSD map of the same region of polycrystalline Cu using the standard EBSD color key. (c), (d), (e), (f) SEM images of representative LPCVD graphene domain shapes grown on different Cu grains [55]

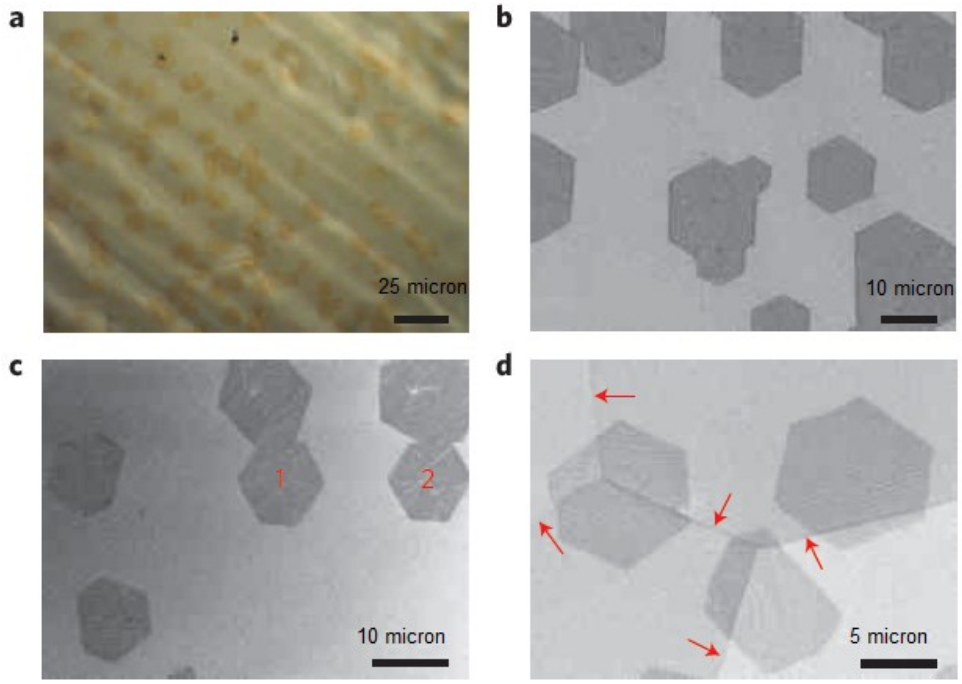

Figure 13: Graphene grains grown on Cu substrates. (a) An optical microscopy image (b) SEM image (c) SEM image of as-grown grains (d) SEM image showing graphene grains across Cu grain boundaries [56]

2.5 Raman spectroscopy of CVD-graphene

A few different techniques have been utilized to characterize the quality as well as the number of layers of CVD deposited graphene. Among them are Raman spectroscopy, scanning electron microscope (SEM), transmission electron microscopy (TEM) and atomic force microscopy (AFM). Of these techniques, Raman spectroscopy has found extensive applications perhaps because the method is simple and non-destructive[57][58]. From the Raman spectra, a great deal of detail on the fine structure of graphene or graphite can be extracted. A typical Raman spectrum for graphene consists of two main bands and a few more very small bands. The two main bands are the G-band found at a Raman shift of ~1582 cm^{-1} and the 2D band found at ~2685 cm^{-1}. A third band although often very weak, the D-band, is found at ~1350 cm^{-1}. These bands are used to discern the quality, the defects, the number of layers and the doping in graphene films[58][59].

What do these bands represent? The D-band is a disorder band and it is sometimes called the defect band. It denotes a ring breathing mode from sp2 carbon rings and the ring must be adjacent to a graphene edge or a defect for the band to be active [58][59]. The band is a result of a single phonon lattice vibrational process and its intensity is an indication of the level of defects in graphene sample. The D-band is a dispersive band and thus its position and shape can be influenced significantly by the excitation laser frequencies. Meanwhile, the G-band is a resonant band and it represents the planar configuration sp2 bonded carbon that constitutes graphene. It arises from the E2g in-plane vibration of the atoms. Unlike the D-band, the G-band position is independent of the excitation laser frequency but depends on the number of graphene layers and perhaps the synthesis conditions. The position of the band shifts to the lower energy with increased layer thickness which connotes softening of the bonds [59]. In addition, the position of the G-band is influenced by the addition of dopants as well as microstrain. These influences must be well considered if the graphene layer thickness is to be accurately evaluated.

The 2D-band (or G/ band as it is called in carbon nanotubes, etc) is an overtone of the D-band and represents the second order of the D-band[60][61]. It is due to a two-phonon lattice vibrational process, but does not need to be close to a defect before being active unlike the D-band. As a result the 2D-band is always a strong band and often present in graphene. This band is also used to estimate graphene layer thickness or the number of graphene layers. As was pointed out with the G-band, care must be taken to ensure that the influences of micro-strain and synthesis conditions are considered because the differences between single and bilayer graphene are more complex than a simple band shift in the 2D-band. Apart from the wave number shift to a higher value, the band shape

changes due to an increased number of the active components. A single layer graphene has one active component while a bilayer graphene has up to four active components causing a band shape distortion.

In a study reported by Li et al.[7] Raman spectroscopy was used to characterize graphene films with different numbers of stacked layers as shown In Figure 14 . The graphene layers were deposited on Cu substrate and then transferred onto a 100 mm diameter silicon wafer containing 300 nm thick SiO2. Based on the Raman plot, it is clear that the peak intensities of the G and 2D bands and the number of layers are well correlated. This behavior is attributed to the random orientations of the hexagonal lattices between any pairs of graphene layers. It is also observed that the 2D-band position shifts to the higher wave number especially between a single and bilayer graphene. The ratio of the peak intensity of 2D-band to that of G-band (I_{2D}/I_G) has been used to distinguish monolayer graphene from others as well as to quantify the uniformity of the graphene layers (by Raman mapping)[50][62].

Also the intensity maps of the G band can give further evidence of the uniformity of the as-grown graphene film [7]. Typically the G-peak intensity of graphene on copper is uniform except in regions corresponding to wrinkles or graphene grain boundaries [7]. An intensity ratio I_{2D}/I_G between ~2 and 4 is considered as a fingerprint of monolayer graphene films[50][62]. In addition, a symmetric 2D peak located at 2698 cm^{-1} [50] or ~2700 cm^{-1} [52] is an indication of a monolayer film.

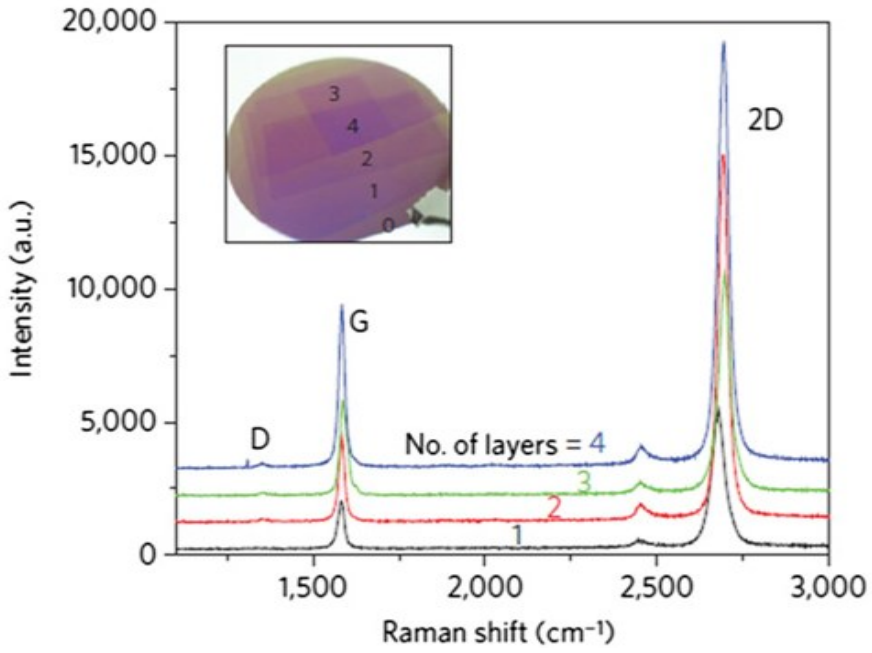

Figure 14: Raman spectra of graphene films with different numbers of stacked layers[7]

A part of these characteristics is demonstrated by Geng et al. [50] who utilized Raman spectroscopy to characterize uniform, single-crystalline and hexagonal graphene flakes (HGFs) deposited by CVD on liquid Cu surfaces. They observed that a monolayer graphene has I_{2D}/I_G = ~2.5 – 4 and a symmetric 2D peak located at 2698 cm^{-1} with a full width at half-maximum (FWHM) of ~35–40 cm^{-1} (**Figure 15**). This finding does not significantly differ from that of Rasool et al. [52] who observed a symmetric 2D band at ~2700 cm^{-1} with FWHM of 32 cm^{-1}. The 2D-band intensity is more than twice as intense as the G band which is found at ~1600 cm^{-1}. To quantify the uniformity of the as-deposited graphene film by Raman mapping, it was shown that 93% of the grown graphene is single layer [62]. In addition, the authors investigated the degree of disorder of graphene grown on a thin film as well as on a copper foil. They concluded that the quality of graphene grown in both cases is comparable (**Figure 16 (b), (c)**).

Furthermore, no increase of the D-band peak was observed after transfer in either case suggesting that no defect was induced during the transfer process [62]. In addition, the I_{2D}/I_G ratios for both cases were comparable indicating that the number of layer is probably the same. However, the intensity of the D- band peak was found to increase with the number of transferred graphene layers which points to the fact that defects are induced more easily in multilayer graphene films (**Figure 16(d)**). The relative peaks intensity of the D-band to the G-band (I_D/I_G) is a measure of the relative degree of disorder in graphene and also the grain size [59]. A higher value denotes more defective film compared to a lower value. In other words, lower value (or zero) is desirable.

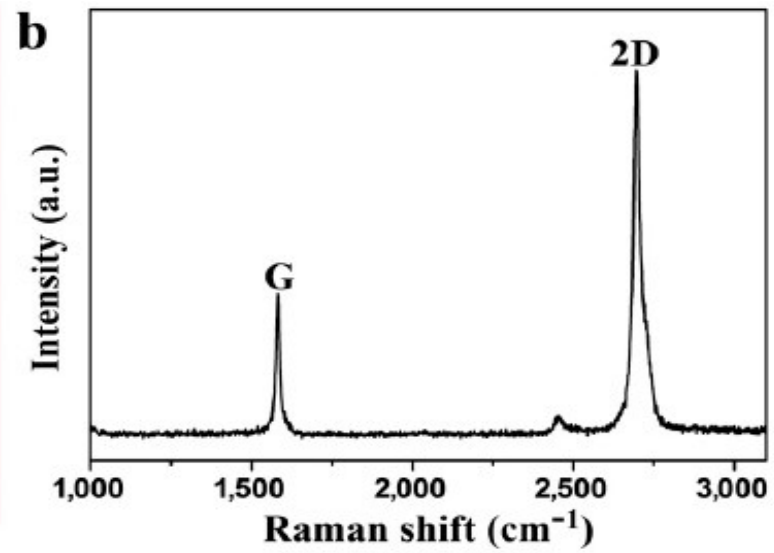

Figure 15: Raman characterizations of HGFs transferred onto 300 nm SiO_2/Si substrate [50]

Recently, attention has been shifted to studying the influence of the substrate orientation on the quality and thickness of LPCVD graphene [55]. It is shown that I_{2D}/I_G ratio is perfectly correlated with crystallographic orientations of the Cu substrate. Given the Raman map showing in **Figure 17** single-layer graphene preferentially forms on

Cu{103}, Cu{111} and some planes slightly aligned to Cu{535} and Cu{335}. Similarly, bilayer graphene forms on Cu{001} indicating that single and multilayer graphene form on Cu{111} and Cu{001}, respectively. Graphene domains spanning across Cu{535} and Cu{001} show both single and bilayer spectra, dictated by the underlying Cu grain. From these results, it is concluded that the crystallographic orientation of the Cu substrate therefore strongly influences the type of LPCVD graphene that forms [55]. This orientation dependent thickness variation is believed to be due to the differences in the interaction between the domains and the substrate surface.

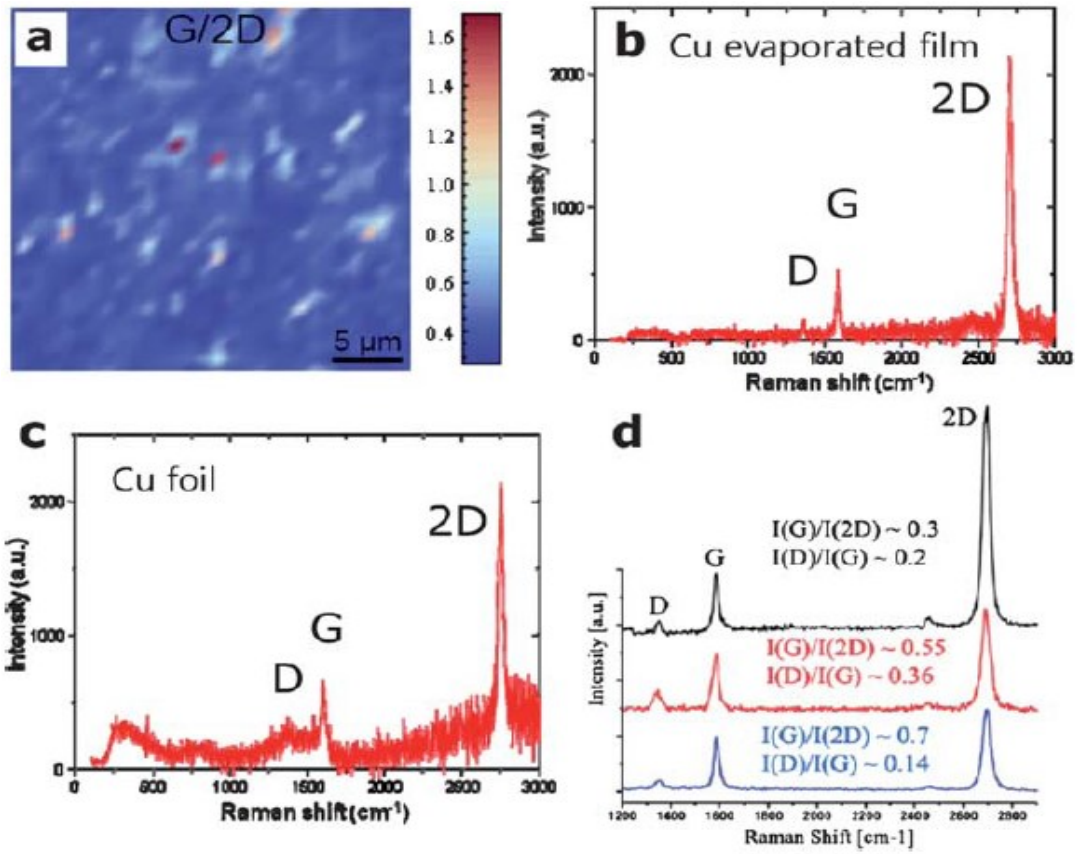

Figure 16: Raman map of a single layer graphene grown on bulk Cu substrate and transferred onto an insulating substrate [63]

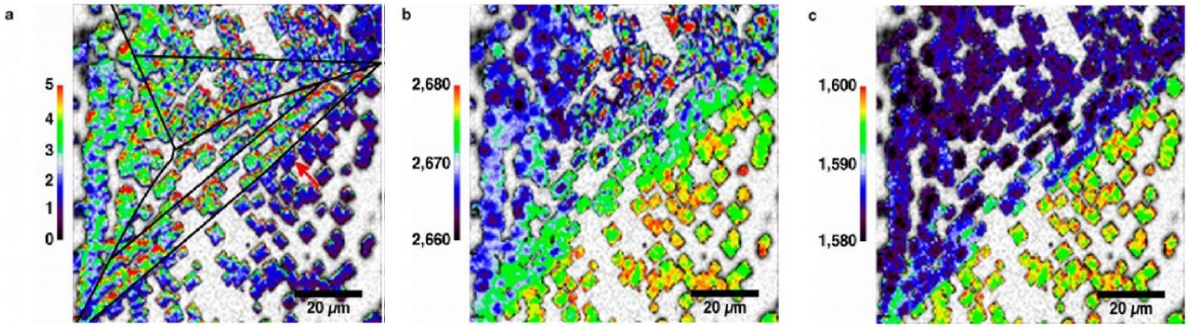

Figure 17: Raman Spectroscopy maps (90x90μm2). (a)I_{2D}/I_G map, (b) 2D peak position map and (c) G peak position map[55]

Yu, et al. [56] also had used Raman spectroscopy and mapping for studying a single graphene grain, and two coalesced graphene grains as shown in **Figure 18**, respectively. They found that, almost I_{2D} values are more than twice that of I_G, confirming single layer graphene samples. Furthermore, almost I_D intensity values throughout the investigated areas are very small (indicating a low defect content) except, notable few isolated spots of relatively high I_D located mostly at the grain centers, edges and grain boundaries. They indicated later, these high defect regions are responsible to cause weak localization and impede electrical transport capability of synthesized graphene.

Raman mapping was also exploited by Li, et al. [7] to investigate monolayer, bilayer and multilayer graphene coverage percentages on the copper substrate surface. Their LPCVD graphene synthesis regime gave approximately 95% monolayer graphene coverage, while only small fraction of bilayer and few-layer (<5%) were found on the copper surface, as can be observed from **Figure 19**. The growth parameters were as follows; H2: 2 sccm, 40 mTorr (before reaction) and CH4: 35 sccm, 500 mTorr (during reaction and cooling periods), and growth time was in the range from 10 to 60 minutes.

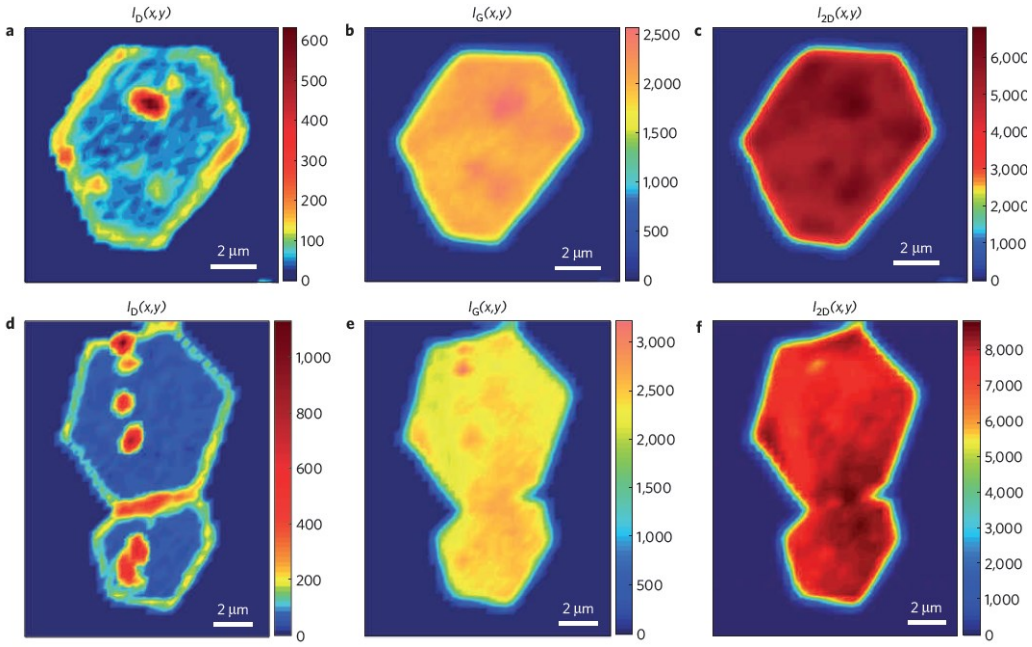

Figure 18: Spectroscopic Raman mapping of graphene grains and grain boundaries. (a–c) Intensity maps of the D, G and 2D bands, respectively, for a two coalesced graphene grains with a single grain boundary [56]

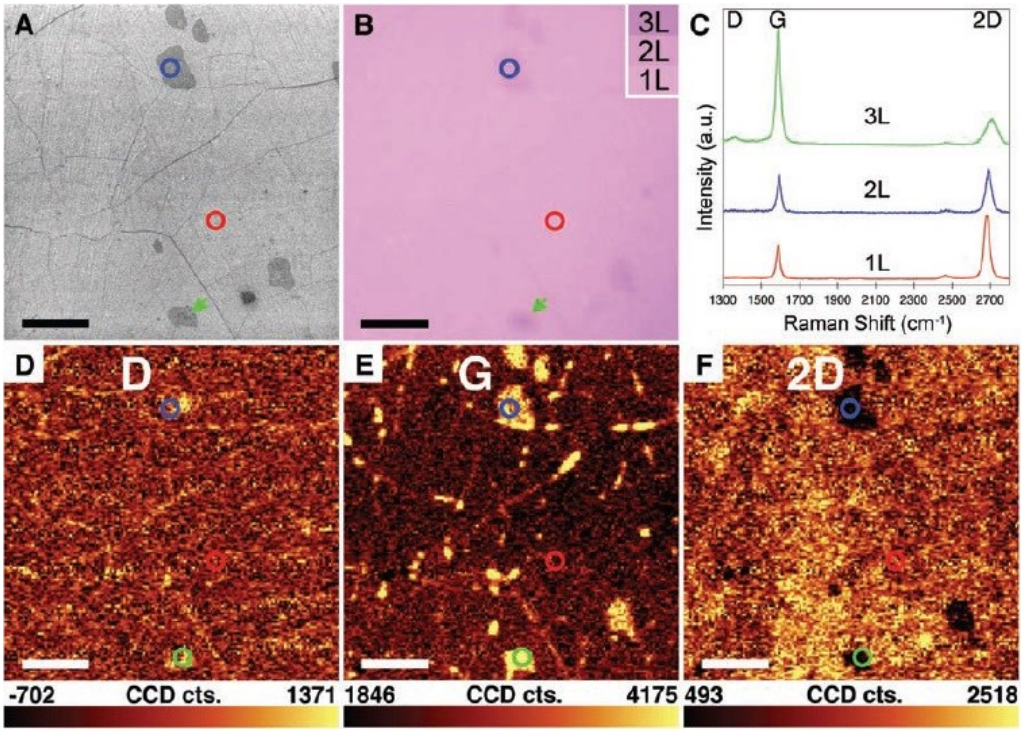

Figure 19: (a) SEM image of graphene transferred on SiO_2/Si (b) Optical microscope image of the same regions as in (a). (c) Raman spectra from the marked spots ,(d to f) Raman maps of the D , G and 2D bands [7]

CHAPTER 3

EXPERIMENTAL WORK

This chapter is devoted to explain all the experimental methods and techniques that conducted during graphene synthesis, transfer and characterization

3.1 Pre-cleaning of Cu substrate

Cu substrates were first cleaned before graphene deposition in order to remove surface contaminations and hence ensure growing good quality graphene. In the present work graphene was grown on two different Cu substrates. The first one was 25 μm thick, 99.8% purity from Alfa Aesar (Product No.13382). The second one was 35 μm thick, 99.9% purity purchased from Nippon Mining & metals–Japan. These Cu substrates were cut into 2 cm x 2 cm pieces and then cleaned by dipping into acetic acid for 5 minutes followed by ethanol (5 min) and de-ionized (DI) water bath (5 min). Then they were dried by pressurized nitrogen gas. After drying, these substrates were slightly pressed between two clean glass slides to keep them flat

3.2 CVD process

CVD systems can be classified into the following categories; (1) Atmospheric Pressure Chemical Vapor Deposition (APCVD), (2) Low Pressure Chemical Vapor Deposition (LPCVD), Plasma Assisted Chemical Vapor Deposition (PACVD) or Plasma Enhanced Chemical Vapor Deposition (PECVD). APCVD is one of the common techniques used to synthesize graphene, because it is simple, needs short time to produce full coverage of

graphene on Cu substrate. On the other hand, it needs very delicate control over the gas flow rate, growth temperature and time, as it involves high amounts of gases at elevated temperature. CVD is a chemical process in which the precursor is fed into the chamber at high temperature in presence of the catalyst/substrate leading to deposition of the desired film. As a result of this reaction some volatile by products can occur but they are removed from the chamber by the carrier gases. During that reaction the atmosphere inside the tube should be kept inert in order to avoid any reactions that can occur between oxygen and the reaction gases.

In the present work, all graphene films were grown in FirstNano-CVD reactor with 3'' diameter quartz tube using the growth conditions as summarized in **Table** 1**.** The geometry of this quartz tube and the other CVD components are y shown in **Figure 20.** After cleaning the Cu substrate, it was inserted into the CVD reactor and heated from room temperature to 1000 ^{o}C in the presence of argon (Ar) and hydrogen (H_2) gas mixture with a total flow rate of 1500 sccm. The ratio H_2: Ar = 37:1463 (sccm) was kept constant during heating and cooling steps for all prepared samples. After heating to 1000^{o}C, the Cu substrates were annealed for 30min at different H_2 concentration (0, 2.5, 20 and 50%) in the total gas mixture. Annealing step is very important to improve the Cu surface characteristics by reducing surface oxides, volatile impurities and surface contaminations [10, 11]. Moreover, annealing increases the Cu grains size and hence reducing the overall density of grain boundaries, resulting in lower density of multilayer graphene domains on Cu grain boundaries. After annealing, graphene growth step starts by introducing CH_4 (5 sccm) into the quartz tube at high temperature (1000°C) and in presence of the Cu substrate. Due to the surface reaction between the CH_4 gas and the Cu substrate, CH_4 will be decomposed

into C and H_2 species, these C atoms will be utilized for graphene nucleation and growth. The flow rate of H_2, Ar and CH_4 gases are controlled by means of mass-flow controllers. The whole CVD cycle including heating, annealing, growth and cooling stages is shown in **Figure 21.**

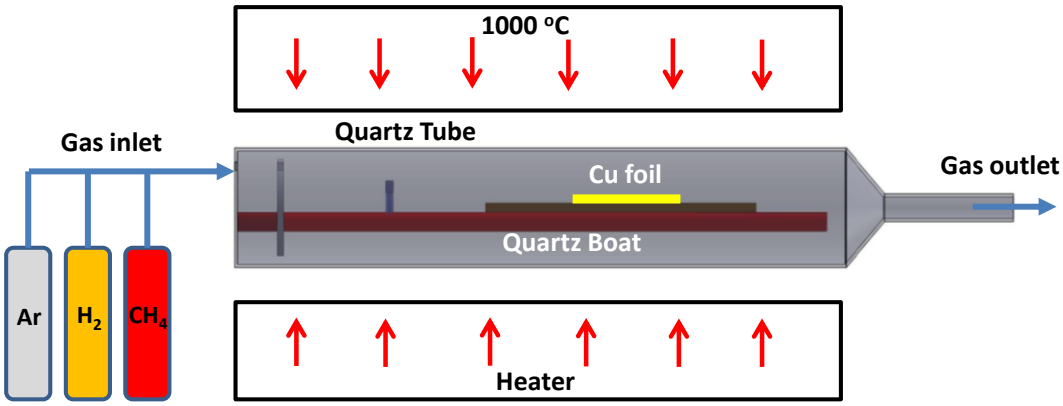

Figure 20: Schematic diagram of the CVD process for growing graphene on Cu substrate

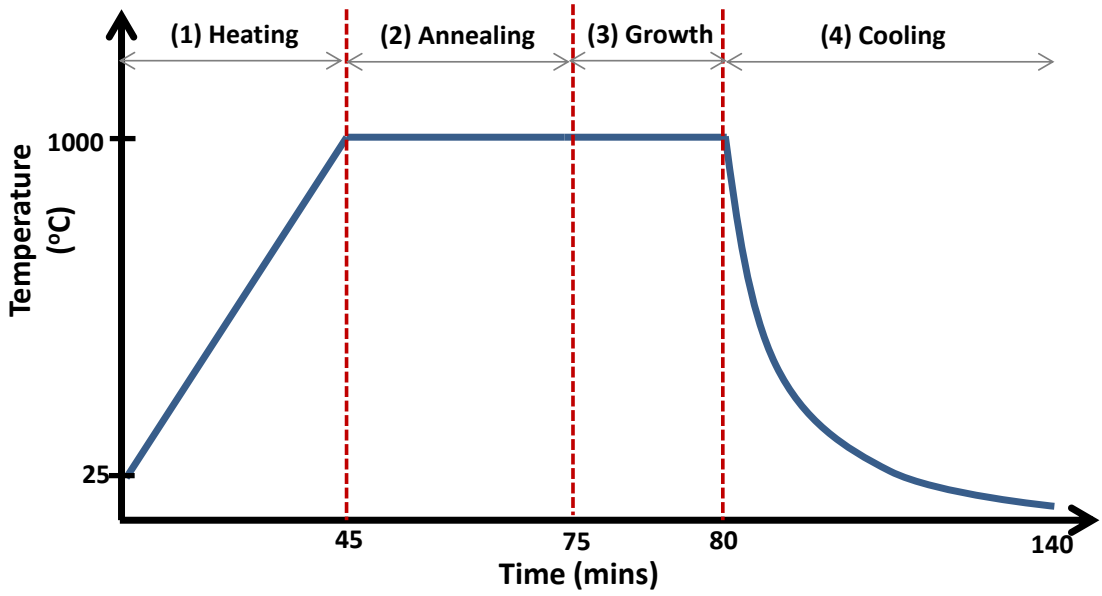

Figure 21: CVD-graphene growth cycle

Table 1: Graphene growth recipe by APCVD

Step Number	Process	Temperature (C^o)	Gases flow rate (sccm)			Duration (min.)
			Ar (sccm)	H_2 (sccm)	CH_4 (sccm)	
1	Heating	25- 1000	1450	50	0	45
2	Annealing	1000	**x**	**y**	0	30
3	Growth	1000	1460	36	5	5
4	Cooling	1000-25	1500	36	0	50

3.3 Graphene transfer

After graphene growth, it is usually transferred onto other insulating substrate in order to be either characterized (e.g. by OM, Raman and AFM) or to be used to fabricate other devices. Graphene transfer consists of the following steps as shown in **Figure 22**: (1) Graphene is coated by PMMA using spin coater (2500 rpm for 1 min); in order to support and protect the graphene film during mechanical handling. (2) Then the backside graphene is removed by floating PMMA/graphene/Cu on APS bath for 7 min, followed by rinsing in DI water for 5 min. (3) Cu substrate that hold PMMA/Graphene membrane is etched by APS for 2h, followed by rinsing the remaining PMMA/Graphene stack in 3 D.I water baths, 10 min for each. (4) PMMA/Graphene membrane is transferred onto 300 nm SiO_2/Si substrate and then it is dried on hot plate for 15 min at 90^{o}C. During this step care should be taken to avoid leaving any residual water between PMMA/Graphene and underlying SiO_2/Si substrate in order to improve the adhesion between them (5) PMMA is dissolved in hot acetone bath followed by isopropanol, 5 min for each at 65^{o}C. Finally,

the stack was placed in DI water bath for 10 min to remove any organic residuals followed by drying with Nitrogen.

3.4 Graphene Characterization

After growing graphene using APCVD, it is crucial to characterize its characteristics in terms of thickness uniformity and quality in order to correlate them to the CVD growth parameters. As a result, we can optimize efficiently graphene growth process using CVD. There are a lot of characterization tools mentioned in literature including scanning electron microscopy (SEM), optical microscopy (OM), Raman spectroscopy, atomic force microscopy (AFM) and transmission electron microscopy (TEM).

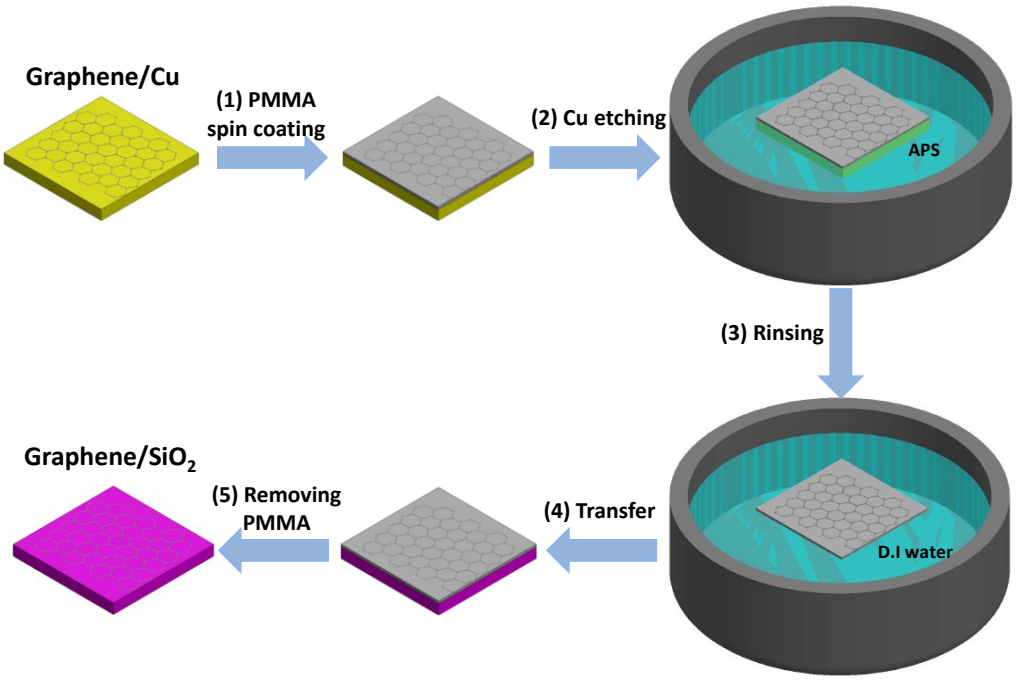

Figure 22: Graphene transfer process

3.4.1 Scanning Electron Microscopy (SEM)

Scanning electron microscopy (SEM) is used extensively to characterize the as-grown graphene films on Cu substrates. It gives very important information regarding the morphology, size and distribution of graphene domains. Besides, it assists in characterizing the evolution of Cu surface morphology as affected by annealing and graphene growth stages. SEM micrographs of graphene on Cu substrates not only can help in estimating the number of layer, morphology and distribution of graphene areas, but also it can assist correlating the obtained graphene characteristics to other features of Cu surface morphology like, surface steps, terraces, striations (rolling lines), grain boundaries and reconstructed surface particles. This provides better insight into the relationship between CVD parameters and the obtained graphene characteristics.

In this work we utilized field emission scanning electron microscopy (FE-SEM) manufactured by (TSCAN-MIRA 3 LMP). The incident electron beam was accelerated by low voltage (1.5-5 kv). Both of secondary electrons (SE=85%) and backscattered electrons (BSE=15%) were collected to form the final micrograph of graphene on Cu sample in order to capture both of the Cu surface topographical changes along with the grown graphene morphology.

3.4.2 X-Ray Diffraction (XRD)

X-ray diffraction (XRD) is an efficient technique utilized for phase identification of a crystalline material and can provide information on unit cell dimensions, crystallographic orientation and crystallite size. In this work XRD technique (Bruker, AXSD-8) was utilized to find out the crystallographic orientation of Cu substrate before and after

graphene growth so that we could understand the impact of these graphene layers on both of the Cu crystallographic orientation and its crystallite size. All Cu substrates were characterized by XRD within a range of diffraction angles from 20 to 120^{o}, with angular interval equal to 0.02.

3.4.3 Optical Microscopy (OM)

Optical microscopy (Lumenera's INFINITY1) is used during the present work basically to characterize transferred graphene films onto SiO_2/Si wafers. It gives useful information regarding the graphene film continuity and uniformity.

3.4.4 Raman Spectroscopy

Raman spectroscopy is a technique employed to observe vibrational, rotational, and other low-frequency modes in a system. It has a wide range of applications in chemistry as it provides an easy way to identify various types of molecules. Raman spectroscopy is very common technique for graphene characterization. In this technique a laser light interacts with the graphene film, consequently its energy is shifted up or down, according to the graphene characteristics in terms of number of layers and quality. Raman spectrum of any carbon allotropes contains basically three characteristics bands; from these bands we can identify the number of layers and quality of deposited graphene. The main advantages of Raman spectroscopy are that it is very simple, nondestructive and providing accurate results. In present work, Raman spectroscopy (HORIBA) is used to characterize as-grown graphene over Cu-substrates and as-transferred graphene on 300 nm SiO_2/Si wafers.

3.4.5 Atomic Force Microscopy (AFM)

Atomic force microscopy (AFM) provides high-resolution images on the order of fractions of a nanometer. The general principle of AFM operation is depicted in **Figure 23.** The relative motion between the tip and sample surface is recorded by the means of laser beam, detector and feedback electronics. AFM operation is usually described as one of three modes, according to the nature of the tip motion: contact mode, tapping mode and non-contact mode.

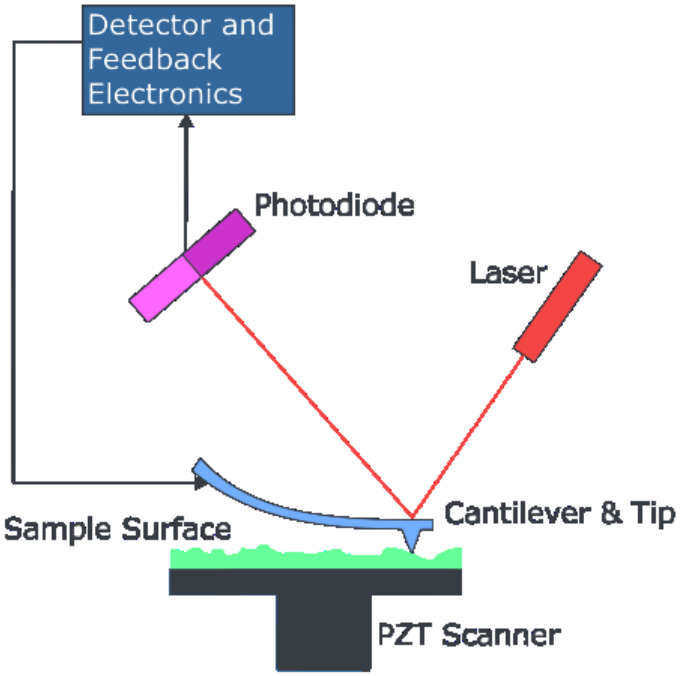

Figure 23: Schematic diagram of AFM instrument [64].

In this work we manipulated AFM (Dimension Icon- Bruker) to characterize the Cu surface morphology evolution as influenced by annealing and graphene growth. This is accomplished by using *Scanasyst* mode (combining contact and tapping modes). Some AFM images of measured Cu surfaces were post-processed by Gaussian filtration approach in order to isolate the fine features from the coarse ones to get better

understanding about these delicate structures as a function of H_2 content during annealing step. Separation of waviness component from the primary measured profile was necessary to obtain representative information regarding short-range wavelength irregularities of the Cu foil. In addition AFM was utilized to characterize as-transferred graphene films onto SiO_2/Si wafers in order to check its morphology, uniformity, thickness and continuity.

3.4.6 Transmission Electron Microscopy (TEM)

Transmission electron microscopy (TEM) manufactured by (JEOL, 200 KV) was utilized for obtaining high magnification images of the transferred graphene films to study the impact of Cu substrate on graphene growth and transfer onto other insulating substrates. In addition energy dispersive spectroscopy (EDS) in TEM was performed to identify the nature of the some observed particles originating from different Cu substrates. Furthermore, selected area electron diffraction (SAED) patterns were implemented to check crystalline structure of obtained graphene samples. Finally, TEM was used to resolve the lattice planes of graphene and identify the number of layers at the folding edges.

CHAPTER 4

RESULTS AND DISCUSSION

4.1 Effect of hydrogen on Cu surface during annealing stage

Extensive work has been done by previous researchers in studying the role of H_2 during different CVD steps in controlling the nucleation and growth of deposited graphene. Wang et al. [16] reported that prolonged annealing of Cu substrate in presence of H_2 was beneficial for deposition of single layer, large-area graphene because Cu surface became smoother and consequently exhibited less nucleation sites. Gan et al. [17] explained that although H_2 was able to reduce Cu surface roughness during annealing step but it promoted the formation of nanoparticles which played a crucial role in the nucleation and growth of graphene domains.

In contrast, Shin and Kong [19] mentioned that H_2 induced a roughening effect on Cu surface due to the formation of voids and hillocks, resulting in high density of active sites and hence formation of multilayer graphene domains. Jung et al. [20]showed that increasing H_2 (from 0 to 6.25 % of the total Ar and H_2 gas mixture) during annealing produced dense graphene domains, indicating a high nucleation density. Yang et al. [18] reported that annealing Cu under H_2 atmosphere increased the nucleation density and consequently promoted multilayer graphene domains located mostly along the rolling lines. Also, they mentioned that H_2 annealing promoted the high density of unsaturated Cu atoms on dense ledge areas.

On the basis of above studies, it was realized that the detailed mechanism of CVD process including the role of H_2 on Cu surface during annealing (whether it has smoothening or roughening effect) and on graphene characteristics is unclear yet. It is thus important to perform a systematic study to understand and underpin the influence of H_2 on Cu surface morphology evolution during annealing stage and investigate its effect on the quality and morphology of deposited graphene. In this regard, the following experimental approach was adopted: first, a set of commercially available Cu foils purchased from Alfa Asear (AA-Cu) were annealed only at 1000^{o}C for 30 min using different H_2 concentrations; 0, 2.5, 20 and 50% of the total gas mixture consisting of Ar and H_2 with a total flow rate of 1500 sccm. Second, another set of similar AA-Cu substrates were annealed again using the same conditions mentioned above, followed by growing graphene by introduction of 5 sccm of CH_4 to the gas mixture (Ar: H_2= 1458: 37 sccm) for a short period of 30 s to observe the graphene growth at early stages. This approach enabled us to investigate the: (1) role of H_2 on Cu surface during annealing, (2) impact of H_2-annealed Cu foil on graphene formation, and (3) impact of graphene growth on Cu surface morphology.

Considering the importance of the Cu substrate characteristics in graphene synthesis, the surface morphology and roughness of as-received AA-Cu substrate was evaluated using optical microscope (OM), scanning electron microscope (SEM) and atomic force microscope (AFM). **Figure 24** shows the surface morphology of as-received AA-Cu, it is

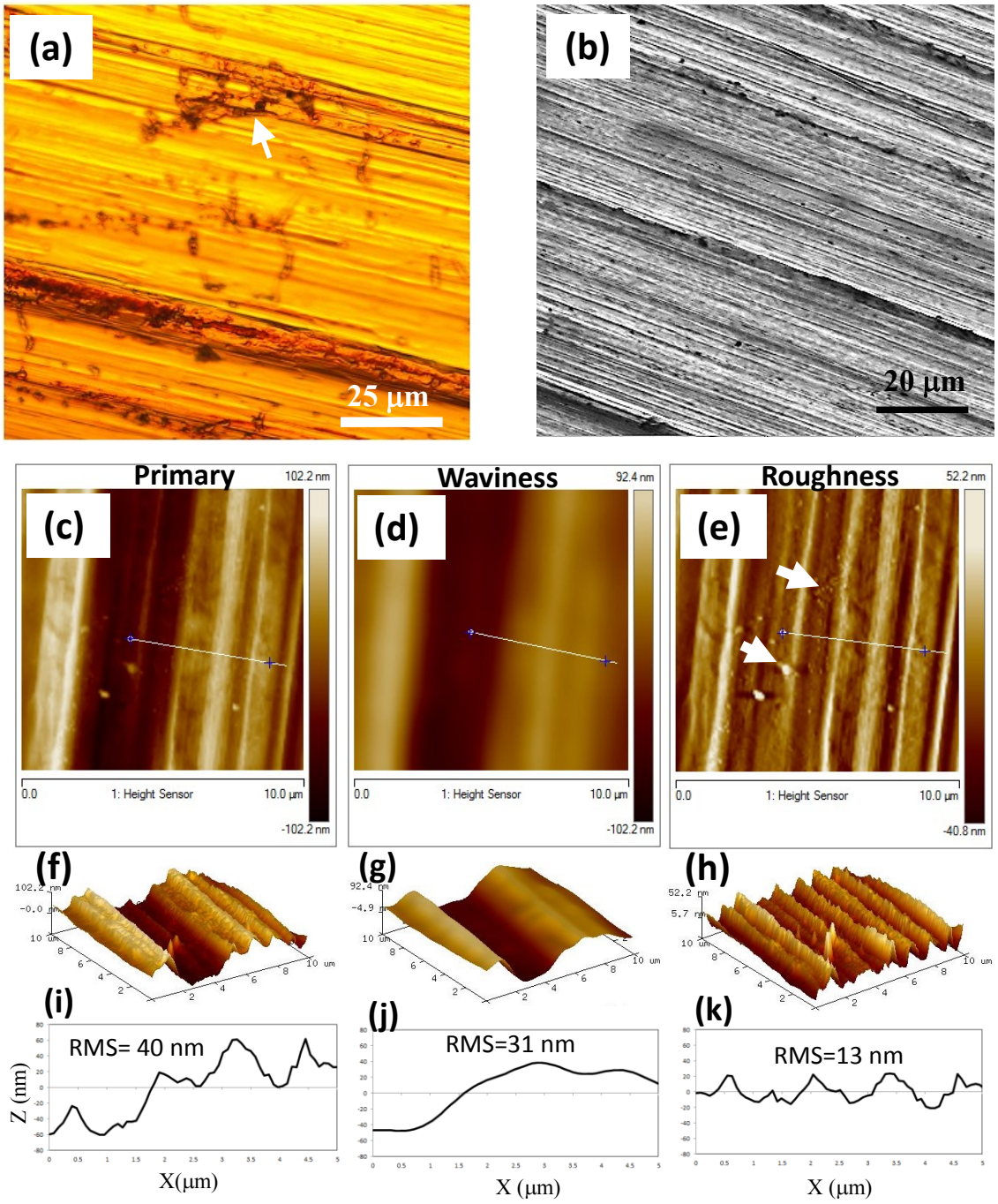

Figure 24: Surface morphology characteristics of as-received AA-Cu foil. (a, b) OM and SEM images of as-received Cu surface morphology, (c, d, e) 2D AFM images of primary , waviness and roughness surface profiles respectively (f, g, h) corresponding 3D AFM images, (i, j, k) surface height profiles corresponding to the locations indicated by the scan lines shown in (c, d, e), the length of scan line was 5 µm in each case

dominated by striation lines that are characteristic of the rolling process during Cu foils manufacturing. In addition to these rolling features, there were also some surface pits, tears and impurity particles (**Figure 24(a),(b)**). Cu surface texture can be considered as a combination of waviness (long-range irregularities) and roughness (short-range irregularities) components as indicated in **Figure 24 (c-e)**. Waviness component must be filtered out of primary surface to obtain roughness only; consequently, it provides a more representative and accurate estimate of computed surface roughness parameters. Root mean square (RMS) roughness parameter was utilized to evaluate the roughness degree of as-received AA-Cu surface. **Figure 24(i-k)** shows the line profiles of primary, waviness and roughness features corresponding to the locations indicated by scanning lines shown in 3D AFM images (**Figure 24(c-e)**) along with their computed RMS values (40, 31, and 13 nm respectively). It is obvious that waviness comprises about 78 % of primary profile, and the remaining 22 % is the roughness contribution, which suggests that primary surface profile is dominated mainly by waviness component.

To elucidate the role of hydrogen concentration on the evolution of Cu surface morphology during the annealing step, AA-Cu foils were systematically pre-heated and annealed in the CVD system under different H_2 concentrations (0, 2.5, 20 and 50 % of the total gas flow rate, including H_2 and Ar) at a fixed temperature (1000^oC) and time (30 min). Other parameters were kept fixed during pre-heating and cooling steps for all runs (see **Table 2**).

Evolution of surface morphology and roughness of these annealed samples was examined by SEM and AFM as shown in **Figure 25** and **Figure 26** respectively. It is clear that

Table 2: CVD parameters to study the effect of H_2 concentration on Cu surface morphology evolution during annealing stage

Exp. No.	H_2%	Heating (H_2:Ar) sccm	Annealing			Cooling			
			Ar (sccm)	H_2 (sccm)	Time (min)	Ar (sccm)	H_2 (sccm)	CH_4 (sccm)	Cooling rate (^oC/min)
1	0	50:1450	1500	0	30	1500	30	0	20
2	2.5	50:1450	1462	38	30	1500	30	0	20
3	20	50:1450	1200	300	30	1500	30	0	20
4	50	50:1450	750	750	30	1500	30	0	20

excluding H_2 during annealing stage yielded relatively rough Cu surface consisting of narrow-spaced steps, high density of surface particles (with average size around 170 nm) grown preferentially along Cu surface striation lines, around surface-hillocks and grain boundaries (**Figure 25 (a,e)**). Wang et al [65] indicated that presence of oxygen impurities in Cu-foil led to formations of step-like structure as a result of Cu reconstruction.

After introducing H_2 in the range from 2.5 to 50%, it is seen that Cu surface became smoother and flatter due to a reduction effect of rolling lines, associated with recrystallization of larger grains (**Figure 25 (b-d)**). However, it also promoted formation of other Cu surface features like; dents, facets, and Cu nanoparticles (average size is around 250 nm) as shown in **Figure 25 (f-h)**. Our results are consistent with earlier reports indicating that preheating and annealing of Cu in presence of H_2 not only reduces surface irregularities (e.g. surface bumps and striation marks) [15] [17], but also it promotes formation of Cu particles with increased density as H_2 concentration was increased, due to H_2-induced etching effect [17]. This 'etching' effect refers to the

reduction of Cu oxide particles, formed during pre-heating stage of Cu foil, into Cu metal particles after the introduction of H_2 during Cu annealing.

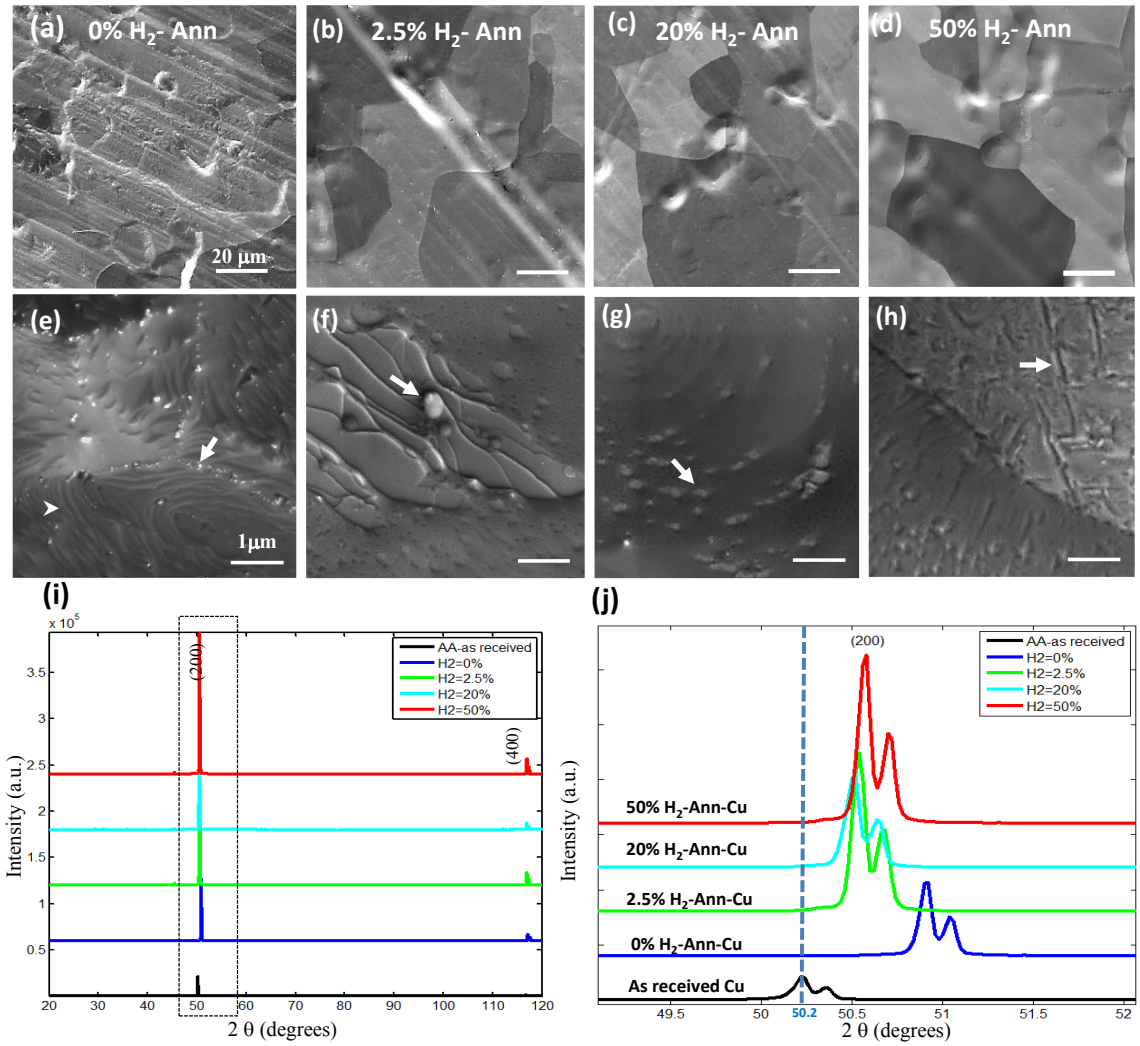

Figure 25: Effect of H_2 during annealing stage on evolution of Cu surface morphology.(a-d) SEM micrographs of Cu annealed at different H_2 concentration corresponding to 0, 2.5, 20 and 50% respectively, (e-h) high magnification images of Cu foils shown in (a-d), (i) XRD spectra of as-received and annealed Cu foils, (j) zoomed–in plot of Cu(200) reflections shown in (i). Scale bars corresponding to 20 µm for (a-d) and 1 µm for (e-h)

The actual mechanism for the formation of the surface defects observed particularly at 50% H_2 (**Figure 25(h)**) in our work is not clear at the moment. However, during annealing at 1000°C in the presence of H_2 content, it is reported that a high amount of H_2 diffuses into Cu (e.g. diffusion coefficient of H_2 in Cu at 1000°C is 3.3×10^{-4} cm^2/s) [67],

thus during annealing stage (30 min) Cu foil became saturated with H_2 . At subsequent CVD stages during growth and cooling to room temperature, H_2 diffuses out of Cu (degassing) [47], which we believe will induce a restructuring of Cu surface, including the formation of surface defects.

RMS roughness values of Cu foils before and after annealing stage reveal that Cu surface became considerably smoother after being heat-treated under different H_2 concentrations. RMS roughness of as received Cu was 13 nm (**Figure 24(k)**), however after annealing all Cu samples give RMS values in the range from1 to 4 nm (**Figure 26 (i-l)**, while it is observed that Ar-annealed sample exhibited the highest RMS roughness value about 4 nm. This indicates that H_2 annealing promoted smoother and flatter Cu surface if compared to that obtained by Ar (0% H_2) annealing.

In order to evaluate the crystallinity changes of Cu foil, XRD patterns were measured for each annealed Cu foil under different H_2 concentrations and compared to the corresponding XRD reflections of as-received Cu as shown in **Figure 25(i),(j)**. It is observed that Cu samples were still dominated by Cu (100) crystals after being annealed at different H_2 concentrations associated with increased peak intensity and peak shift towards higher diffraction angles. The increase of peak intensity indicates that annealing process enhanced Cu crystallinity (as confirmed by increased crystallite size as shown in **Table 3**). In addition the peak shift towards higher diffraction angles indicates that the lattice parameter is decreased, however it is obvious that H_2-annealing exhibited larger lattice parameter compared to Ar-annealed one. It is clear from **Table 3** that 50% H_2

promoted the largest crystallite size (138 nm), associated with increased lattice size compared to that obtained after Ar-annealed sample.

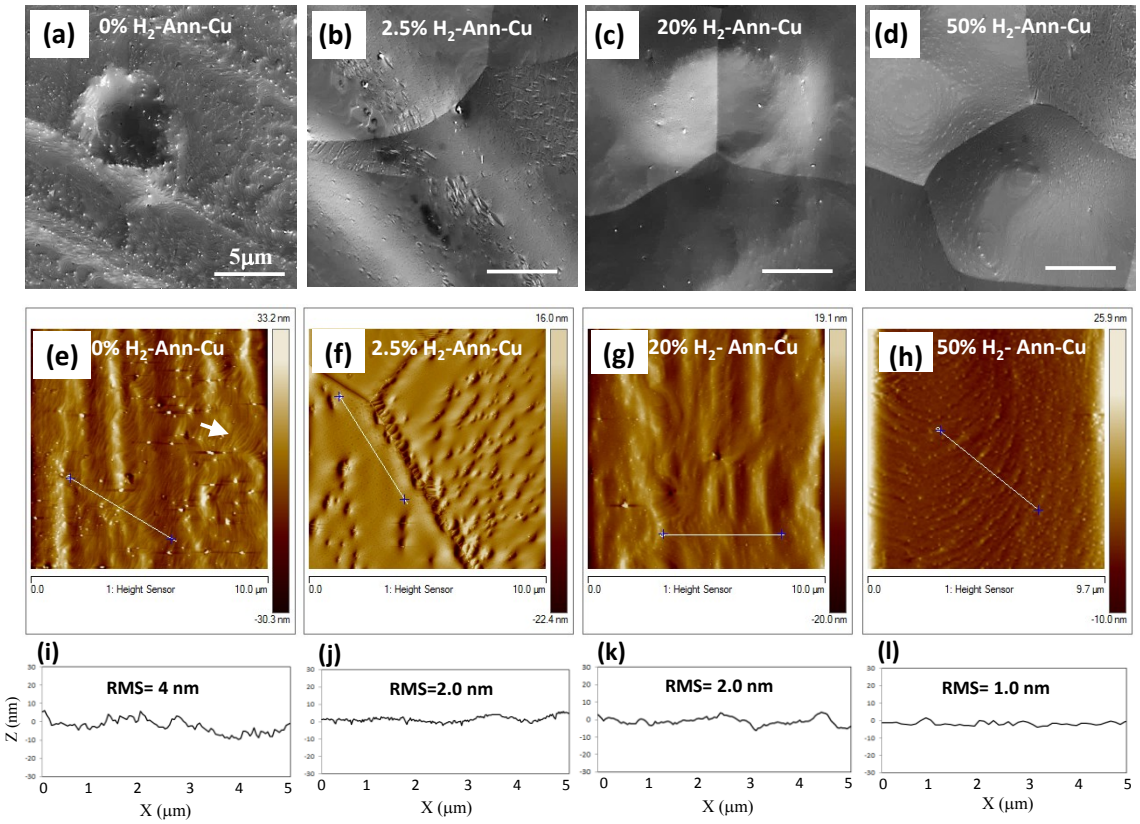

Figure 26: Effect of H_2 on Cu surface evolution after annealing only. (a-d) SEM micrographs of Ann-Cu samples at different H_2 concentrations corresponding to 0, 2.5, 20 and 50% respectively (e-h) 2D AFM images of Cu surfaces shown in (a-d), (i-l) cross-sectional surface profiles at locations indicated by the scan lines

Table 3 Crystallite size calculations of annealed Cu samples as a function of H_2 concentrations

Cu(200)	As-received Cu (200)	H_2 concentrations during annealing			
		0%	2.5%	20%	50%
Position	50.2265	50.9075	50.5371	50.5059	50.5693
FWHM	0.08643	0.06819	0.07162	0.08115	0.06649
Crystallite size (nm)	106	135	128	113	138

4.2 Effect of hydrogen during Cu annealing on nucleation and growth of graphene

To elucidate the role of hydrogen concentration on the as-grown graphene on Cu substrates, another set of Cu-foils were annealed under the same conditions mentioned in previous section. Afterwards, graphene was grown for a short time (30s) in order to investigate the graphene nucleation and growth at early stage. All CVD parameters for these set of samples are shown in **Table 4. Figure 27 (a-d)** show SEM micrographs of as-grown graphene on Cu foils corresponding to different H_2 concentrations. At 0 and 2.5 % H_2, individual graphene domains with different size and shape, grown over another continuous single graphene layer as reported elsewhere [16][18][68]. These graphene domains were preferentially nucleated on the step edges while less on the flat terraces (**Figure 27 (a)**), suggesting that Cu-step acted as lower energy barrier for graphene [69].

Increasing H_2 concentrations to 20% of total gas mixture resulted in formation of small size, high density multilayer graphene domains, preferentially nucleated along the surface striation lines and/or Cu grain boundaries (**Figure 27 (c**), **Figure 28(c)**). At 50% H_2 concentration, these multilayer domains were increased in size and density as shown in **Figure 27 (d**), **Figure 28(d).** These results are consistent with previous reports which indicates that graphene selectively grow along the striation features of Cu surface[18].

To have better insight into the grown graphene characteristics, all graphene films were transferred onto SiO_2/Si substrates as shown in **Figure 28(a-d)**. It was clear that excluding H_2 during annealing step resulted in discontinuous graphene film associated with high amount of surface residuals (mostly Cu oxides).

Table 4: CVD-graphene growth parameters to study the effect of H_2 concentration (during annealing stage) on Cu surface morphology evolution and deposited graphene properties

Exp. No.	H_2%	Heating (H_2:Ar) sccm	Annealing			Graphene Growth			
			Ar (sccm)	H_2 (sccm)	Time (min)	Ar (sccm)	H_2 (sccm)	CH_4 (sccm)	Time (sec)
1	0	50:1450	1500	0	30	1464	36	5	30
2	2.5		1462	38	30				
3	20		1200	300	30				
4	50		750	750	30				

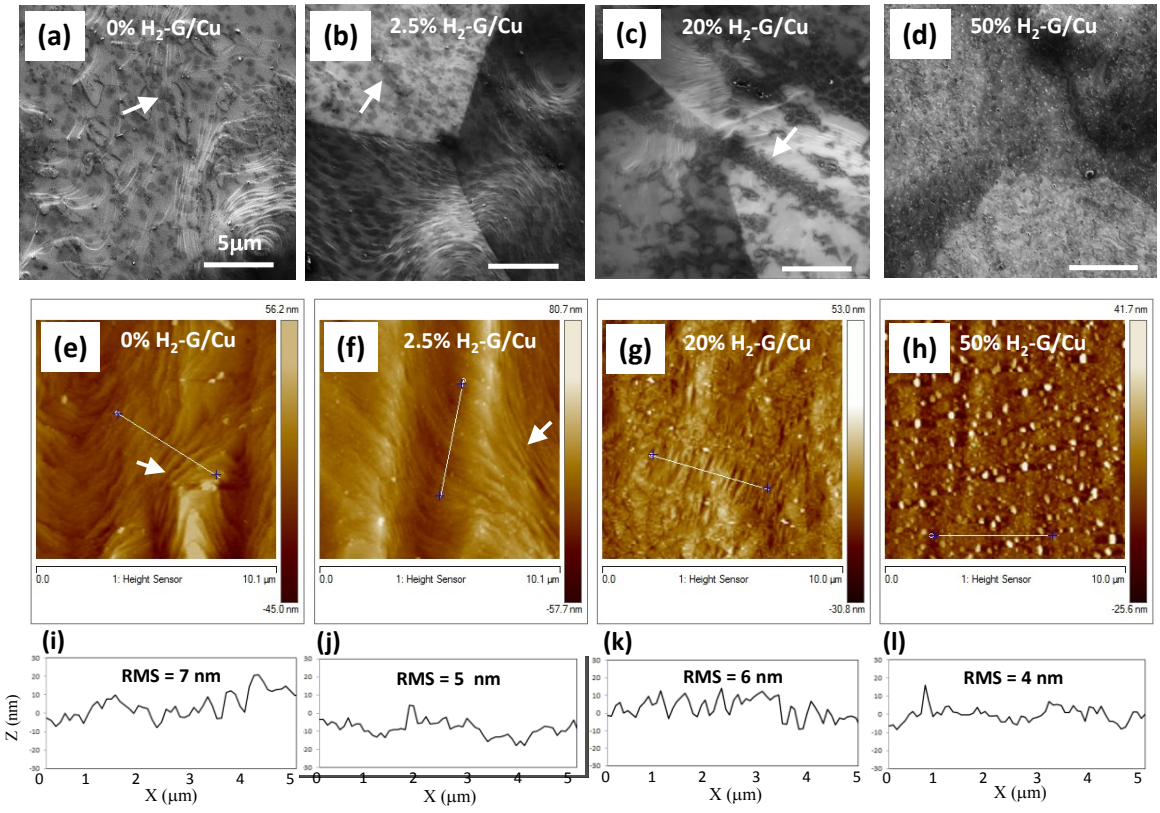

Figure 27: (a-d) SEM micrographs of graphene/Cu that pre-annealed at different H2 concentrations (0 to 50%). Some graphene domains are indicated by white arrows in a, b, and a particle with white arrowhead in (c)

On the other hand, graphene grown at H_2 (2.5%) was more continuous and cleaner associated with presence of relatively small darker domains along surface striations and grain boundaries (mostly bilayer domains) as shown in **Figure 28(b)**. At higher H_2 concentrations corresponding to 20 and 50 % however, multilayer, very small, graphene domains were grown on Cu surface striations and/or grain boundaries, with increased number and size at H_2 content of 50% (**Figure 28(c),(d)**). These results demonstrated that H_2 played crucial role in determining the final properties of grown graphene films in terms of continuity, uniformity, number of layers, and quality.

Quality of transferred graphene films onto SiO_2/Si substrates were further studied using Raman spectroscopy as shown in **Figure 28(e),(f)**. It is seen that all spectra display common bands of graphitic material, e.g. D, G and 2D. At low H_2 (0 and 2.5%) during annealing stage, bilayer graphene films were produced as confirmed by the I_{2D}/I_G ratios (~1.5), where I_{2D} and I_G are the intensities in arbitrary units for 2D and G bands respectively. Raman spectra of these graphene films show rather low I_D/I_G ratios (0.2 and 0.4 corresponding to 0 and 2.5% H_2 respectively); indicating that excluding H_2 during annealing step is beneficial for producing better quality graphene. It is worth noting that D-band originates due to existence of certain factors which can produce defects in a crystal such as; lattice distortion at graphene domain edges [23][70], surface contamination, amorphous carbon [58] and multilayer domains [12] [71] [72]. On the other hand, multilayer graphene films were grown when higher H2 (20 and 50%) were used during the annealing process, as judged by I_{2D}/I_G ratios (~0.7). In addition, relatively higher I_D/I_G ratios (~0.6-0.8) were observed, indicating a highly defective graphene films.

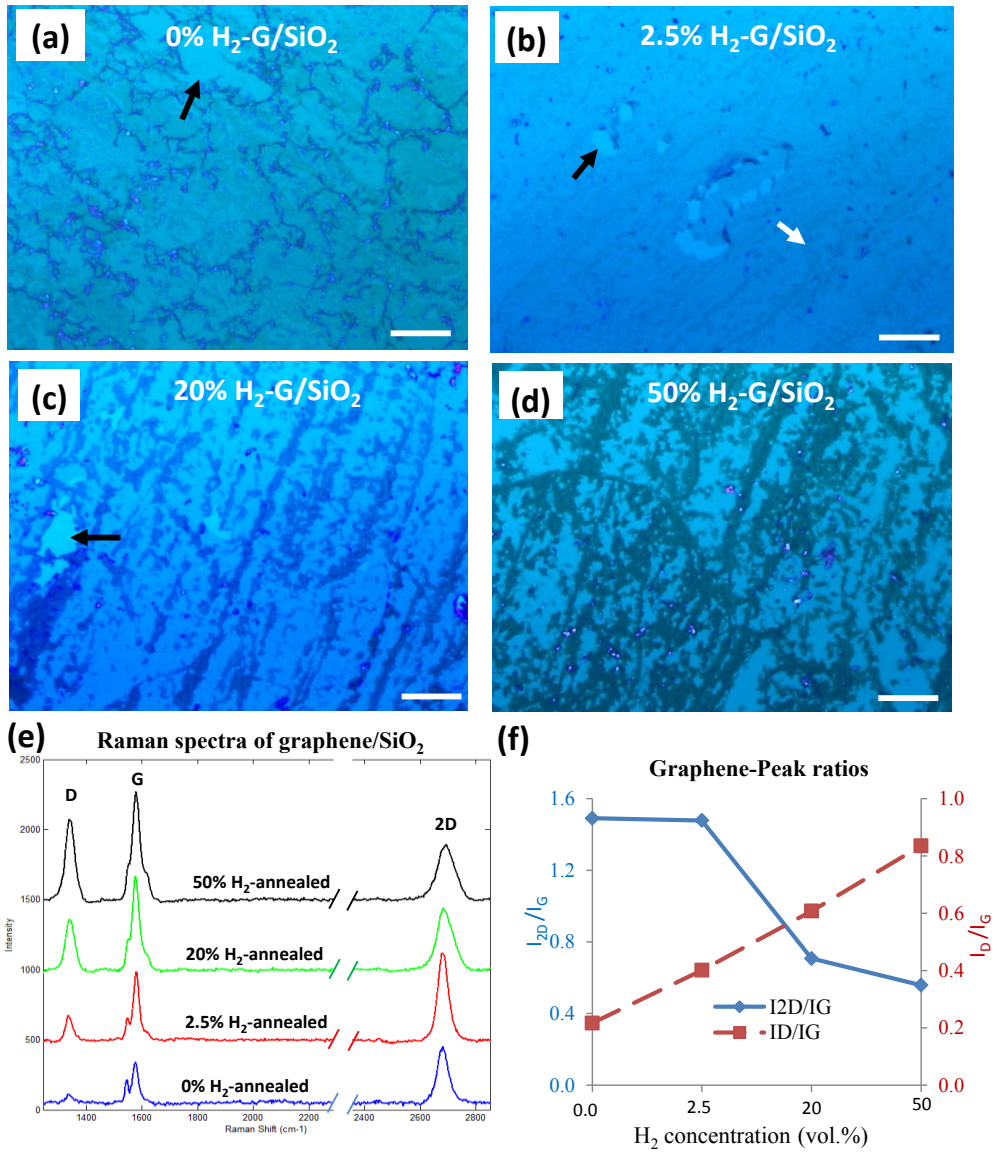

Figure 28: OM images and Raman spectra of transferred graphene onto 300 nm SiO_2/Si wafers, (a-d) OM images of transferred graphene grown on Cu-foils that annealed at different H_2 concentrations (0-50%), (i) Raman spectra of transferred graphene samples and (j) plot of I_{2D}/I_G and I_D/I_G ratios measured from Raman spectra shown in (i)

These results suggest that annealing of Cu in Ar or in the presence of low H_2 concentration promotes a fewer number of layers and better quality graphene films compared to those obtained at excessive H_2 concentrations during annealing. These results are consistent with those mentioned in previous reports [19] [12].

Evolution of Cu surface morphology after graphene growth was studied by AFM as shown in **Figure 27 (e-i).** It is observed that Cu surface became smoother again after annealing followed by graphene growth, as confirmed by the decreased RMS roughness from 13 nm (of as-received) to approximately 6 nm in average (corresponding to different H_2 concentrations). 0%H_2 concentration exhibited more complex surface morphology consisting of wide-spaced steps with RMS roughness value about 7 nm. However, by increasing H_2 to 2.5 and 20% respectively, Cu surface became slightly smoother and flatter as validated by decreased RMS values. However at 50% H_2 Cu surface became very smooth dominated by high density of large size particles as confirmed by RMS value (4 nm). Similar particles were reported in previous works [16][23]. Comparing surface morphologies of as-annealed Cu and as-grown graphene on Cu substrates reveals that surface became slightly rougher after graphene growth as confirmed by the increase in RMS roughness values from (2 to 6 nm on average) as shown in (**Figure 26 (e-l)** and **Figure 27 (e-l)**).

According to the above results graphene growth mechanism can be hypothesized as follows: (1) at low H_2 concentration, present active sites such as impurity particles, Cu-particles, step-edges, surface striations and grain boundaries were probably oxidized and passivated, leading to formation of low number of nucleation sites. This associated by few surface-bound active H_2 atoms, resulting in less adsorption, and dissociation of CH_4 to carbon species. As a result, little amount of carbon atoms will be available leading to less nucleation points, and less number of graphene layers (double layers growth) associated with slow growth rate. (2) at high H_2 concentration, however all Cu surface features would be very active, increasing the density of surface-bound active H_2 atoms,

leading to stronger adsorption and dehydrogenation of CH_4 into carbon adatoms, along with presence of very dense nucleation sites (located mainly on surface striations and grain boundaries). Consequently, this promotes higher growth rate and formation of multilayer graphene domains with higher defect density as confirmed by Raman results shown in **Figure 28(e),(f)**. Besides, it promoted formation of high density, larger nanoparticles (of average size around 200 nm) that are more pronounced at 50% H_2 concentration (**Figure 29(d)**).

Although the origin of these particles is not yet completely understood, some research groups claimed that they might originate from the: CVD quartz tube [20], Cu surface impurities [16], and/or reconstructed Cu particles formed during H_2 annealing at elevated temperature [28,29]. Furthermore, Fan et al [73] observed that some of these particles were carbon aggregates, indicating that they might be originated from the carbon precursor (CH_4). In present study EDX analysis (**Figure 30**) of some particles revealed that they were SiO_2, since the percentage of Si element (~1.86 wt. %) obtained from this analysis was much higher than that found in as-received Cu (~ 0.05 wt. %). It is suggested that some Si particles might be formed from either the CVD-quartz tube or segregated from Cu foil [20] [74]. Our results revealed that higher H_2 concentration promoted higher density of those particles. We suspect that high H_2 content leads to more reaction with the surrounding including the quartz tube, which is believed to be one of the sources of Si element in addition to impurities in the Cu substrate [65][73]. These Si particles could have been oxidized by the oxygen residual in the Ar gas during cooling stage. Similar SiO_2 particles were observed at high H_2 concentration by Jung et al [20].

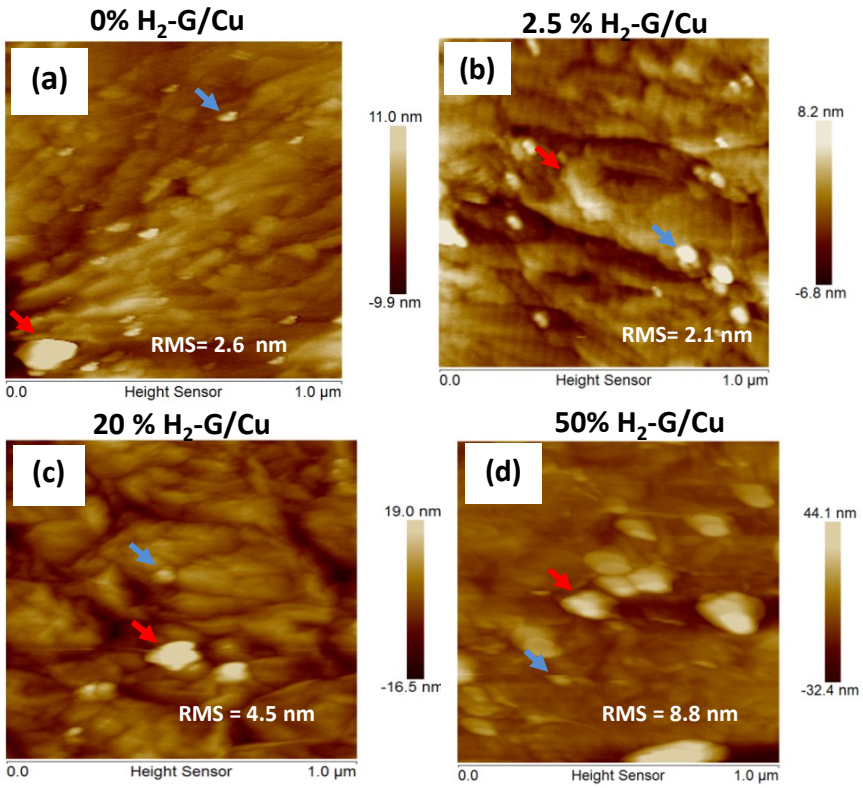

Figure 29: AFM micrographs of as grown graphene on Cu foils; the foils were annealed at 0% (a), 2.5% (b), 20% (c) and 50% of H2 (d). The micron-sized particles were emerged on the Cu foils both as individuals (blue arrows) and aggregates (red arrows)

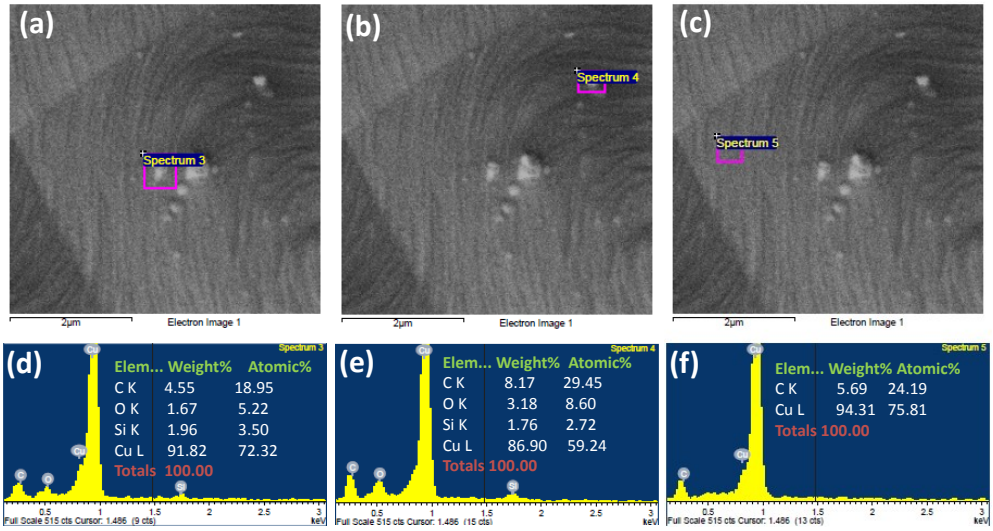

Figure 30: Elemental analysis composition of particles formed on Cu surface after graphene growth (Cu was annealed at 0% H_2), (a-c) SEM images of investigated Cu areas, (d- f) corresponding EDX spectra of areas highlighted by square shapes, as shown in (a- c)

The evolution of Cu surface morphology before and after graphene growth (as being annealed under 0%H_2 (Ar) or at higher H_2 concentrations) can be summarized schematically as shown in **Figure 31**. (1) when Cu is annealed under Ar only (H_2 = 0%), it would most likely be oxidized by oxygen residuals present either in Ar gas or in the CVD system [17]. These surface oxides could impede surface diffusion during annealing at elevated temperature and create high density narrow-spaced steps along with smaller Cu grains (**Figure 31 (b)**, the inset shown below). (2) Graphene will nucleate and grow preferentially along these evolved Cu-steps, consequently it will prevent Cu atom diffusion and evaporation underneath, leading to "step bunching" effect, thus Cu surface becomes more rougher consisting of wide-spaced steps [75] [76] as demonstrated in **Figure 31 (d)**. (3) However, annealing in H_2 would effectively reduce the Cu oxides throughout the surface via an exothermic reaction [77], resulting in better mobility and enhanced diffusion leading to smooth surface morphology (no presence of steps structure as shown in the inset of **Figure 31 (c)**) and larger Cu grains [78] despite, it also promotes formation of various surface features like surface dents, facets and nanoparticles. These features are considered the most preferable sites for nucleation and growth of bilayer/multilayer graphene. (4) After graphene growth on such smooth surface (inset of **Figure 31 (c)**), Cu surface turned out into wavy structure consisting of narrow-spaced wrinkles (**Figure 31 (e)**), due to the graphene-induced reconstruction effect on Cu. These Cu-wrinkles are mostly occurred to relax the strain from a large lattice mismatch between graphene and Cu lattice at a high temperature during the cooling stage as reported Wang et al [65]. These results reveal that Cu surface morphology prior to graphene deposition is

very important in controlling and dictating the Cu surface structure after graphene growth.

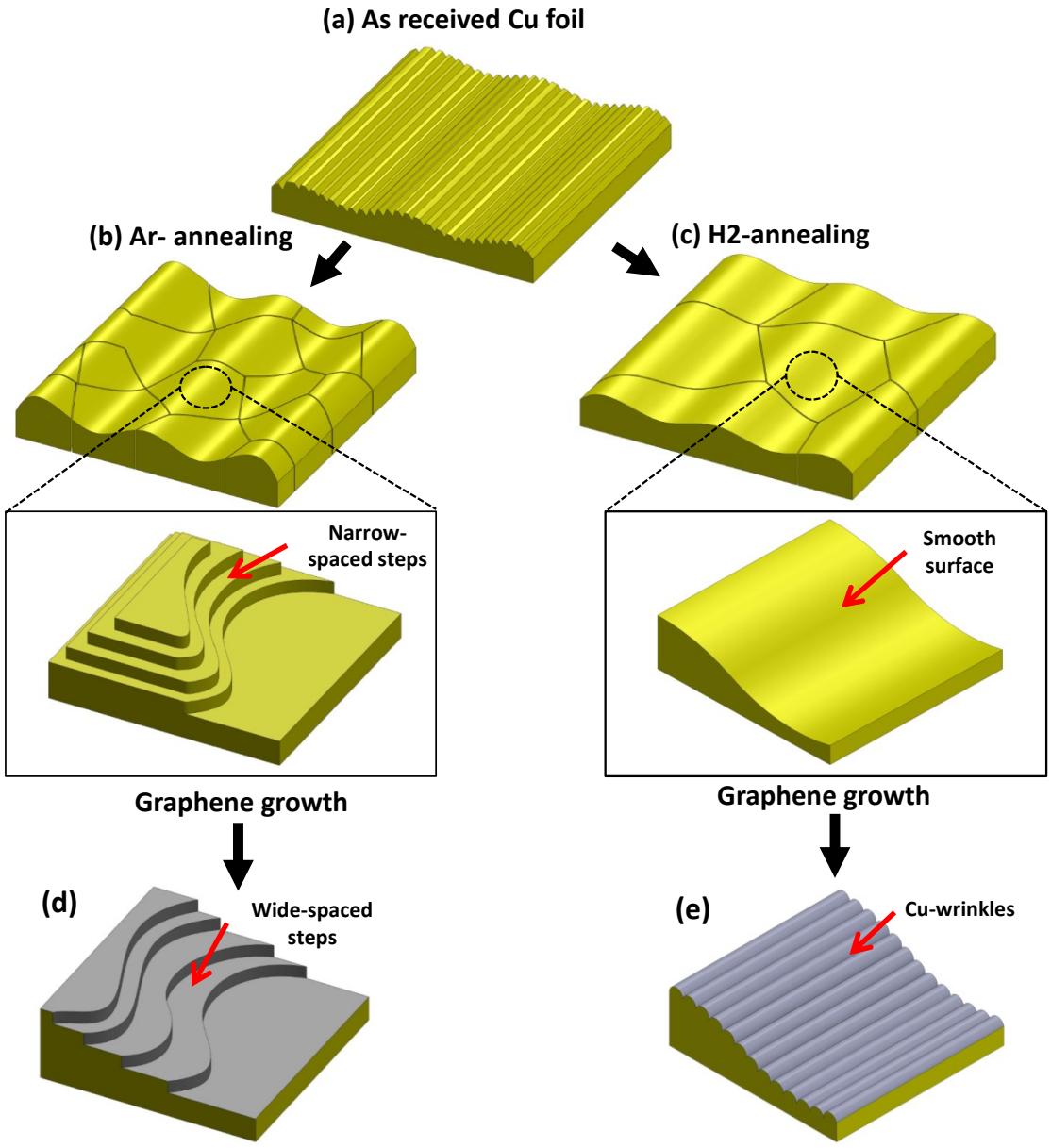

Figure 31: Schematic illustration of Cu surface morphology evolution of only annealed-Cu and graphene/Cu. (a) surface morphology of as-received Cu, (b, c) after Ar and H_2-annealing respectively, the insets are zoomed-in views of annealed-Cu and (d, e) Cu surface morphologies after graphene growth on Cu shown in the insets of (b, c)

In previous section, we studied the effect of H_2 concentration during Cu annealing stage on the deposited graphene morphology and quality but for short time growth (30s). In this section we extended the growth time to 3min in order to investigate the effect of increased growth time on synthesized graphene characteristics along with the evolution of underlying Cu surface morphology.

Figure 32 (a-d) shows the SEM and AFM images of the deposited graphene/Cu samples as a function of H_2 concentration during annealing stage. It is seen that 0% H_2 exhibited continuous, large area graphene film associated with formation of homogenously distributed small graphene domains (of darker contrast). By increasing H_2 to 2.5%, the size of graphene domains were increased as indicated by the darker areas (bilayer), where brighter regions are thought to be monolayer graphene.

Higher H_2 concentrations (20 and 50%) promoted formation of irregular graphene domains of different sizes and thicknesses; where brighter regions are due to monolayer, the gray color regions are due to bilayer, and the darker regions are due to multilayer or amorphous carbon aggregates. The density and areas of these multilayer graphene domains grown at 20% H_2 were higher than those obtained at 50%.

In addition, it was observed that different H_2 concentrations exhibited different Cu surface morphologies as shown in **Figure 32 (e-h)**. Again 0%H_2 leaded to the roughest surface (RMS=11 nm) consisting of widely-spaced very dense step structure (**Figure 32 (a), (e), (i))**; however by introducing H_2 during annealing Cu surface became smoother (RMS = 7 nm) as demonstrated by line profiles shown in **Figure 32 (j)**. In contrast at higher H_2 concentrations (20 and 50%), Cu surface was more dominated by high density of nanoparticles of

different sizes compared to low H_2 concentrations (**Figure 32 (f-h)**). These particles are mostly located at the centers of various darker graphene domains

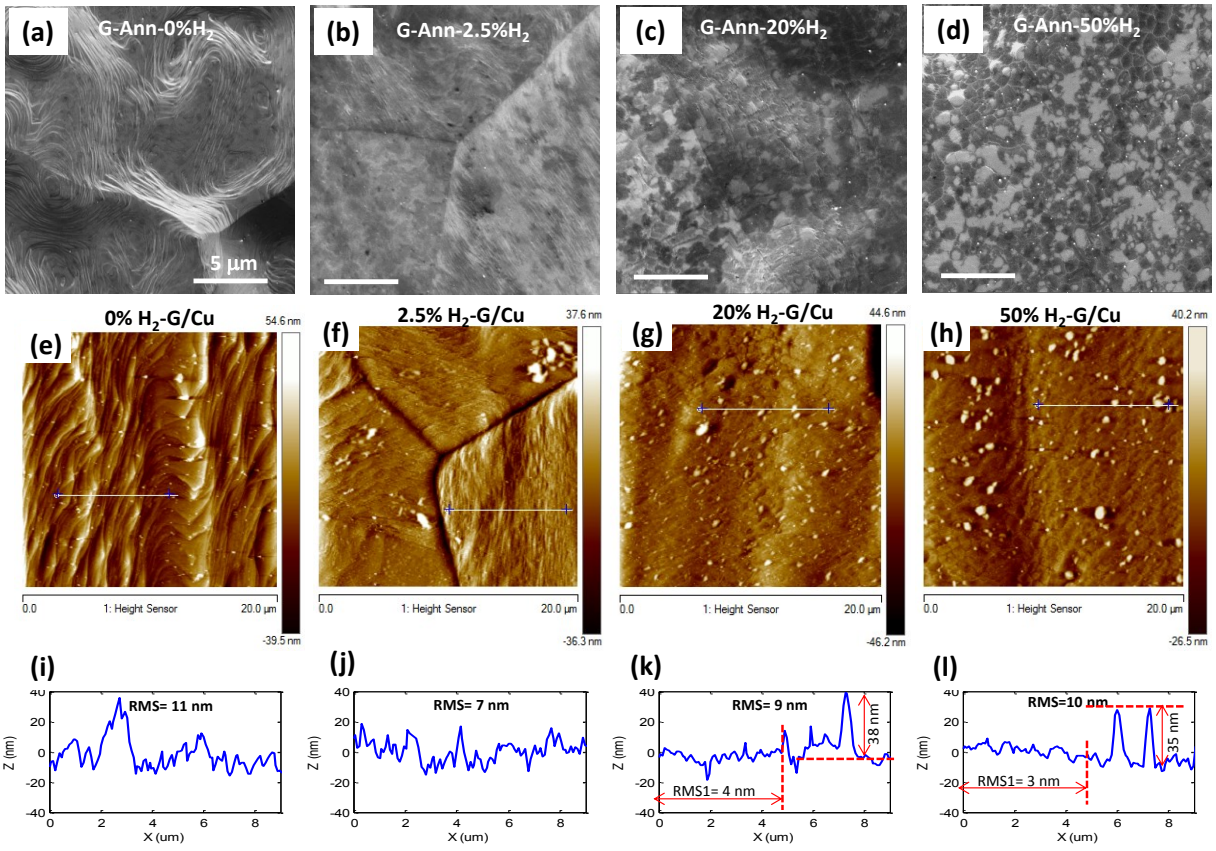

Figure 32: (a-d) SEM images of G-Cu samples (3 min growth) as a function of different H2 concentrations (0-50%), (e-h) 2D AFM images of corresponding SEM images shown in (a-d), (i-l) surface profiles of 2D AFM images shown in (e-h) corresponding to the cross-sectional lines indicated by white color

It is worth mentioning that, high H_2 concentrations (20 and 50%) exhibited smoother Cu surface compared to those obtained at 0 or 2.5% H_2 as confirmed by the decreased RMS roughness values to 4 and 3 nm as calculated from the measured surface profiles in the range from 0 to 5 µm as shown **Figure 32 (k), (l),** despite that the overall RMS values of corresponding measured surface profiles is high (around 10 nm) including those surface particles into the overall surface profiles. This indicates these surface particles contribute strongly in increasing the roughness of Cu surface. These results suggest H_2 concentration

during annealing stage not only controls the nucleation and growth of graphene film but also it dictates the irregularity degree of Cu surface. Consequently, these Cu surface morphologies may have significant effect on transferred graphene performance especially in case of graphene membrane applications such as gas and liquid filtration.

In order to evaluate the morphology and quality of previous deposited graphene films (after 3 min growth), all grown graphene were transferred onto SiO_2/Si wafers and consequently characterized by OM and Raman spectroscopy as shown in **Figure 33.** It is clear that 0%H_2 annealed Cu sample promoted formation of monolayer, large area and uniform graphene film associated with some surface residuals originating mainly from un-etched surface Cu oxides particles (**Figure 33(a))**. In contrast 2.5%H_2 exhibited bilayer and non-uniform as indicated by presence of high density of bilayer domains mainly located either on the striation lines or grain boundaries (**Figure 33(b))**. Interestingly, by increasing the H_2 concentration to 20 and 50% respectively, multilayer, non-uniform graphene film was obtained more pronounced along surface rolling lines and Cu grain boundaries (**Figure 33(c),(d)),** however it is observed that nucleation density of these multilayer domains was higher in 20%H_2 compared to that observed at 50%H_2.

Quality of transferred graphene onto SiO_2/Si wafers was further studied using Raman spectroscopy as shown in **Figure 33(e),(f)**. It is seen that all spectra display common bands of graphitic material, e.g. D, G and 2D. Again Ar annealing (0%H_2) Cu sample promoted

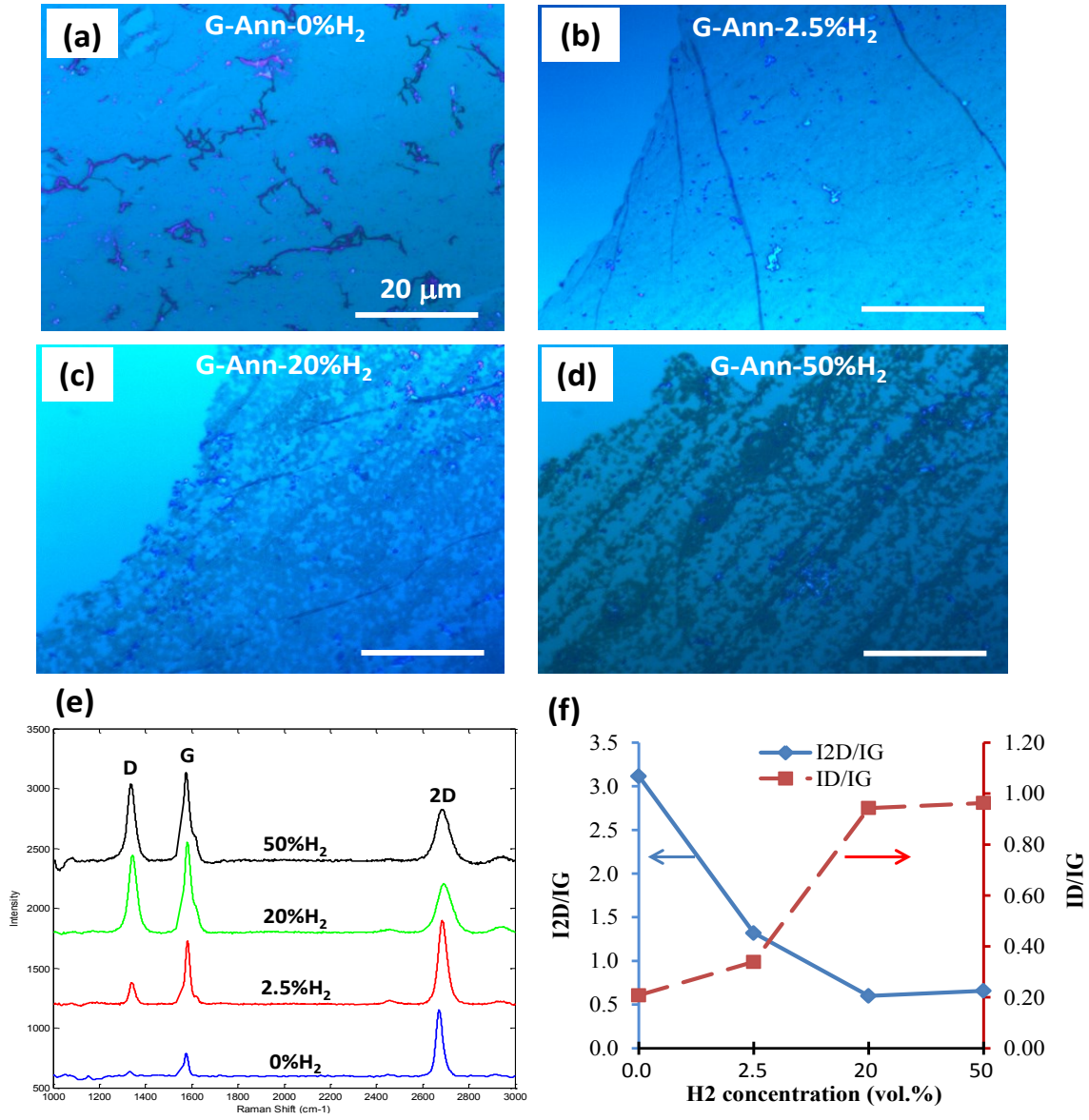

Figure 33: (a-d) OM images of transferred graphene/SiO_2 which grown on Cu substrates, which pre-annealed at different H_2 concentrations (0- 50%) of the total gas mixture consisting of Ar and H_2, (e) Raman spectra of graphene/SiO_2 samples shown in (a-d), (f) plot of I_{2D}/I_G and I_D/I_G ratio of corresponding spectra shown in (e)

Table 5: Calculations of I_D/I_G and I_{2D}/I_G ratios for Raman spectra shown in Figure 33(e)

Sample	D-band	G-band	2D-band		I_D/I_G	I_{2D}/I_G
	I_D	I_G	I_{2D}	FWHM		
G-Ann-0%H_2	2.3	11.1	34.7	37.7	0.21	3.1
G-Ann-2.5%H_2	170.3	502.2	663.1	48.4	0.34	1.3
G-Ann-20%H_2	605.6	642.1	385.5	76.0	0.94	0.6
G-Ann-50%H_2	390.7	405.7	267.0	73.7	0.96	0.7

monolayer graphene film as indicated by the I_{2D}/I_G ratios (~3), and FWHM (~38 cm^{-1}) along with low defects density as confirmed by low I_D/I_G ratio (~0.2). However, 2.5% H_2sample showed bilayer graphene film (I_{2D}/I_G= 1.3) with slightly increased defects density (I_D/I_G = 0.3). By further increasing the H_2 concentrations in the range from 20 and 50% respectively, it was observed that I_{2D}/I_G ratio was decreased to approximately 0.6 and 0.7 respectively, indicating that the number of deposited graphene layers was increased accordingly, resulting in formation of multilayer, non-uniform graphene film. the increase in number of deposited graphene layer is further associated with increase of defects density as confirmed by the increase of the I_D/I_G ratio to about 1 corresponding to 20 and 50% H_2 concentrations. These results demonstrated that H_2 played crucial role in determining the final characteristics of grown graphene films in terms of continuity, uniformity, number of layers, and quality.

Figure 34 shows 2D AFM micrographs of transferred graphene/SiO_2 wafers. It is seen that at 0%H_2 concentrations (Ar), graphene film exhibited some tears and cracks associated with presence of some uniformly distributed pores of different sizes (~120 nm) (**Figure 34** (a) as marked by black arrow). Till now, it is unclear what are the main reasons behind formation of these pores, but it might stem from the presence of high density Cu oxides particles formed on Cu surface during annealing stage (in Ar only). In addition, it seems that the obtained graphene film is thinner than those obtained at higher H_2 (2.5-50%). 2.5%H_2 yielded formation of bilayer graphene domains on the continuous graphene film as marked by yellow arrows in **Figure 34 (b)**. by further increasing H_2 to 20 and 50%, multilayer, flower shape (of dendritic shape)graphene domains were

observed, with increased density in case of 20% H_2 compared to those found in 50% H_2 case (**Figure 34(c),(d)**).

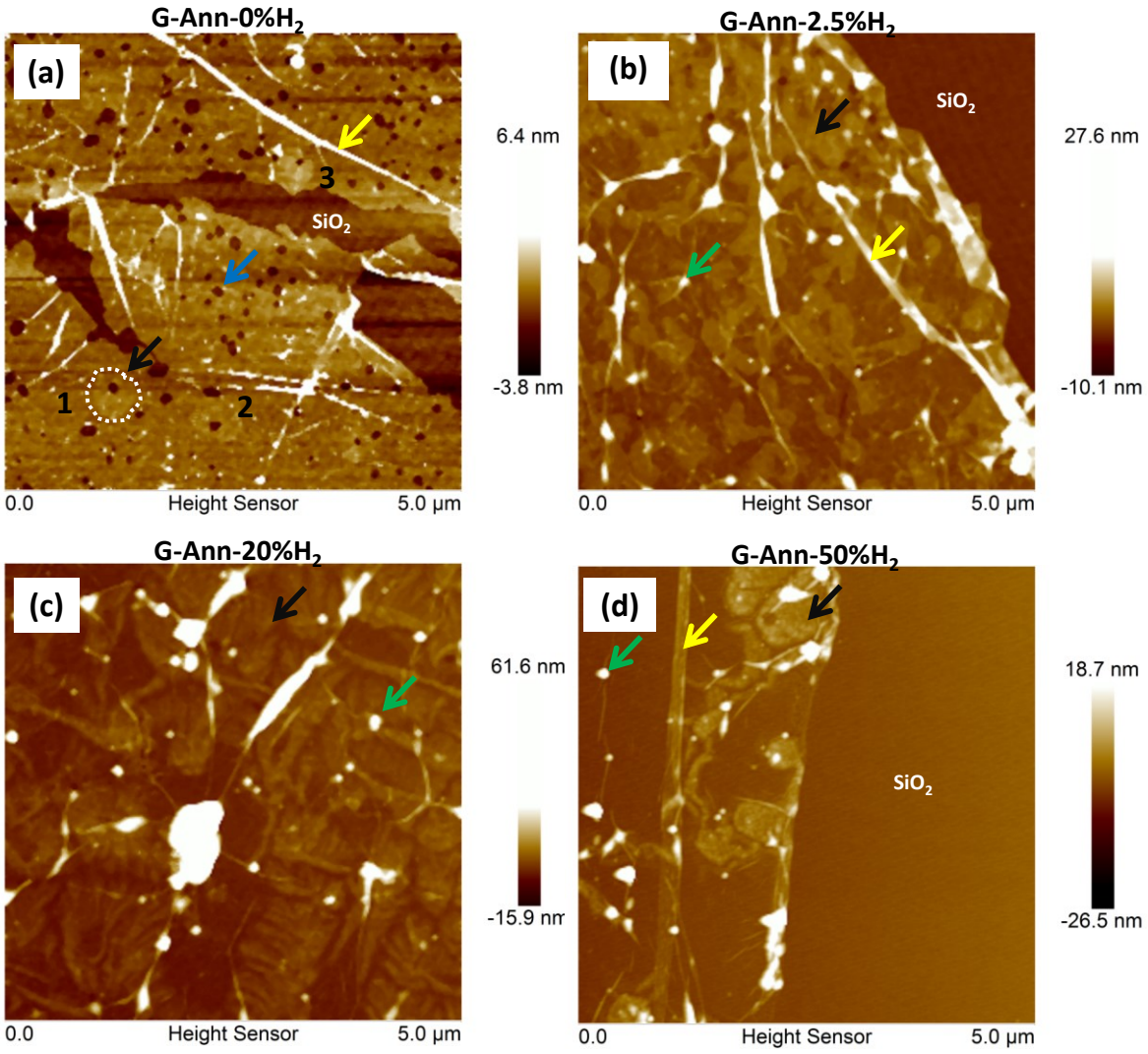

Figure 34: AFM images of transferred graphene onto SiO_2 which were deposited on Cu substrates (pre-annealed at different H_2 concentrations corresponding to (a) 0%, (b) 2.5%, (c) 20% and (d) 50% of the total gas mixture consisting of Ar and H_2

4.3 Effect of hydrogen during graphene growth step

It was a big controversial in literature regarding the actual role of H_2 gas supply during graphene growth step. It was reported in many articles that presence of H_2 was crucial for growing large area, high quality graphene, as it (1) encourages conversion of adsorbed methane into its hydrocarbon radicals which is essential for formation of graphene [42]. Consequently, activating surface bound carbon which was necessary to grow monolayer [43] and/or bilayer graphene [44]. (2) H_2 could also regulate the diffusion of carbon species on the surface of the copper, thus affording a balanced carbon environment to further ensure the quality of the graphene formed [42]. (3) In addition, H_2 is playing as etching reagent which could control both size, morphology, and the number of layers of grown graphene [42] [43].

Therefore, many researchers found that after excluding H_2 from growth step, amorphous carbon batches were grown on Cu surface, as absence of H_2 lead to formation of weak carbon coverage, consisting mostly of oxidized and amorphous carbon obtained on the copper catalyst. The oxidation originates from the inevitable occurrence of residual oxidizing impurities in the quartz tube, leading to oxygen-related functional groups (H_2 was considered as defect suppressor agent) [15] [42] [45].

On the other hand, many researchers gave completely different explanation concerning H_2 role during growth. H_2 competes with CH_4 dehydrogenation leading to suppression of graphene formation and growth, associated by formation of defective graphene consisting basically of C-H defects [46], high H_2 supply can cause also SP3-style defects resulting in increased I_D/I_G ratio [44]. Other researchers claimed that H_2 could be the main reason

behind growing few-layer graphene, leading to thick and discontinuous multilayer flakes observed mainly at high H_2 concentrations, as it could prevent the transport and adsorption of active carbon species, leading to aggregation of the activated C atoms around the active sites to form stacked graphene flakes, associated by low growth rate [47]. Therefore, by excluding H_2 during growth step, high quality graphene with large area could be synthesized similarly to those obtained by LPCVD confirming that absence of H_2 might convert the growth kinetics from mass-transport to surface-reaction regime [19].

According to the above studies, it is found that the detailed mechanisms of CVD process including the role of H_2 on deposited graphene morphology and quality during growth step is unclear yet. It is thus important to perform a systematic study to understand and reveal the actual role of H_2. In this regards, we grow different samples of graphene on Cu substrates as a function of H_2 concentration during graphene growth stage. The detailed description of adopted CVD parameters is shown in **Table 6**.

Table 6: CVD-graphene growth parameters to study the effect of H_2 concentration (2.5-20%) during growth on the deposited graphene characteristics

Sample	H_2 %	Heating		Annealing			Growth			
		Ar (sccm)	H_2 (sccm)	Ar (sccm)	H_2 (sccm)	Time (min)	Ar (sccm)	H_2 (sccm)	CH_4 (sccm)	Time (min)
G-2.5%	2.5	1450	50	1462	38	30	1457	38	5	3
G-10%	10						1345	150	5	3
G-20%	20						1195	300	5	3

Figure 35 shows the effect of H_2 concentration on evolution of graphene morphology and quality. It is seen that at low H_2 concentration (2.5%), bilayer graphene domains were deposited on underlying continuous graphene film as indicated by irregular darker color contrast domains in **Figure 35 (a),(d)**. In contrast, higher H_2 (10%) promoted growth of multilayer and/or amorphous carbon aggregates with high density **(Figure 35 (b),(e))**. By further increasing H_2 to 20%, Cu surface exhibited lower density of multilayer graphene domains with larger domains size (**Figure 35 (c),(f)**) compared to those obtained at 10% H_2 concentration.

The quality of above deposited graphene was further studied by OM and Raman analysis of transferred graphene onto 300 nm SiO_2/Si wafer as shown in **Figure 35 (d),(h).** Raman results suggest that all H_2 concentrations yielded approximately bilayer graphene with different densities of multilayer/amorphous carbon regions as confirmed by the ratio between 2D and G bands (I_{2D}/I_G ~ 1.3-2.1) and by the FWHM values of 2D-band (~45-48 cm^{-1}). It is seen that as H_2 increases, the area and density of multilayer domains increases as well. It is also observed that as H_2 concentration increases the density of defects induced into the deposited graphene film increases as indicated by the increased ratio of I_D/I_G from 0.3 to 0.7 corresponding to H_2 concentrations from 2.5 to 20% respectively. These results suggest that low H_2 (2.5%) promote lower defective graphene but with thicker graphene film compared to 10 and 20% H_2 samples.

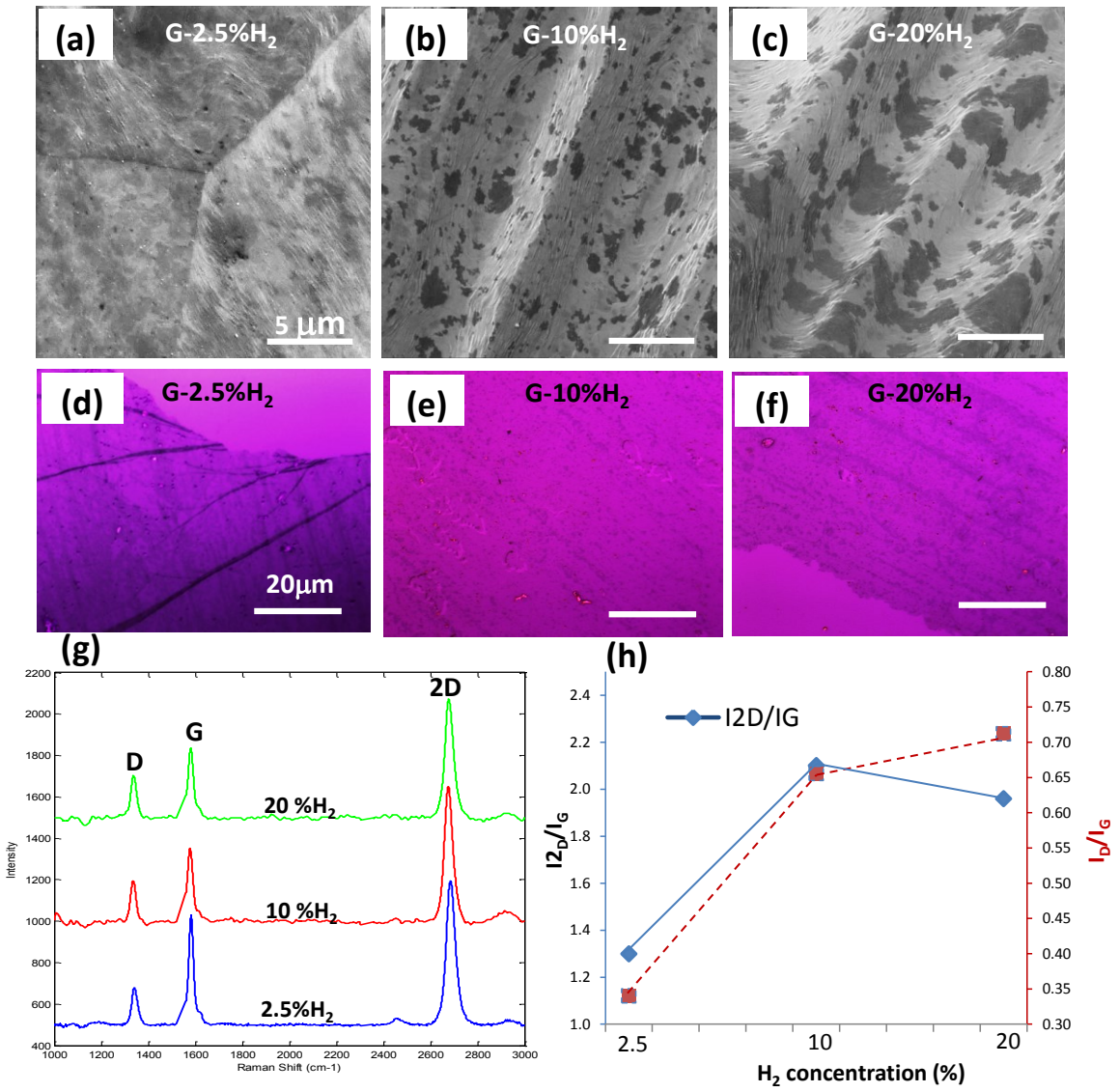

Figure 35: Effect of H_2 concentration during growth step on graphene characteristics (a-c) SEM micrographs of as-grown graphene/Cu substrates under different H_2 concentrations corresponding to 2.5, 10 and 20% respectively, (d-f) OM images of graphene/SiO_2 wafers, (g-i) Raman spectroscopy analysis of graphene/SiO_2

4.4 Effect of Cu substrate on growth and transfer of graphene

This study is intended to investigate the evolution of Cu surface morphology of two commercial foils after being annealed, and their impact on the quality of both deposited and transferred graphene films. This work is thought to give better insight into the relationship between the graphene properties and the underlying Cu substrate surface morphology. Graphene films were synthesized on two different copper foils, purchased from Alfa Aesar (AA), and Nippon Mining & metals (HA). Cu foils were cut into 1 cm x 3 cm pieces, and pre-cleaned using acetic acid (5min), followed by ethanol and DI water. Cu foils specifications along with CVD growth parameters are shown in **Table 7**. After growing graphene on both Cu substrates it was transferred onto 300 nm SiO_2/Si wafers, as demonstrated in previous sections.

Table 7: CVD-graphene growth parameters to study the effect of Cu substrate on graphene properties

Cu substrate	Purity %	Thickness (μm)	Annealing			Growth			
			Ar (sccm)	H_2 (sccm)	Time (min)	Ar (sccm)	H_2 (sccm)	CH_4 (sccm)	Time (min)
AA	99.8	25	1500	0	30	1465	35	5	5
HA	99.96	30	1500	0	30	1465	35	5	5

Figure 36(a),(b) show SEM micrographs of graphene on AA and HA Cu substrates respectively. The contrast variation throughout the image can reflect the different thicknesses of graphene domains. The dark regions on those SEM images indicate bilayer and/or multilayer graphene and the bright areas correspond to the monolayer graphene. Due to the complex structure of AA, it exhibited irregular shaped, small size bi and/or multilayer, high density graphene domains nucleated mostly on the Cu surface step edges. In contrast HA yielded more uniform shaped (hexagonal or circular), larger size

(~2μm) and lower density of graphene domains along with presence of wrinkles and cracks. These wrinkles are formed during cooling step because of the thermal expansion mismatch between graphene and Cu substrate [79].

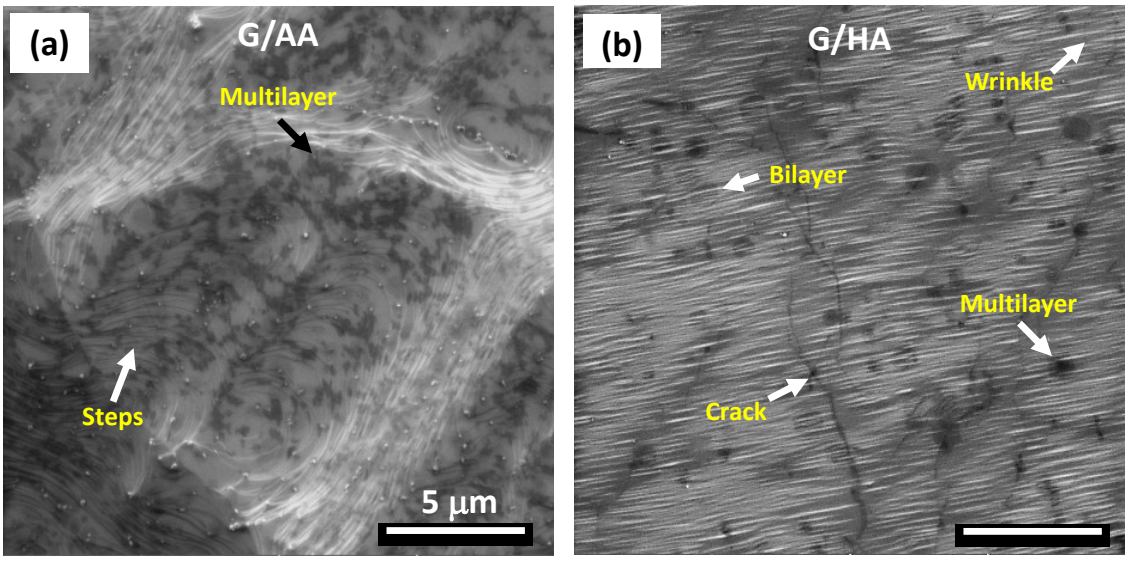

Figure 36: SEM micrographs of grown graphene on (a) AA and (b) HA Cu respectively. It is obvious that AA exhibited higher density of multilayer; irregular graphene domains nucleated mostly on Cu step edges, in contrast HA showed less number of nucleation sites with bi and multilayer, hexagonal graphene domains on monolayer graphene with increased number of wrinkles and cracks indicating its one atom thickness

It seems that because HA promoted monolayer graphene (as confirmed later on by Raman spectra results), it exhibited more pronounced wrinkles and cracks since the interaction between this monolayer graphene and underlying Cu substrate will be more stronger than that in case of multilayer over Cu substrate.

In order to better understand the correlation between Cu surface morphology and the growth mechanisms of graphene on these Cu foils, AFM was utilized to investigate the evolution of both Cu substrates before and after graphene growth as shown in **Figure 37.** It is clear that both Cu foils (as-received) exhibited a lot of surface striations which resulted from the rolling process of these Cu sheets during manufacturing process.

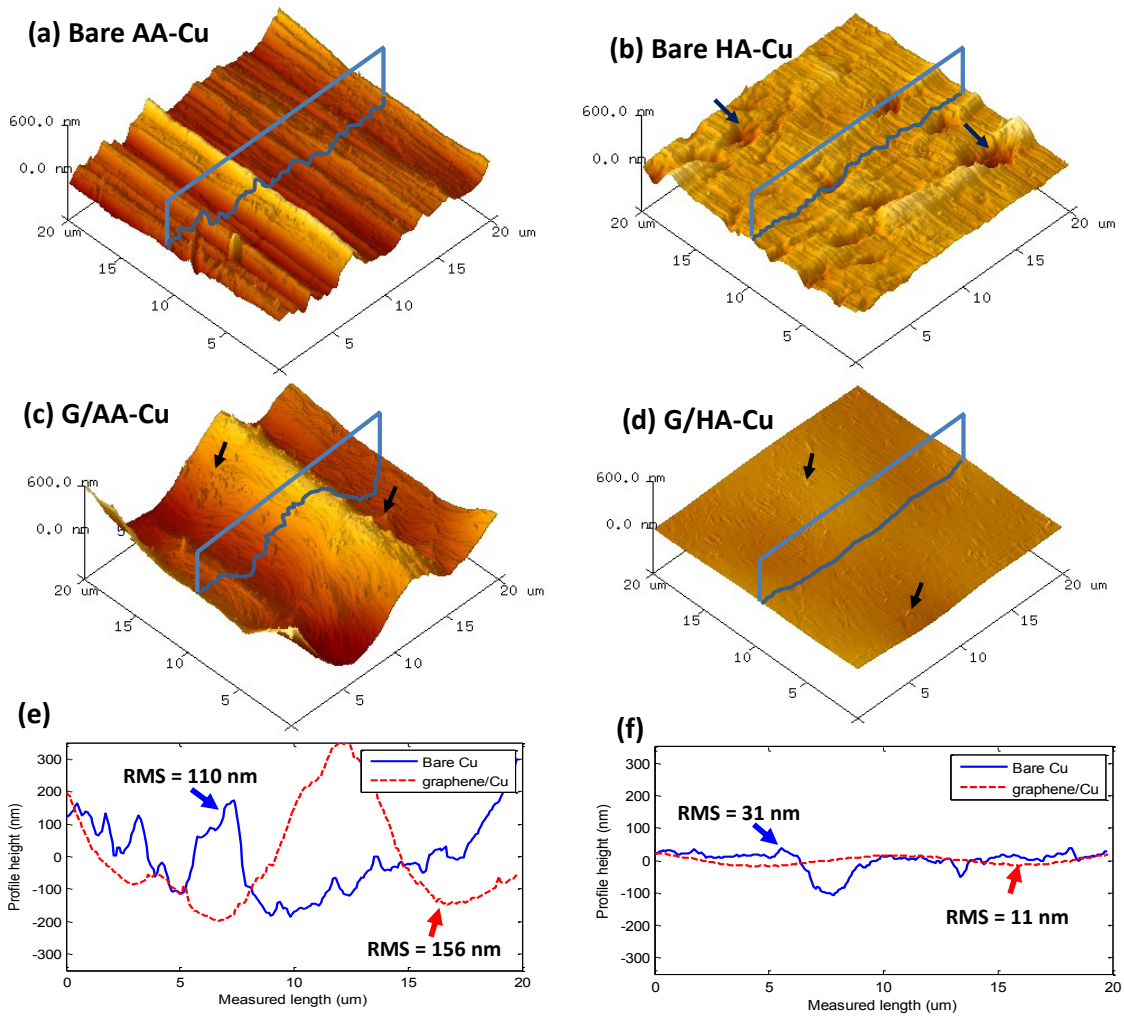

Figure 37: Surface morphology and roughness of Cu substrate before and after graphene growth. AFM micrographs of (a) bare AA, (b) graphene/HA, (c) bare HA, (d) graphene/HA. (e, f) surface roughness profiles of as-received(blue line) and as-grown graphene(red line) on AA and HA Cu foils respectively, associated with their corresponding RMS roughness values

Although HA showed lower height striations compared to those in AA (**Figure 37 (a),(b)**), it exhibited some surface voids which may be attributed to sever deformation during its manufacturing. RMS roughness parameter was employed to evaluate the irregularity degree of Cu substrates. RMS roughness value of HA-Cu was very low (~ 31nm) compared to AA (~110 nm), indicating that HA is much smoother than AA Cu although it has some surface voids as shown in **Figure 37(b)**. After graphene growth it is observed that both Cu surfaces underwent great changes. For AA, rolling lines were evolved to

stepped structure associated with formations of nanoparticles. On the other hand, HA exhibited completely smoother surface associated with presence of some nanoparticles (of lower density than AA). It is clear that the overall surface roughness of HA (RMS= 11 nm) is much lower than AA (RMS= 156 nm) as shown in **Figure 37(e),(f).**

These observed nanoparticles (average size~250 nm) in both cases, are mostly Cu oxides formed during annealing Cu foils under Ar only that included some oxygen residues.

To get better insight into the surface morphology changes between AA and HA substrates as influenced by graphene growth step, high magnification AFM images **(Figure 38 (a), (b))** were obtained from the same investigated Cu foils as shown in **Figure 37 (c),(d)** for AA and HA respectively. **Figure 38(a-d)** show the AFM micrographs and surface roughness profiles of graphene/AA and HA Cu foils respectively, it is observed that graphene/AA exhibited much rougher surface morphology (RMS=8 nm) compared to the obtained very smooth graphene/HA (RMS= 1 nm), as indicated by the roughness profiles obtained corresponding to white color lines as shown in **Figure 38 (a), (b).** In addition, AA exhibited higher density of nanoparticles than that observed in HA, although their lateral size are comparable (~250 nm) in average, however their height is lager in case of AA (~70 nm) compared to those ones in HA (~15 nm) as indicated by the corresponding particles height profiles shown in **Figure 38(a),(b)** corresponding to AA and HA respectively. The surface morphology evolution of both Cu foils before and after graphene deposition is schematically depicted in **Figure 39**. These differences in surface morphology between these Cu foils indicate that they underwent different reconstruction mechanisms during annealing and graphene growth step.

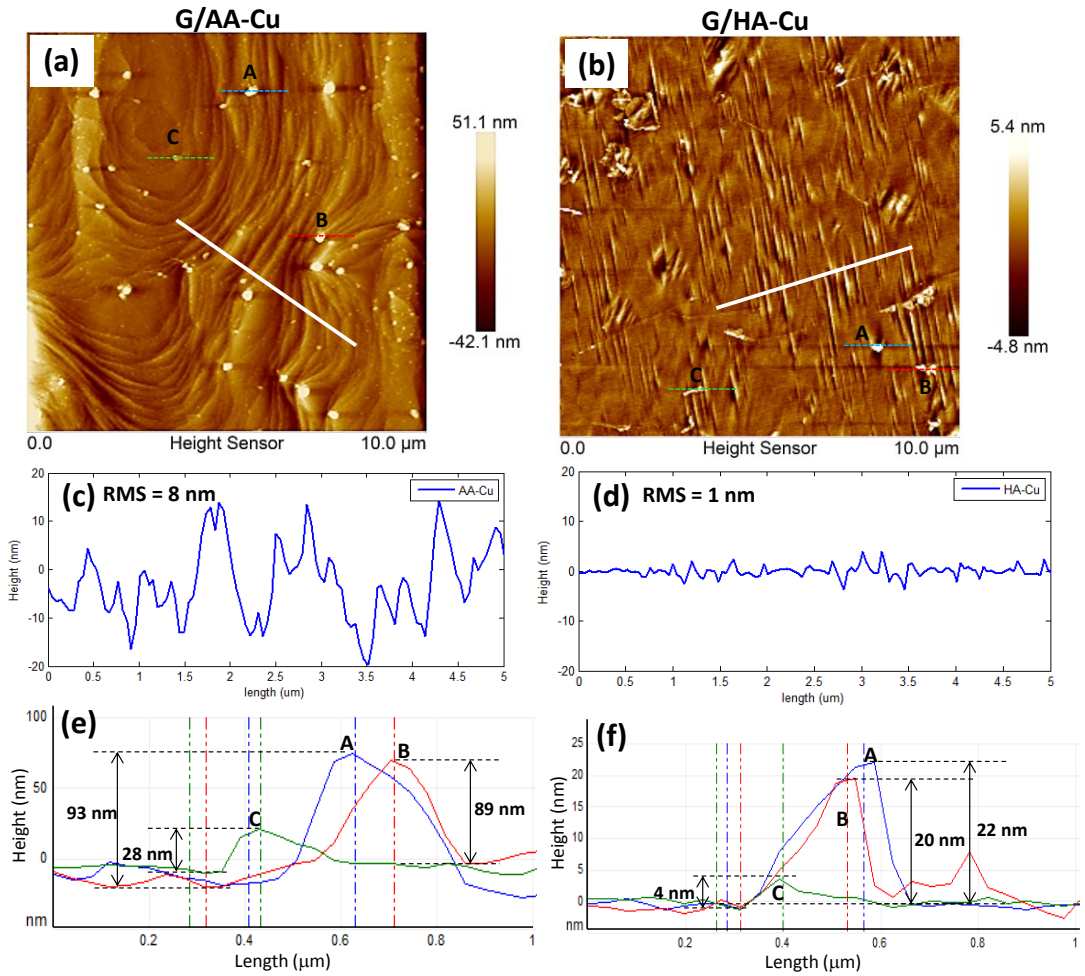

Figure 38: High magnification AFM images (shown in Figure 1 (b), (c) respectively) of Cu foils after graphene growth, (a, c) AA-Cu surface morphology, and corresponding height profile of surface nanoparticles, (b, d) HA-Cu surface morphology and its corresponding particles heights analysis. It is observed particles emerged on AA case are larger in size (~ 70 nm) than found on HA Cu whose size (~15 nm)

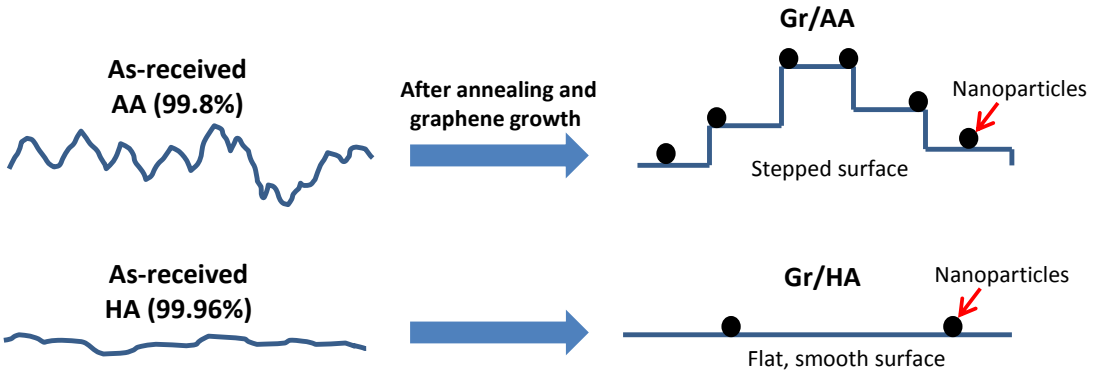

Figure 39: Schematic diagram shows the evolution of AA and HA Cu foils after annealing and graphene growth steps

Since AA exhibited much rougher morphology with dense steps, and more particles. While, HA showed relatively smoother surface with low particles density. The high density of surface steps in AA could be attributed to (1) AA has larger heights of striations compared to HA, (2) the higher evaporation rate of AA (99.8% purity) compared to HA (99.9% purity) since it is suggested that AA will melt at lower temperatures than HA as it contains more impurities. (3) the effect of graphene "step bunching" as mentioned in [79] would be more pronounced in AA.

The higher density of particles in AA may be attributed to the higher contents of impurities compared to HA. In addition, it was mentioned in [73] that these particles may be nucleated and deposited on the same graphene nucleation points, and because AA has much density of surface steps and edges, it is suggested that it will promote higher number of particles. These particles may be SiO_2, or any other types of impurity particles. It is expected that these evolved Cu surface features will have significant effect not only on the characteristics of as-grown graphene but also on its morphology and quality after transfer process. The main reasons behind deposition of high density, multilayer and irregular graphene on AA compared to the low density, bi/multilayer, uniform hexagonal graphene domains on HA could be attributed to the following reasons; (1) the complex morphology of AA, which consisting of dense and sharp corrugations combined by its low purity level (99.8%) would increase catalytic activity of Cu substrate, leading to higher methane decomposition, and consequently dissociation of much higher quantity of carbon atoms on the surface [68]. (2) rough features on Cu are likely to promote higher density of nuclei due to their significant lower nucleation barrier, since the mobility of carbon-adatoms species on rough surface is very low compared to its high mobility on

smooth surfaces [69]. (3) the increased density of steps and terraces in AA compared to HA will decrease the mobility of dissociated carbon adatoms on the surface, as the free travel distance by these atoms on the densely stepped surface would be shorter, this leads to formation of rough growth front and anisotropic growth of graphene resulting in dendritic graphene domains morphology [80].

These results suggest that complex structure of AA compared to the smooth and flat morphology of HA promoted higher density of nucleation sites, leading to multilayer and irregular graphene domains preferentially grown on the step edges. It is suggested that these bilayer/multilayer domains were nucleated and grown under the top-layer monolayer graphene [79][81]. This monolayer is almost invisible due to its atomic thickness and can be only identified by the presence of wrinkles.

In addition to the Cu surface morphological changes, we evaluated the crystallinity changes of both Cu foils by measuring XRD patterns of Cu substrates before and after graphene growth. It is obvious from **Figure 40** that although as-received AA was dominated by Cu(100) crystals, it remained textured at the same direction after graphene deposition , however it is intensity was decreased, and shifted towards higher 2θ angle, this may be related to the presence of staking faults, or oxides.

In contrast, although the XRD reflections of as-received HA Cu showed three peaks corresponding to Cu (200), (220) and (311) planes respectively, which indicates its poly-crystallinity nature, it did not exhibit any defined XRD peaks in the range from 20 to 120 degrees after graphene deposition, indicating that HA-Cu substrate became amorphous after being annealed in Ar atmosphere. It is unclear completely what are the actual

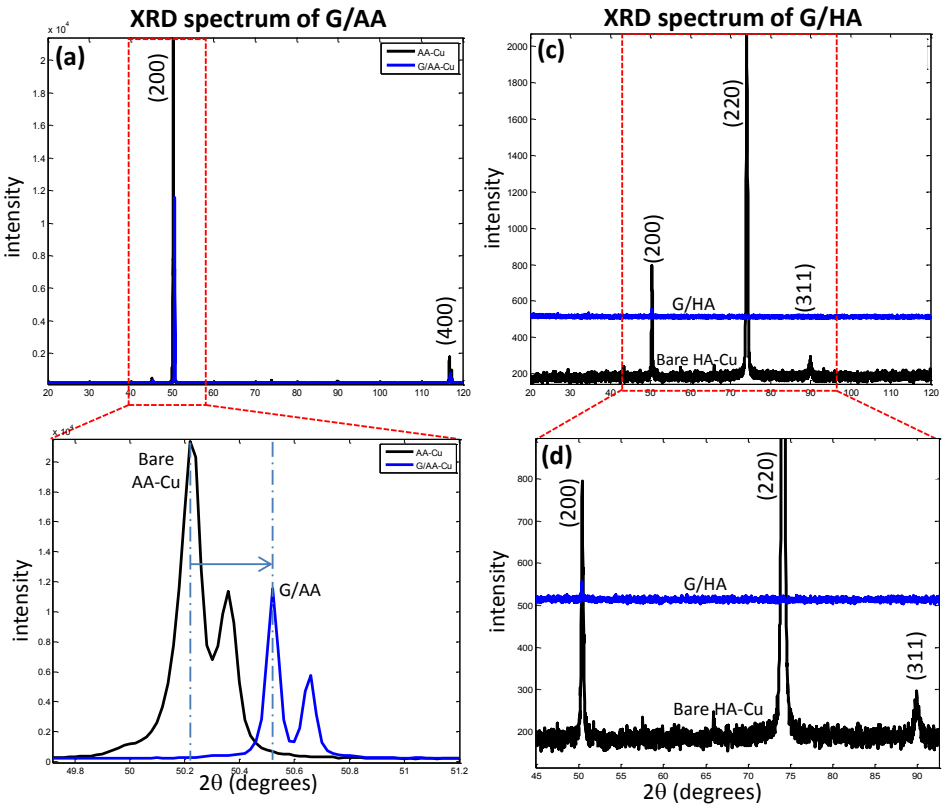

Figure 40: XRD patterns of AA and HA C1gu substrates before and after graphene growth (a,b) of AA and (c,d) for HA

reasons behind that, and why other Cu foil (AA) did not exhibit the same results, however, this might be beneficial for reducing grain boundaries defects, which are responsible for increasing graphene nucleation density and formation of defective, multilayer graphene domains. Based on the finding that HA yielded smoother surface morphology compared to AA, we investigated the effect of each of these Cu substrates on the morphology and quality of synthesized graphene.

It is obvious from above results that although both Cu foils were underwent the same annealing and graphene growth condition, they yielded different graphene properties. It is evidenced that both the Cu morphology and purity play crucial role in determining and controlling the final deposited graphene uniformity and quality.

In order to better evaluate the morphology and quality of grown graphene on both Cu foils, these graphene films were transferred onto 300 nm SiO_2/Si wafer as shown in **Figure 41(a), (b).** It is observed that both Cu foils yielded large area, continuous graphene films associated with presence of un-etched Cu residuals (indicated by black arrows) mostly representing the underlying Cu grain boundaries. However, AA Cu promoted growth of high density darker domains (multilayer) of very small size, distributed homogenously throughout the graphene film (**Figure 41 (a)** denoted by white arrow). In contrast, HA copper exhibited better uniformity, with no obvious bilayer/multilayer graphene regions (**Figure 41 (b**)) associated with low defects as confirmed by the low intensity D-band in Raman spectra, indicating high-quality graphene. These results suggest that flatter Cu surface, with low density of surface imperfections (e.g. surface striations, stepped structures and grain boundaries) is advantageous for growing more uniform, thinner, higher quality graphene.

Figure 41(c), (d) show Raman spectra of transferred graphene onto SiO_2/Si wafer that previously grown on AA and HA-Cu foils respectively. The I_{2D}/I_G ratio of about 2 and the FWHM of 2D bands (~43 cm^{-1}) indicate graphene film is bilayer. However HA Cu exhibited I_{2D}/I_G ratio of 3 and the FWHM of 2D bands (~38cm^{-1}), which suggest graphene film is monolayer. Both AA and HA showed low intensity D-band suggesting good quality graphene compared with relatively negligible D-bands of examined graphene/Cu substrates as depicted by blue color spectra. This suggests that those observed D-bands of graphene/SiO_2 wafers were originated due to transfer process and there is no evidence of having intrinsic graphene defects due to growth process.

In order to investigate the effect of Cu substrates on the graphene properties in microscopic **scale,** tapping mode AFM was carried out to previously transferred graphene films (**Figure 41 (a), (b))** where the scan size was 5x5 μm^2 for each sample. **Figure 42 s**hows 2D AFM surface morphology of transferred graphene after removing PMMA with acetone. It is clear that AA exhibited higher density of cracks, tears, wrinkles and pores compared to HA Cu foil (**Figure 42(a), (b))**. It is worth noting that these pores (~113 nm) distributed uniformly throughout the graphene film, whose thickness was measured to be 1.86 nm as indicated **Figure 42 (c).**

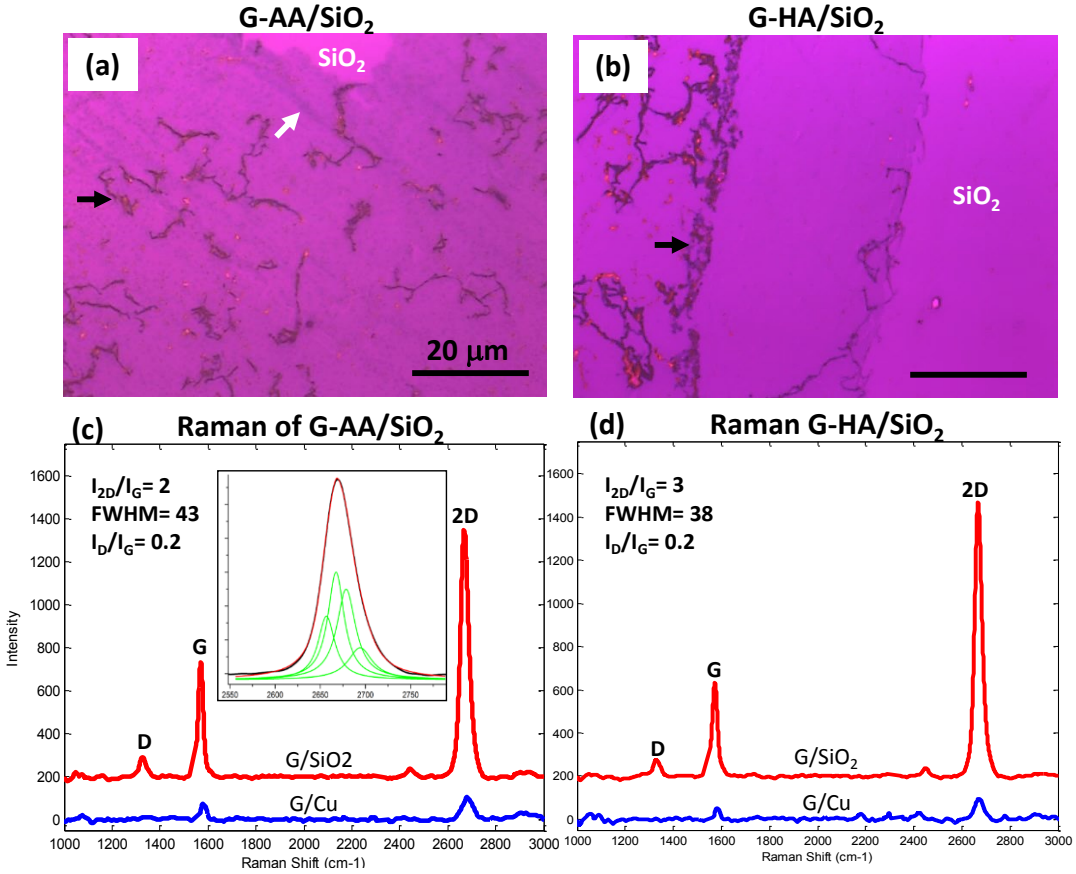

Figure 41: OM and Raman spectroscopy analysis of grown graphene on AA and HA Cu substrates respectively, (a, b) OM images of graphene/AA and HA respectively after transferred onto SiO2 wafer, (c, d) Raman spectra of graphene/SiO2 shown in a, b respectively

In contrast, HA-grown graphene (**Figure 42 (b)**) exhibited more uniform graphene, with no presence of pores and tears into graphene film. The measured thickness graphene film grown over HA copper substrate was 1.12 nm, indicating that deposited graphene on HA was monolayer compared to the bilayer graphene film grown on AA. Both graphene films grown on AA and HA showed some contaminations (indicated by bright spots) mostly originated from PMMA residues left over graphene film after transfer process. The observed differences among the measured graphene films thicknesses and the theoretical ones may be attributed to the presence of PMMA and/or un-etched Cu particles in between the graphene and SiO_2 substrate. These contaminations will certainly lead to that observed increase in measured thickness of graphene films.

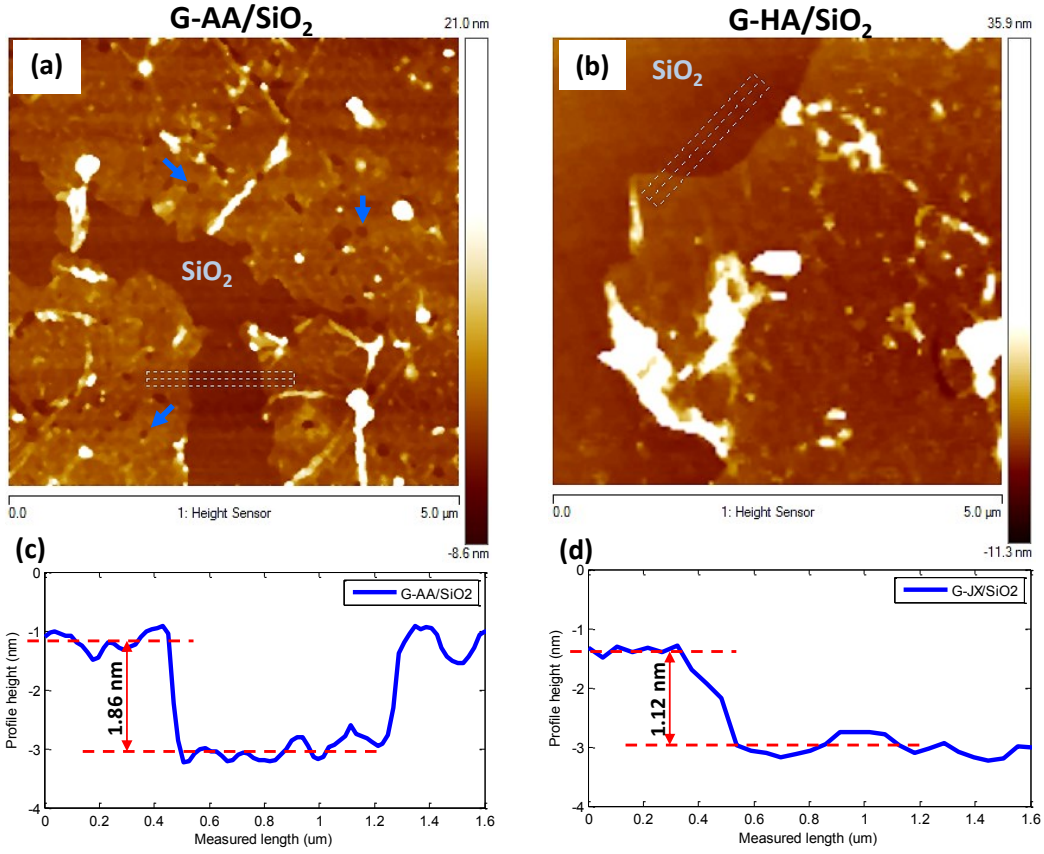

Figure 42: AFM micrographs of graphene transferred onto SiO_2/Si substrate, (a,b) graphene grown on AA and HA respectively, (c, d) height profiles along the rectangles marked in (a) and (b) respectively

The quality and effect of substrate on transferred graphene was studied and number of graphene layers was identified by using transmission electron microscopy (TEM). TEM results are shown in **Figure 43**. Graphene synthesized on AA-Cu has both individual particles and cluster of several particles (**Figure 43(a))**; the average size of the cluster is around 200 nm which is consistent with AFM observation. Since TEM provided much higher resolution than AFM, it can be hypothesized that the particulates seen in **Figure 38(a) and (b)** are comprised of several individual particles which are about 50 nm in size. Along with clusters, we also found individual particles of same size that of found in clusters. Interestingly, we found one graphene domain around 50 nm in diameter surrounding a round particle, similar domains were also observed by SEM (**Figure 36 (a)**). To identify the nature of the particles, energy dispersive spectroscopy (EDS) was performed in the TEM. Certain impurity elements were identified in both cases by EDS, such as Si, S and Cr etc. However, concentration of chromium (Cr) was higher in AA-Cu foil than HV-Cu. Selected area electron diffraction (SAED) patterns showed that graphene produced on both substrates were of good crystalline structure. The main crystalline planes for hexagonal crystal were identified and indexed in each case.

Furthermore, we performed the high resolution TEM to resolve the lattice planes of graphene and identify the number of layers at the folding edge of graphene in case of G/HA-Cu. Folding edges of graphene enabled us to take high resolution images of these areas to estimate the number of layers by measuring the spacing between them, the spacing between two layers is around 0.335 nm. We measured this distance around 0.34

nm and 3-4 graphene layers were identified, see intensity profile in the inset of **Figure 43(g)**.

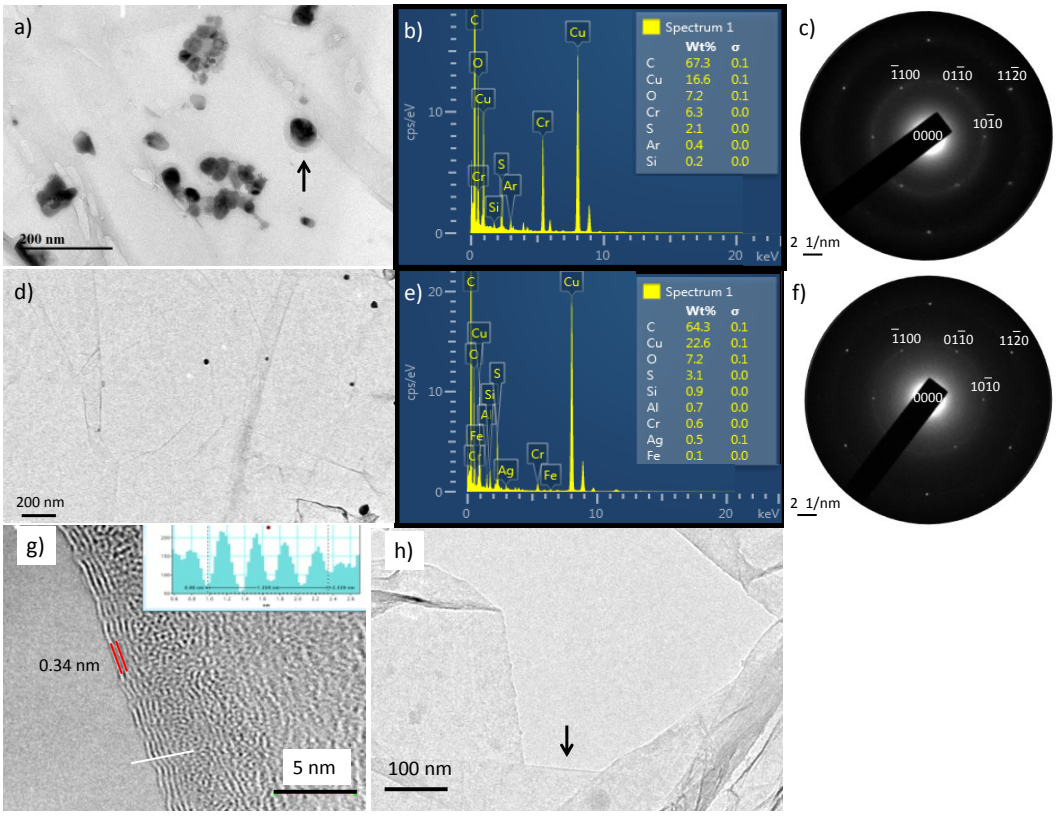

Figure 43: TEM analysis of graphene (a,d) transferred from AA and HA Cu foils respectively, (b,e) EDS spectra of corresponding images (a,d), (c, f) Typical selected area electron diffraction (SAED) patterns of graphene taken from the flat area in each case, (g) High resolution image taken from the folding edge of graphene (as marked with black arrow in (h) where, the inset is the intensity profile taken from the indicated area (white line) show 3-4 layers of graphene

The origin of these defects (including tears, cracks and pores) which observed mainly in graphene film that transferred from AA may be attributed to the complex morphology of AA substrate that evolved after graphene deposition step (**Figure 37 (c)** and **Figure 38(a)**) consisting of high density, sharp step-edges associated with those high density, large size surface nanoparticles. Generation of these pores into transferred graphene films can be explained as shown in **Figure 44**.

It is suggested that (1) this stepped structure along with those reconstructured surface nanoparticles (whether they are impurity particles or Cu oxide particles) promoted formation of high density, very small multilayer domains in the graphene film [25], [69], this graphene film will be discontinuous around those surface nanoparticles, since it is very difficult for the deposited graphene film to cover these particles [25], (2) upon etching the underlying Cu substrate during graphene transfer process, these nanoparticles might be etched or left a way during mechanical handling of graphene film, leaving behind these nanometer pores in the final transferred graphene film, and make it more subjected to formation of tears and cracks during mechanical handling of graphene film from the etchant solution to the SiO_2 substrate. (3) Because of the complex structure of AA Cu surface morphology compared to HA as schematically depicted in **Figure 44 (a), (c)** respectively. Based on the above findings, we can suggest that the complex morphology of AA Cu surface including surface steps, edges, and existing nanoparticles would likely promote this non-uniform, bilayer, porous graphene film. In contrast, HA-Cu promoted more uniform, better continuity, thinner graphene film as it exhibited very smooth surface with low evidence of nanoparticles formations as shown in **Figure 44 (b), (d)** respectively.

This observation can be verified by conducting etching-pit experiment on graphene/Cu surface. Etching tests were conducted in order to quantify graphene structural defects after being deposited on AA and HA Cu substrates respectively. In this experiment, APS Cu-etchant was utilized to etch graphene/Cu surface for 5 sec, afterwards the sample was rinsed thoroughly by deionized water followed by N_2 drying.

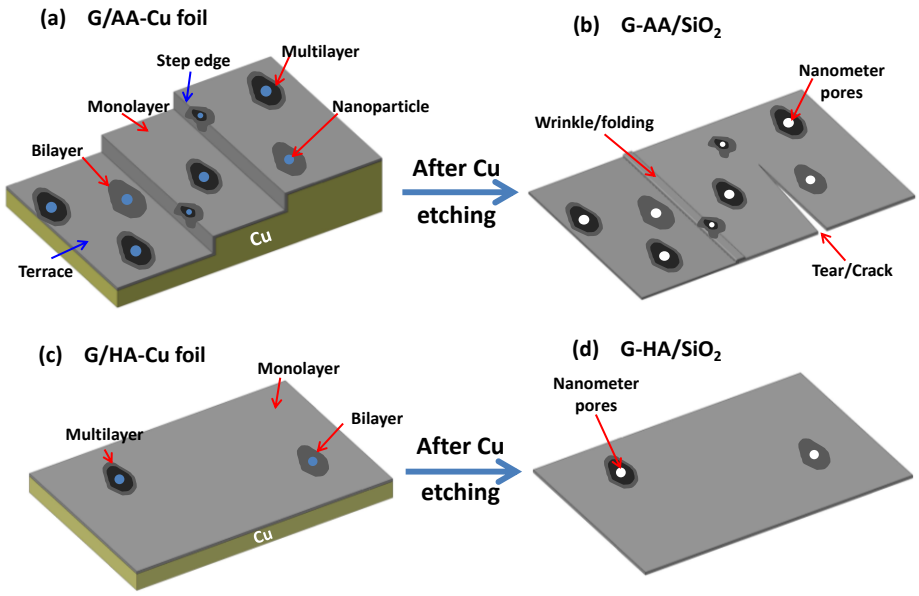

Figure 44: Schematic diagram shows the transfer of graphene from Cu substrate to SiO_2/Si wafer and generation of graphene nanometer pores as a result of Cu-etching process

Surface morphology of etched graphene/Cu-samples were characterized by OM and AFM as shown in **Figure 45**. It is clear that surface pits density found on graphene/AA surface **(Figure 45(a),(b))** is much higher than those found on graphene/HA **(Figure 45((d), (e))**, although it is bigger and deeper in HA case as depicted by AFM and profile height measurements shown in **Figure 45((c), (f)** for AA and HA respectively. The origin of these pits could be attributed to the partial growth of graphene and/or presence of impurity particles and/or graphene lattice defects [18] and [82].

Above results confirmed that smooth Cu surface was beneficial in deposition of monolayer, large area, homogeneous graphene, and consequently, it provided better protection for the underlying Cu substrate against the attack of APS-Cu etchant. In contrast, rough Cu surface showed bilayer, inhomogeneous, pores graphene film of less passivating ability of Cu substrate underneath. Results indicated also that transfer step by using PMMA increased the defectiveness of graphene films either grown on AA or HA substrates as indicated by

induced D-band after transfer process along with contaminating transferred graphene with PMMA and/or un-etched Cu residues.

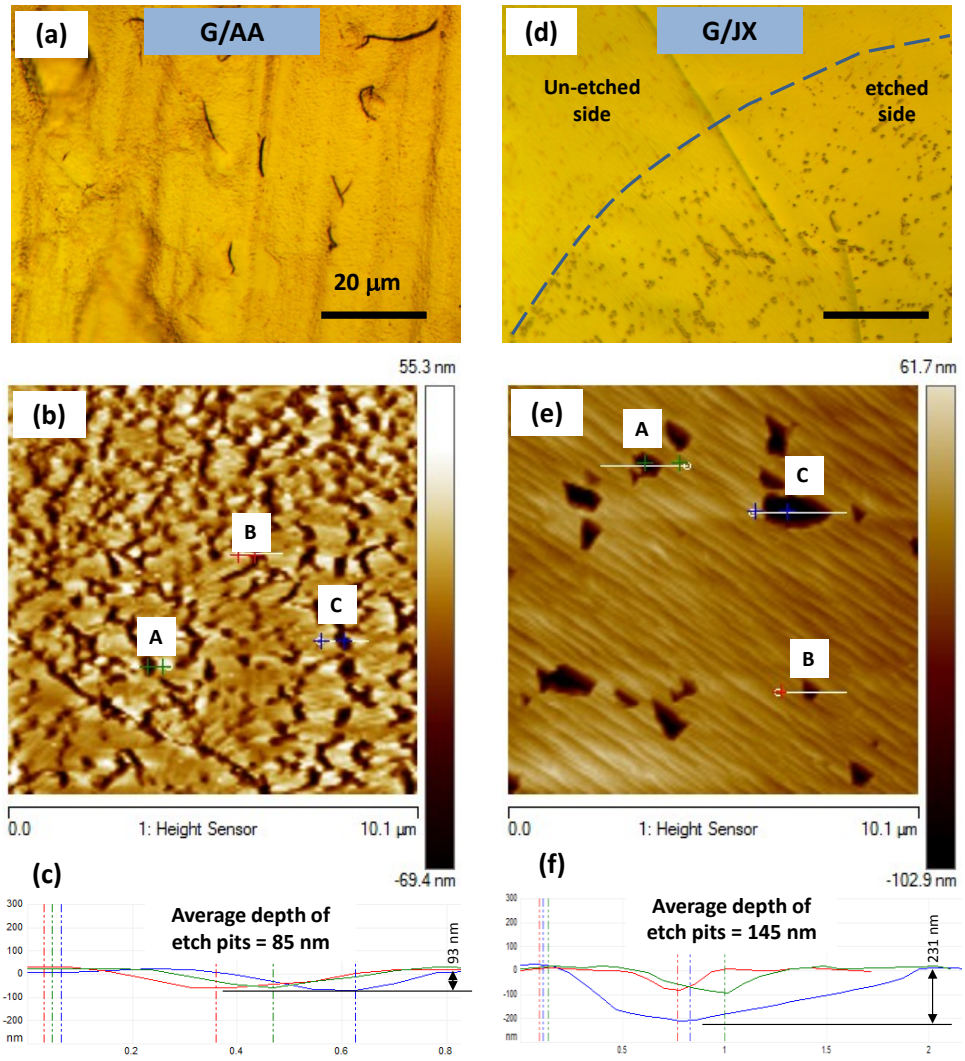

Figure 45: OM and AFM images of etched graphene/ AA and HA Cu foils respectively. (a, b, c) graphene grown by AA, (d, e, f) graphene grown on HA

4.5 Effect of growth temperature on the quality and thickness uniformity of graphene film

Previous graphene samples were deposited on AA and HA Cu foils that pre-annealed for 30 min at 0% H_2. This is to suppress the nucleation sites on Cu surface during annealing stage by oxidizing the surface or in other words, by increasing the oxygen content on the surface. In next section we will study the combined effects of H_2 concentration (during heating and annealing stages) and the growth temperature on graphene growth on the same AA and HA Cu substrates. The growth time was set to be 30 sec, the growth temperature was 1040^{o}C, and the H_2/Ar ratio was fixed during heating and annealing stages as shown in **Table 8.**

Table 8: CVD-graphene growth parameters to study the effect of H_2 concentration (during annealing stage) and increased growth temperature (1040^{o}C) on deposited graphene properties on AA and HA-Cu substrates respectively

Sample	H_2%	Heating		Annealing			Graphene Growth			
		Ar	H2	Ar (sccm)	H_2 (sccm)	Time (min)	Ar (sccm)	H_2 (sccm)	CH_4 (sccm)	Time (sec)
G-0%H_2	0	1500	0	1500	0	30	1464	36	5	30
G-2.5%H_2	2.5	1462	38	1462	38	30				
G-20%H_2	20	1300	200	1200	300	30				

Figure 46 shows the growth of graphene on AA-Cu that pre-heated and annealed at different H_2 concentrations (0, 2.5 and 20%). It is seen that 0%H_2 treatment promoted bilayer graphene film associated with some thicker multilayer domains concentrated mainly on the steps and terraces of Cu substrate. Furthermore, it was observed that narrow-spaced steps promoted formation of graphene ribbons as indicated by black arrows in **Figure 46 (a)**. 2.5%H_2 exhibited also bilayer graphene associated with

multilayer domains indicated by black arrow in panel (b). These domains were uniformly distributed throughout the Cu surface as shown by panels (b,e) associated with increased density of surface particles indicated by bright spots (marked by white arrow) in (b). At increased H_2 concentration corresponding to 20%, multilayer, more defective graphene film was obtained located mainly along surface striations and grain boundaries as indicated by **Figure 46 (c),(f).**

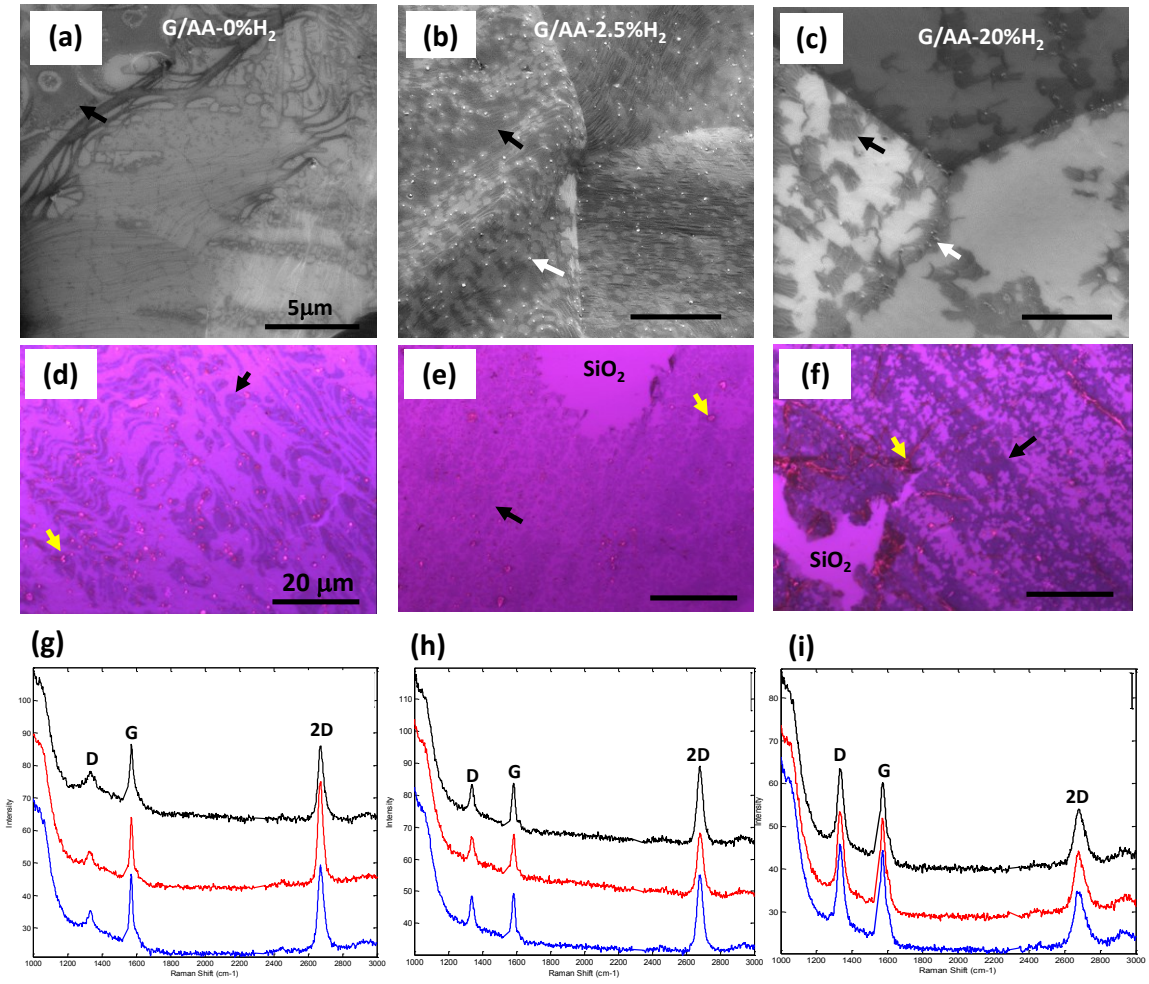

Figure 46: Effect of H_2 concentration on graphene grown on AA-Cu at 1040 ^oC for 30 sec growth time. (a- c) SEM micrographs of deposited graphene/AA-Cu foils, which preheated and annealed under different H_2 concentrations corresponding to 0, 2.5 and 20% respectively of the total gas mixture consisting of Ar and H_2 gases, (d-f) OM images of transferred graphene onto SiO_2 wafers shown in panels a-c , (g-i) Raman spectra of graphene/AA-Cu samples shown in panels (d-f). It is clear that as H_2 concentration increases, the defects density measured by D-band increases, indicating that high H_2 exposure during Cu pre-heating and annealing promotes formation of multilayer, highly defective graphene films

Raman spectra shown in **Figure 52 (g-i)** reveal that as H_2 concentration increases (from 0 to 20%) the density of defects increase accordingly as indicated by the increased D-band intensity, where the highest defects density is attained at 20%H_2. Comparing the 2D and G peaks ratios as a function of H_2 concentrations (0, 2.5 and 20%) as shown in Figure 52 (g-i) indicates that 2.5%H_2 promotes more uniform, fewer number of graphene layers if compared to those graphene films deposited at other H_2 concentrations, despite its defects density is higher slightly than that obtained in graphene film at 0% H_2 concentration.

Figure 47 shows growth of graphene on HA foils as a function of different H_2 concentrations (0, 2.5 and 20% respectively) during heating and annealing stages. It is observed that 0%H_2 led to deposition of bilayer graphene associated with formation of high density, very small multilayer uniformly distributed throughout the Cu surface and more pronounced on grain boundaries **Figure 47(d)**. As H_2 increases to 2.5%, it is seen that graphene film became monolayer, associated with presence of low density, bilayer/multilayer graphene areas (marked by black arrow in panel (b)). By further increasing H_2 concentration from 2.5 to 20%, multilayer graphene was obtained along with formation of high density, small size multilayer/amorphous carbon areas (indicated by black arrow). In addition, it is observed that as H_2 concentration increases the density of defects increases accordingly as indicated by the increased D-band intensity as a function of H_2 concentrations (**Figure 47(g-i)**). This confirms that the higher the H_2 exposure to Cu during heating and annealing, the higher the formation of amorphous carbon aggregates mostly designated by darker, thick irregular areas as shown in panels (a-c) and (d-f).

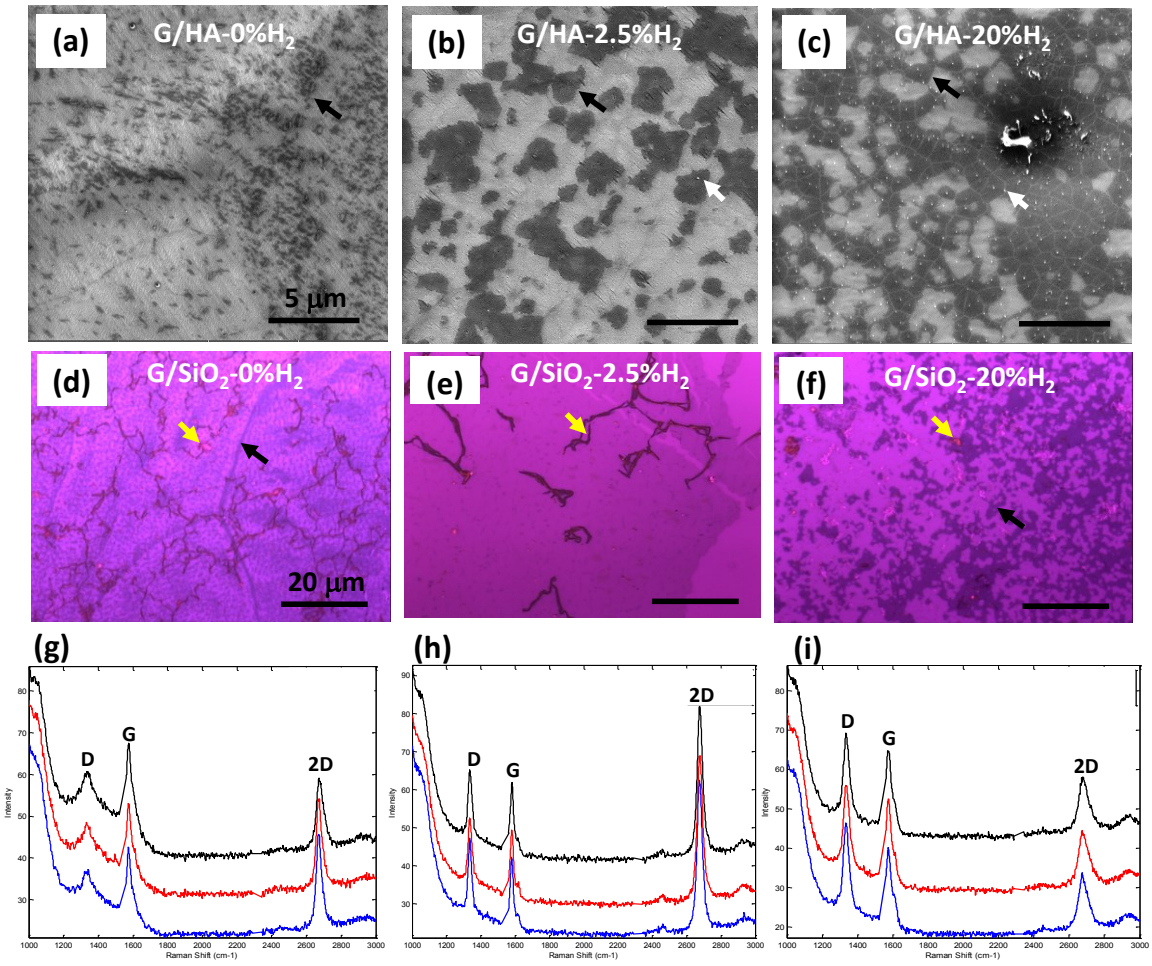

Figure 47: Effect of H_2 concentration on graphene grown on HA-Cu at 1040°C for 30 sec growth time. (a- c) SEM micrographs of deposited graphene/HA-Cu foils, which preheated and annealed under different H_2 concentrations corresponding to 0, 2.5 and 20% respectively of the total gas mixture consisting of Ar and H_2 gases, (d-f) OM images of transferred graphene onto SiO_2/Si substrates shown in panels a-c , (g-i) Raman spectra of as-transferred graphene films shown in panels (d-f). It is clear that as H_2 concentration increases, the defects density measured by D-band increases, indicating that high H_2 exposure during Cu pre-heating and annealing promotes formation of multilayer, highly defective graphene films

It is also observed that as H_2 increases from 2.5 to 20% the density of surface-particles were increased correspondingly. These particles are located approximately at the same nucleation sites of observed multilayer/amorphous carbon areas (**Figure 47(b),(c)**). Till now, it is unclear whether these particles are formed before or after graphene growth. It is mentioned in [73] that these particles were likely to nucleate after graphene deposition at the same nucleation sites of grown graphene areas. In other words, Cu active sites promoted nucleation not only of graphene domains but also surface particles formations.

The EDX elemental analysis of these particles reveals that they may be clusters of many elements like, C, Si, Cu and O.

At higher H_2 exposure (20%) it is clear that the density of multilayer domains in HA is higher than that observed in AA despite HA is smoother than AA, which suggesting that HA should exhibit lower nucleation or active sites than AA. This phenomenon could be related to the kinetics of nucleation, and growth of graphene on Cu substrate. This observation can be explained as follows; it was mentioned in [69] that the Cu surface with varying rough and smooth areas is likely to exhibit average less graphene nucleation density if compared to that found on completely uniform, flat surface. When carbon adatoms are dissociated from CH4 they will diffuse on the Cu surface, they will nucleate in large number on rough regions (because of their low mobility), forming a lot of nuclei on rough features, which will capture more carbon species for growth (this is referred by nucleation exclusion zone) [36]. This will result in less carbon resources on smoother regions, leading to less nucleation sites, less number of layers and better quality graphene. Therefore, we can say that rough features may promote less nucleation density on nearby smooth, flat regions.

According to the above results, we can conclude that low H_2 concentration (~2.5 %) is favorable for growing large area, more uniform, less number of graphene layers on both AA and HA-Cu substrates, despite it promoted slightly more defects than those obtained in deposited graphene at 0%H_2.

Figure 48 shows growth of graphene on AA and HA Cu foils that pre-treated at 0%H_2 concentration for 30 min, at 1040 ^{o}C, where the growth time was increased to 5 min. It is

observed that AA-Cu promoted formation of multilayer graphene film, associated with formation of high density of amorphous carbon aggregates (appear as flower-shape domains and/or dots and/or ribbons) as shown in **Figure 48 (a, c).** Moreover, Raman spectra shown in **Figure 48(e)** suggests that high growth temperature exhibited multilayer graphene (I_{2D}/I_G= 0.5) with high defect density (I_D/I_G= 0.7) compared with that negligible defects (I_D/I_G= 0.2) obtained at lower temperature growth corresponding to 1000^{o}C (**Figure 41 (c)**)

In contrast, HA-Cu exhibited bilayer graphene film associated with emergence of high density, very small size and thicker carbon clusters, with increased density of graphene grain boundaries as shown in **Figure 48 (b),(d)**. Raman results shown in **Figure 48 (f)** shows that the density of defects was increased (I_D/I_G= 0.4) compared to that obtained at lower growth temperature corresponding to 1000^{o}C (I_D/I_G= 0.2) as indicated in **Figure 41.** In contrast to that reported before in literature regarding the role of growth temperature on morphology and quality of synthesized graphene. The effect of increased temperature on promoting high density, multilayer, irregular graphene domains with high defects density (AA) can be explained by the fact that high growth temperature accompanied with increased growth time would increase high diffusion of carbon into Cu substrate (as the solubility of carbon into Cu will increased-leading to increased amount of carbon atoms in Cu), during cooling these carbon adatoms will segregate out of Cu substrate resulting in formation of multilayer, and inhomogeneous graphene.

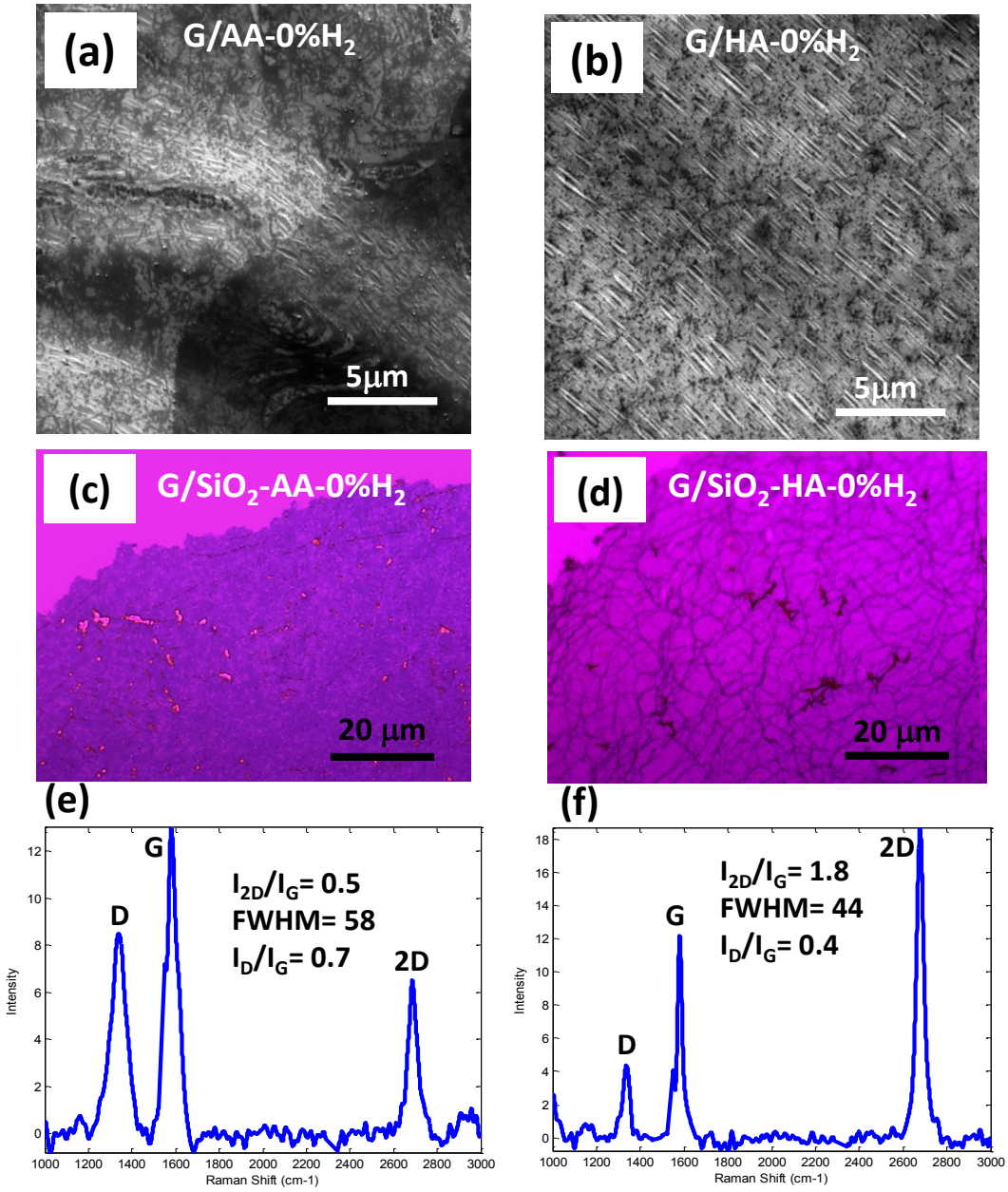

Figure 48: SEM and OM images of growth graphene on AA and HA Cu foils at elevated temperature corresponding to 1040 oC. Other growth parameters were set as follows; H2: Ar = 0 (during annealing step-30 min), 5 sccm CH4, for 5 minutes (a, b) SEM images of graphene/AA and HA respectively, (c,d) OM images of transferred graphene (shown in (a,b)) onto 300 nm SiO2/Si wafer, (e,f) Raman spectra of transferred graphene samples shown in (c,d). It is clear that AA promoted multilayer, high density, very small, high defective graphene, however, HA exhibited bilayer, low defective graphene with high density of graphene grain boundaries

It was suggested that these multilayer graphene regions grow underneath the first homogeneous, large area and single layer graphene film. This is more confirmed by previous reports [81] which indicated carbon segregation promotes formation of multilayer and inhomogeneous graphene formation. These carbon atoms were stored mainly in Cu substrate's defects such as, screw dislocations and grain boundaries [83].

Based on the above mentioned discussion, there are two ways to reduce these carbon in-homogeneities, the first is by suppressing the surface defects in Cu before graphene deposition (using high purity Cu surface, or single crystal metal, epitaxial thin films). The second method is by minimizing the amount of used CH4 during growth step and/or decreasing the growth time (less time for storing carbon inside Cu substrate).

CHAPTER 5

CONCLUSIONS

Our results revealed that H_2 plays an important role in controlling the characteristics of both Cu surface morphology and graphene film grown by CVD. Our annealing study on Cu demonstrated that the reconstructed Cu surface strongly depends on the H_2 concentration. At 0%H_2 annealing Cu exhibited step-like structure consisting of narrow-spaced steps. Increasing H_2 up to 50%, Cu surface became smoother associated with other features such as dents, particles and facets. In addition, we elucidated that Cu surface morphology prior to graphene deposition played crucial role in controlling and dictating the Cu surface reconstruction mechanism. Our results revealed that when graphene is grown on narrow-spaced steps structure (Ar-annealed), it will pin the steps motion which causes step bunching effect and produce wide-spaced steps structure. In contrast, when graphene is deposited on smooth surface (H_2-annealed) it will promote formation of narrow-spaced wrinkles structure. These Cu-wrinkles are mostly occurred to relax the strain from a large lattice mismatch between graphene and Cu lattice at a high temperature during the CVD process. Even though high H_2 concentration reduced Cu surface roughness, it promoted formation of defective and multilayer graphene. In contrast, a low H_2 concentration yielded a slightly rougher surface; but it yielded bilayer and good quality graphene.

In addition, we investigated the influence of Cu substrate surface morphology on the deposited graphene properties and its subsequent transfer onto SiO2/Si substrate.

Smoother, relatively higher purity copper (HA) yielded more uniform, continuous, single graphene film associated with low density of bilayer/multilayer regular graphene domains. In contrast rough and low purity Cu (AA) exhibited non-uniform, high density of bilayer/multilayer irregular graphene domains. AA surface evolved to complex surface texture consisting of dense steps associated with high density of large-sized particles after graphene growth, while HA yielded relatively flat surface accompanied by low density of surface particles. The complex structure of G/AA promoted high density of pores, tears and cracks into the transferred graphene film compared to the smoother Cu morphology of G/HA, which gave rise to more continuous, uniform graphene film with negligible pores after subsequent transfer.

According to the above results; it is clear that graphene grown on smooth Cu (G/HA) provided better protection for the underlying Cu substrate against the attack of APS etchant, confirming that G/HA had lower structural defects compared to that found for G/AA which exhibited less-protection to the underlying Cu substrate during etching-pit experiment.

References

[1] A. K. Geim and K. S. Novoselov, “The rise of graphene,” *Nat Mater*, vol. 6, no. 3, pp. 183–191, Mar. 2007.

[2] C. Lee, X. Wei, J. W. Kysar, and J. Hone, “Measurement of the Elastic Properties and Intrinsic Strength of Monolayer Graphene,” *Science*, vol. 321, no. 5887, pp. 385–388, Jul. 2008.

[3] S. C. O’Hern, C. A. Stewart, M. S. H. Boutilier, J.-C. Idrobo, S. Bhaviripudi, S. K. Das, J. Kong, T. Laoui, M. Atieh, and R. Karnik, “Selective Molecular Transport through Intrinsic Defects in a Single Layer of CVD Graphene,” *ACS Nano*, vol. 6, no. 11, pp. 10130–10138, Nov. 2012.

[4] S. C. O’Hern, M. S. H. Boutilier, J.-C. Idrobo, Y. Song, J. Kong, T. Laoui, M. Atieh, and R. Karnik, “Selective Ionic Transport through Tunable Subnanometer Pores in Single-Layer Graphene Membranes,” *Nano Lett.*, vol. 14, no. 3, pp. 1234–1241, 2014.

[5] Y. Hernandez, V. Nicolosi, M. Lotya, F. M. Blighe, Z. Sun, S. De, I. T. McGovern, B. Holland, M. Byrne, Y. K. Gun’Ko, J. J. Boland, P. Niraj, G. Duesberg, S. Krishnamurthy, R. Goodhue, J. Hutchison, V. Scardaci, A. C. Ferrari, and J. N. Coleman, “High-yield production of graphene by liquid-phase exfoliation of graphite,” *Nat Nano*, vol. 3, no. 9, pp. 563–568, Sep. 2008.

[6] K. S. Novoselov, A. K. Geim, S. V. Morozov, D. Jiang, Y. Zhang, S. V. Dubonos, I. V. Grigorieva, and A. A. Firsov, “Electric Field Effect in Atomically Thin Carbon Films,” *Science*, vol. 306, no. 5696, pp. 666–669, Oct. 2004.

[7] X. Li, W. Cai, J. An, S. Kim, J. Nah, D. Yang, R. Piner, A. Velamakanni, I. Jung, E. Tutuc, S. K. Banerjee, L. Colombo, and R. S. Ruoff, "Large-Area Synthesis of High-Quality and Uniform Graphene Films on Copper Foils," *Science*, vol. 324, no. 5932, pp. 1312–1314, Jun. 2009.

[8] X. Li, W. Cai, L. Colombo, and R. S. Ruoff, "Evolution of Graphene Growth on Ni and Cu by Carbon Isotope Labeling," *Nano Lett.*, vol. 9, no. 12, pp. 4268–4272, Dec. 2009.

[9] Q. Yu, J. Lian, S. Siriponglert, H. Li, Y. P. Chen, and S.-S. Pei, "Graphene segregated on Ni surfaces and transferred to insulators," *Applied Physics Letters*, vol. 93, no. 11, p. 113103, Sep. 2008.

[10] W. Wu, Q. Yu, P. Peng, Z. Liu, J. Bao, and S.-S. Pei, "Control of thickness uniformity and grain size in graphene films for transparent conductive electrodes," *Nanotechnology*, vol. 23, no. 3, p. 035603, Jan. 2012.

[11] P. Trinsoutrot, C. Rabot, H. Vergnes, A. Delamoreanu, A. Zenasni, and B. Caussat, "High quality graphene synthesized by atmospheric pressure CVD on copper foil," *Surface and Coatings Technology*, vol. 230, pp. 87–92, Sep. 2013.

[12] S. Bhaviripudi, X. Jia, M. S. Dresselhaus, and J. Kong, "Role of Kinetic Factors in Chemical Vapor Deposition Synthesis of Uniform Large Area Graphene Using Copper Catalyst," *Nano Lett.*, vol. 10, no. 10, pp. 4128–4133, Oct. 2010.

[13] I. Vlassiouk, S. Smirnov, M. Regmi, S. P. Surwade, N. Srivastava, R. Feenstra, G. Eres, C. Parish, N. Lavrik, and P. Datskos, "Graphene Nucleation Density on

Copper: Fundamental Role of Background Pressure," *The Journal of Physical Chemistry C*, vol. 117, no. 37, pp. 18919–18926, 2013.

[14] V. T. Nguyen, H. D. Le, V. C. Nguyen, and T. T. T. Ngo, "Synthesis of multi-layer graphene films on copper tape by atmospheric pressure chemical vapor deposition method."

[15] N. Reckinger, A. Felten, C. N. Santos, B. Hackens, and J.-F. Colomer, "The influence of residual oxidizing impurities on the synthesis of graphene by atmospheric pressure chemical vapor deposition," *Carbon*, vol. 63, pp. 84–91, 2013.

[16] H. Wang, G. Wang, P. Bao, S. Yang, W. Zhu, X. Xie, and W.-J. Zhang, "Controllable Synthesis of Submillimeter Single-Crystal Monolayer Graphene Domains on Copper Foils by Suppressing Nucleation," *J. Am. Chem. Soc.*, vol. 134, no. 8, pp. 3627–3630, Feb. 2012.

[17] L. Gan and Z. Luo, "Turning off Hydrogen To Realize Seeded Growth of Subcentimeter Single-Crystal Graphene Grains on Copper," *ACS Nano*, vol. 7, no. 10, pp. 9480–9488, Oct. 2013.

[18] F. Yang, Y. Liu, W. Wu, W. Chen, L. Gao, and J. Sun, "A facile method to observe graphene growth on copper foil," *Nanotechnology*, vol. 23, no. 47, p. 475705, Nov. 2012.

[19] Y. C. Shin and J. Kong, "Hydrogen-excluded graphene synthesis via atmospheric pressure chemical vapor deposition," *Carbon*, vol. 59, pp. 439–447, Aug. 2013.

[20] D. H. Jung, C. Kang, M. Kim, H. Cheong, H. Lee, and J. S. Lee, "Effects of Hydrogen Partial Pressure in the Annealing Process on Graphene Growth," *J. Phys. Chem. C*, vol. 118, no. 7, pp. 3574–3580, Feb. 2014.

[21] Z. Luo, Y. Lu, D. W. Singer, M. E. Berck, L. A. Somers, B. R. Goldsmith, and A. T. C. Johnson, "Effect of Substrate Roughness and Feedstock Concentration on Growth of Wafer-Scale Graphene at Atmospheric Pressure," *Chemistry of Materials*, vol. 23, no. 6, pp. 1441–1447, Mar. 2011.

[22] O. I. Sarajlic and R. G. Mani, "Mesoscale Scanning Electron and Tunneling Microscopy Study of the Surface Morphology of Thermally Annealed Copper Foils for Graphene Growth," *Chem. Mater.*, vol. 25, no. 9, pp. 1643–1648, May 2013.

[23] G. H. Han, F. Güneş, J. J. Bae, E. S. Kim, S. J. Chae, H.-J. Shin, J.-Y. Choi, D. Pribat, and Y. H. Lee, "Influence of Copper Morphology in Forming Nucleation Seeds for Graphene Growth," *Nano Lett.*, vol. 11, no. 10, pp. 4144–4148, Oct. 2011.

[24] I. Vlassiouk, P. Fulvio, H. Meyer, N. Lavrik, S. Dai, P. Datskos, and S. Smirnov, "Large scale atmospheric pressure chemical vapor deposition of graphene," *Carbon*, vol. 54, pp. 58–67, Apr. 2013.

[25] S. M. Kim, A. Hsu, Y.-H. Lee, M. Dresselhaus, T. Palacios, K. K. Kim, and J. Kong, "The effect of copper pre-cleaning on graphene synthesis," *Nanotechnology*, vol. 24, no. 36, p. 365602, Sep. 2013.

[26] P. Procházka, J. Mach, D. Bischoff, Z. Lišková, P. Dvořák, M. Vaňatka, P. Simonet, A. Varlet, D. Hemzal, M. Petrenec, L. Kalina, M. Bartošík, K. Ensslin, P. Varga, J. Čechal, and T. Šikola, "Ultrasmooth metallic foils for growth of high quality

graphene by chemical vapor deposition," *Nanotechnology*, vol. 25, no. 18, p. 185601, May 2014.

[27] W. Wen-Rong, L. Chen, L. Tie, Y. Heng, L. Na, and W. Yue-Lin, "Graphene Domains Synthesized on Electroplated Copper by Chemical Vapor Deposition," *Chinese Phys. Lett.*, vol. 30, no. 2, p. 028102, Feb. 2013.

[28] T. Humplik, J. Lee, S. C. O'Hern, B. A. Fellman, M. A. Baig, S. F. Hassan, M. A. Atieh, F. Rahman, T. Laoui, R. Karnik, and E. N. Wang, "Nanostructured materials for water desalination," *Nanotechnology*, vol. 22, no. 29, p. 292001, Jul. 2011.

[29] D. Jiang, V. R. Cooper, and S. Dai, "Porous Graphene as the Ultimate Membrane for Gas Separation," *Nano Lett.*, vol. 9, no. 12, pp. 4019–4024, Dec. 2009.

[30] D. Cohen-Tanugi and J. C. Grossman, "Water Desalination across Nanoporous Graphene," *Nano Lett.*, vol. 12, no. 7, pp. 3602–3608, Jul. 2012.

[31] L. A. David, "Synthesis of large-area few layer graphene films by rapid heating and cooling in a modified apcvd furnace," Thesis, Kansas State University, 2011.

[32] K. S. Kim, Y. Zhao, H. Jang, S. Y. Lee, J. M. Kim, K. S. Kim, J.-H. Ahn, P. Kim, J.-Y. Choi, and B. H. Hong, "Large-scale pattern growth of graphene films for stretchable transparent electrodes," *Nature*, vol. 457, no. 7230, pp. 706–710, Feb. 2009.

[33] S.-Y. Kwon, C. V. Ciobanu, V. Petrova, V. B. Shenoy, J. Bareño, V. Gambin, I. Petrov, and S. Kodambaka, "Growth of Semiconducting Graphene on Palladium," *Nano Lett.*, vol. 9, no. 12, pp. 3985–3990, Dec. 2009.

[34] P. W. Sutter, J.-I. Flege, and E. A. Sutter, “Epitaxial graphene on ruthenium,” *Nat Mater*, vol. 7, no. 5, pp. 406–411, May 2008.

[35] J. Coraux, A. T. N`Diaye, C. Busse, and T. Michely, “Structural Coherency of Graphene on Ir(111),” *Nano Lett.*, vol. 8, no. 2, pp. 565–570, Feb. 2008.

[36] Y. Zhang, L. Gomez, F. N. Ishikawa, A. Madaria, K. Ryu, C. Wang, A. Badmaev, and C. Zhou, “Comparison of Graphene Growth on Single-Crystalline and Polycrystalline Ni by Chemical Vapor Deposition,” *J. Phys. Chem. Lett.*, vol. 1, no. 20, pp. 3101–3107, Oct. 2010.

[37] A. W. Robertson and J. H. Warner, “Hexagonal Single Crystal Domains of Few-Layer Graphene on Copper Foils,” *Nano Lett.*, vol. 11, no. 3, pp. 1182–1189, Mar. 2011.

[38] X. Li, C. W. Magnuson, A. Venugopal, J. An, J. W. Suk, B. Han, M. Borysiak, W. Cai, A. Velamakanni, Y. Zhu, L. Fu, E. M. Vogel, E. Voelkl, L. Colombo, and R. S. Ruoff, “Graphene Films with Large Domain Size by a Two-Step Chemical Vapor Deposition Process,” *Nano Lett.*, vol. 10, no. 11, pp. 4328–4334, Nov. 2010.

[39] J. Zhang, P. Hu, X. Wang, Z. Wang, D. Liu, B. Yang, and W. Cao, “CVD growth of large area and uniform graphene on tilted copper foil for high performance flexible transparent conductive film,” *J. Mater. Chem.*, vol. 22, no. 35, pp. 18283–18290, Aug. 2012.

[40] C. Liang, W. Wang, T. Li, and Y. Wang, “Optimization on the synthesis of large-area single-crystal graphene domains by chemical vapor deposition on copper foils,”

in *2012 International Conference on Manipulation, Manufacturing and Measurement on the Nanoscale (3M-NANO)*, 2012, pp. 144–147.

[41] Rossela Giorgi, Nicola Lisi, Theodoros Dickonimos, Mauro Falconieri, Serena Gagliardi, Elena Salernitano, Piere Morales, and Luciano Pilloni, "Graphene: large area synthesis by Chemical Vapor Deposition — it." [Online]. Available: http://www.enea.it/it/produzione-scientifica/EAI/anno-2011/indice-world-view-3-2011/graphene-large-area-synthesis-by-chemical-vapor-deposition. [Accessed: 19-Jul-2013].

[42] X. Zhang, J. Ning, X. Li, B. Wang, L. Hao, M. Liang, M. Jin, and L. Zhi, "Hydrogen-induced effects on the CVD growth of high-quality graphene structures," *Nanoscale*, May 2013.

[43] I. Vlassiouk, M. Regmi, P. Fulvio, S. Dai, P. Datskos, G. Eres, and S. Smirnov, "Role of Hydrogen in Chemical Vapor Deposition Growth of Large Single-Crystal Graphene," *ACS Nano*, vol. 5, no. 7, pp. 6069–6076, Jul. 2011.

[44] M. Qi, Z. Ren, Y. Jiao, Y. Zhou, X. Xu, W. Li, J. Li, X. Zheng, and J. Bai, "Hydrogen Kinetics on Scalable Graphene Growth by Atmospheric Pressure Chemical Vapor Deposition with Acetylene," *J. Phys. Chem. C*, vol. 117, no. 27, pp. 14348–14353, Jul. 2013.

[45] S. Hussain, M. W. Iqbal, J. Park, M. Ahmad, J. Singh, J. Eom, and J. Jung, "Physical and electrical properties of graphene grown under different hydrogen flow in low pressure chemical vapor deposition," *Nanoscale Res Lett*, vol. 9, no. 1, p. 546, Oct. 2014.

[46] M. Losurdo, M. M. Giangregorio, P. Capezzuto, and G. Bruno, "Graphene CVD growth on copper and nickel: role of hydrogen in kinetics and structure," *Phys. Chem. Chem. Phys.*, vol. 13, no. 46, pp. 20836–20843, Nov. 2011.

[47] Y. Jin, B. Hu, Z. Wei, Z. Luo, D. Wei, Y. Xi, Y. Zhang, and Y. Liu, "Roles of H2 in annealing and growth times of graphene CVD synthesis over copper foil," *J. Mater. Chem. A*, vol. 2, no. 38, pp. 16208–16216, Sep. 2014.

[48] J. D. Wood, S. W. Schmucker, A. S. Lyons, E. Pop, and J. W. Lyding, "Effects of Polycrystalline Cu Substrate on Graphene Growth by Chemical Vapor Deposition," *Nano Lett.*, vol. 11, no. 11, pp. 4547–4554, Nov. 2011.

[49] I. Vlassiouk, S. Smirnov, I. Ivanov, P. F. Fulvio, S. Dai, H. Meyer, M. Chi, D. Hensley, P. Datskos, and N. V. Lavrik, "Electrical and thermal conductivity of low temperature CVD graphene: the effect of disorder," *Nanotechnology*, vol. 22, no. 27, p. 275716, Jul. 2011.

[50] D. Geng, B. Wu, Y. Guo, L. Huang, Y. Xue, J. Chen, G. Yu, L. Jiang, W. Hu, and Y. Liu, "Uniform hexagonal graphene flakes and films grown on liquid copper surface," *PNAS*, Apr. 2012.

[51] L. Gao, W. Ren, J. Zhao, L.-P. Ma, Z. Chen, and H.-M. Cheng, "Efficient growth of high-quality graphene films on Cu foils by ambient pressure chemical vapor deposition," *Applied Physics Letters*, vol. 97, no. 18, pp. 183109–183109–3, Nov. 2010.

[52] H. I. Rasool, E. B. Song, M. J. Allen, J. K. Wassei, R. B. Kaner, K. L. Wang, B. H. Weiller, and J. K. Gimzewski, "Continuity of Graphene on Polycrystalline Copper," *Nano Lett.*, vol. 11, no. 1, pp. 251–256, Jan. 2011.

[53] C. Jia, J. Jiang, L. Gan, and X. Guo, "Direct Optical Characterization of Graphene Growth and Domains on Growth Substrates," *Sci. Rep.*, vol. 2, Oct. 2012.

[54] A.-Y. Lu, S.-Y. Wei, C.-Y. Wu, Y. Hernandez, T.-Y. Chen, T.-H. Liu, C.-W. Pao, F.-R. Chen, L.-J. Li, and Z.-Y. Juang, "Decoupling of CVD graphene by controlled oxidation of recrystallized Cu," *RSC Adv.*, vol. 2, no. 7, pp. 3008–3013, Mar. 2012.

[55] A. T. Murdock, A. Koos, T. B. Britton, L. Houben, T. Batten, T. Zhang, A. J. Wilkinson, R. E. Dunin-Borkowski, C. E. Lekka, and N. Grobert, "Controlling the Orientation, Edge Geometry, and Thickness of Chemical Vapor Deposition Graphene," *ACS Nano*, vol. 7, no. 2, pp. 1351–1359, Feb. 2013.

[56] Q. Yu, L. A. Jauregui, W. Wu, R. Colby, J. Tian, Z. Su, H. Cao, Z. Liu, D. Pandey, D. Wei, T. F. Chung, P. Peng, N. P. Guisinger, E. A. Stach, J. Bao, S.-S. Pei, and Y. P. Chen, "Control and characterization of individual grains and grain boundaries in graphene grown by chemical vapour deposition," *Nat Mater*, vol. 10, no. 6, pp. 443–449, Jun. 2011.

[57] A. K. Geim and K. S. Novoselov, "The rise of graphene," *Nat Mater*, vol. 6, no. 3, pp. 183–191, Mar. 2007.

[58] A. C. Ferrari, J. C. Meyer, V. Scardaci, C. Casiraghi, M. Lazzeri, F. Mauri, S. Piscanec, D. Jiang, K. S. Novoselov, S. Roth, and A. K. Geim, "Raman Spectrum of

Graphene and Graphene Layers," *Phys. Rev. Lett.*, vol. 97, no. 18, p. 187401, Oct. 2006.

[59] D. Stojanović, N. Woehrl, and V. Buck, "Synthesis and characterization of graphene films by hot filament chemical vapor deposition," *Phys. Scr.*, vol. 2012, no. T149, p. 014068, May 2012.

[60] F. Tuinstra, "Raman Spectrum of Graphite," *The Journal of Chemical Physics*, vol. 53, no. 3, p. 1126, 1970.

[61] A. Gupta, G. Chen, P. Joshi, S. Tadigadapa, and P. C. Eklund, "Raman scattering from high-frequency phonons in supported n-graphene layer films," *Nano Lett.*, vol. 6, no. 12, pp. 2667–2673, Dec. 2006.

[62] M. P. Levendorf, C. S. Ruiz-Vargas, S. Garg, and J. Park, "Transfer-Free Batch Fabrication of Single Layer Graphene Transistors," *Nano Lett.*, vol. 9, no. 12, pp. 4479–4483, Dec. 2009.

[63] C. Mattevi, H. Kim, and M. Chhowalla, "A review of chemical vapour deposition of graphene on copper," *J. Mater. Chem.*, vol. 21, no. 10, pp. 3324–3334, Feb. 2011.

[64] "Atomic force microscopy," *Wikipedia, the free encyclopedia*. 05-Feb-2015.

[65] Z.-J. Wang, G. Weinberg, Q. Zhang, T. Lunkenbein, A. Klein-Hoffmann, M. Kurnatowska, M. Plodinec, Q. Li, L. Chi, R. Schloegl, and M.-G. Willinger, "Direct Observation of Graphene Growth and Associated Copper Substrate Dynamics by in Situ Scanning Electron Microscopy," *ACS Nano*, vol. 9, no. 2, pp. 1506–1519, Feb. 2015.

[66] Z. Yan, J. Lin, Z. Peng, Z. Sun, Y. Zhu, L. Li, C. Xiang, E. L. Samuel, C. Kittrell, and J. M. Tour, "Toward the Synthesis of Wafer-Scale Single-Crystal Graphene on Copper Foils," *ACS Nano*, vol. 6, no. 10, pp. 9110–9117, Oct. 2012.

[67] H. Magnusson and K. Frisk, "Self-diffusion and impurity diffusion in the hydrogen, oxygen, sulphur and phosphorous in copper," *Swedish Nuclear Waste Management Company Technical Report TR-13-24*, 2013.

[68] W. Liu, H. Li, C. Xu, Y. Khatami, and K. Banerjee, "Synthesis of high-quality monolayer and bilayer graphene on copper using chemical vapor deposition," *Carbon*, vol. 49, no. 13, pp. 4122–4130, Nov. 2011.

[69] H. Kim, C. Mattevi, M. R. Calvo, J. C. Oberg, L. Artiglia, S. Agnoli, C. F. Hirjibehedin, M. Chhowalla, and E. Saiz, "Activation Energy Paths for Graphene Nucleation and Growth on Cu," *ACS Nano*, vol. 6, no. 4, pp. 3614–3623, Apr. 2012.

[70] B. Zhang, W. H. Lee, R. Piner, I. Kholmanov, Y. Wu, H. Li, H. Ji, and R. S. Ruoff, "Low-Temperature Chemical Vapor Deposition Growth of Graphene from Toluene on Electropolished Copper Foils," *ACS Nano*, vol. 6, no. 3, pp. 2471–2476, Mar. 2012.

[71] J. Song, T. Y. Ko, and S. Ryu, "Raman Spectroscopy Study of Annealing-Induced Effects on Graphene Prepared by Micromechanical Exfoliation," *Bulletin of the Korean Chemical Society*, vol. 31, no. 9, pp. 2679–2682, Sep. 2010.

[72] X. Dong, P. Wang, W. Fang, C.-Y. Su, Y.-H. Chen, L.-J. Li, W. Huang, and P. Chen, "Growth of large-sized graphene thin-films by liquid precursor-based

chemical vapor deposition under atmospheric pressure," *Carbon*, vol. 49, no. 11, pp. 3672–3678, Sep. 2011.

[73] L. Fan, K. Wang, J. Wei, M. Zhong, D. Wu, and H. Zhu, "Correlation between nanoparticle location and graphene nucleation in chemical vapour deposition of graphene," *J. Mater. Chem. A*, vol. 2, no. 32, pp. 13123–13128, Jul. 2014.

[74] S. Suzuki, T. Nagamori, Y. Matsuoka, and M. Yoshimura, "Threefold atmospheric-pressure annealing for suppressing graphene nucleation on copper in chemical vapor deposition," *Jpn. J. Appl. Phys.*, vol. 53, no. 9, p. 095101, Sep. 2014.

[75] K. Hayashi, S. Sato, and N. Yokoyama, "Anisotropic graphene growth accompanied by step bunching on a dynamic copper surface," *Nanotechnology*, vol. 24, no. 2, p. 025603, Jan. 2013.

[76] J. M. Wofford, S. Nie, K. F. McCarty, N. C. Bartelt, and O. D. Dubon, "Graphene Islands on Cu Foils: The Interplay between Shape, Orientation, and Defects," *Nano Lett.*, vol. 10, no. 12, pp. 4890–4896, Dec. 2010.

[77] D. P. Favreau, Y. Shacham-Diamand, Y. Horiike, B. University of California, and Continuing Education in Engineering, Eds., *Advanced metallization for ULSI applications in 1993: proceedings of the conference held October 5-7, 1993, San Diego, California, U.S.A., and October 26-27, 1993, Tokyo, Japan sponsored by Continuing Education in Engineering, University Extension, University of California, Berkeley, U.S.A.* Pittsburgh, PA: Materials Research Society, 1994.

[78] S.-K. Rha, W.-J. Lee, S.-Y. Lee, D.-W. Kim, C.-O. Park, and S.-S. Chun, "Effects of the Annealing in Ar and H2/Ar Ambients on the Microstructure and the Electrical

Resistivity of the Copper Film Prepared by Chemical Vapor Deposition," *Jpn. J. Appl. Phys.*, vol. 35, no. 11R, p. 5781, Nov. 1996.

[79] L. Fan, Z. Li, Z. Xu, K. Wang, J. Wei, X. Li, J. Zou, D. Wu, and H. Zhu, "Step driven competitive epitaxial and self-limited growth of graphene on copper surface," *AIP Advances*, vol. 1, no. 3, p. 032145, Sep. 2011.

[80] M. L. Z Zhang, "Atomistic Processes in the Early Stages of Thin-Film Growth," *Science (New York, N.Y.)*, vol. 276, no. 5311, pp. 377–83, 1997.

[81] S. Nie, W. Wu, S. Xing, Q. Yu, J. Bao, S. Pei, and K. F. McCarty, "Growth from below: bilayer graphene on copper by chemical vapor deposition," *New J. Phys.*, vol. 14, no. 9, p. 093028, Sep. 2012.

[82] Y.-P. Hsieh, M. Hofmann, and J. Kong, "Promoter-assisted chemical vapor deposition of graphene," *Carbon*, vol. 67, pp. 417–423, Feb. 2014.

[83] S. Yoshii, K. Nozawa, K. Toyoda, N. Matsukawa, A. Odagawa, and A. Tsujimura, "Suppression of Inhomogeneous Segregation in Graphene Growth on Epitaxial Metal Films," *Nano Lett.*, vol. 11, no. 7, pp. 2628–2633, 2011.

Curriculum Vitae

Name	:Ahmed Ibrahim Ali Ibrahim
Nationality	:Egyptian
Date of Birth	:1/1/1977
Email	:amdegy@yahoo.com
Address	:King Fahd University of Petroleum and Minerals
Academic Background	:Mechanical Engineering Department

RESEARCH INTERESTS

- Metal Matrix Composites (MMCs).
- Modelling of Process-Microstructure-Property relationship in MMCs.
- Synthesis, characterization and transfer of graphene fabricated by chemical Vapor deposition (CVD)
- Modelling of machining processes.

LIST OF PUBLICATIONS

- A. Ibrahim, A. Owais, M. Atieh, R. Karnik, and T. Laoui, "Evolution of Cu Surface Morphology and its Effect on Graphene Synthesized by Chemical Vapor Deposition," Advances in Science and Technology, vol. 95, pp. 17–22, Oct. 2014 (Conference paper)

- A. Ibrahim, S. Akhtar, M. Atieh, R. Karnik, and T. Laoui, "Effects of annealing on copper substrate surface morphology and graphene growth by chemical vapor deposition," Carbon, vol. 94, pp. 369–377, Nov. 2015

- El-Sonbaty, U.A. Khashaba, A. I. Selmy, and A. Ibrahim "Prediction of Surface Roughness Profiles for Milled Surfaces Using an Artificial Neural Network and Fractal Geometry Approach" Journal of Materials Processing Technology, Volume 200, Issues 1-3, 8 May 2008, Pages 271-278

- Esmail M.A. Mokheimer, Ahmet Z. Sahin, Abdullah Al-Sharafi, A. Ibrahim "Modeling and optimization of hybrid wind–solar-powered reverse osmosis water desalination system in Saudi Arabia" Energy Conversion and Management Volume 75, November 2013, Pages 86–97